Characterization of terrestrial organic carbon in the Amazon system: insights from biomarkers and their isotopic composition (δ^{13}C and Δ^{14}C)

Dissertation

Zur Erlangung des Doktorgrades

der Naturwissenschaften

-Dr. rer. nat. -

Am Fachbereich Geowissenschaften

der Universität Bremen

Vorgelegt von

Shuwen Sun

Bremen

April 2018

Universität Bremen

Erstgutachter:

Prof. Dr. Gesine Mollenhauer

Zweitgutachter:

Dr. Tommaso Tesi

Tag des Prüfungskolloquiums:

28. Juni 2018

Mitlieder der Prüfungskommission:

Prof. Dr. Gesine Mollenhauer

Dr. Tommaso Tesi

Prof. Dr. Sabine Kasten

Dr. Enno Schefuß

Dr. Stefan Mulitza

Herr. Julian Schukies

To my parents and girlfriend

Name / *Name*: _____ Datum / *Date:* _____

Anschrift / *Address:* _____

**Erklärung gem. § 4 Abs. 1 Nr. 3 und 4
der Promotionsordnung vom 15.07.2015 /
*Statement according to § 4 (1) no. 3 and 4
of the Doctoral Degree Rules and Regulations of 15.07.2015***

Ich erkläre, dass ich mich weder einem Promotionsverfahren unterzogen noch ein solches beantragt habe. /
I affirm that I did not undergo a doctoral degree granting procedure, nor did I apply for the examination procedure elsewhere.

Mit einer Überprüfung der Dissertation mit qualifizierter Software zur Untersuchung von Plagiatsvorwürfen bin ich einverstanden. /
I accept scanning of the doctoral thesis with appropriate software for the detection of plagiarism.

_____
(Unterschrift Doktorand/in / *Signature PhD student*)

Versicherung an Eides Statt / *Affirmation in lieu of an oath*

gem. § 5 Abs. 5 der Promotionsordnung vom 15.07.2015 /

according to § 5 (5) of the Doctoral Degree Rules and Regulations of 15 July, 2015

Ich / I,_____

(Vorname / First *Name*, Name / *Name*, Anschrift / *Address*, ggf. Matr.-Nr. / *student ID no., if applicable*)

versichere an Eides Statt durch meine Unterschrift, dass ich die vorliegende Dissertation selbständig und ohne fremde Hilfe angefertigt und alle Stellen, die ich wörtlich dem Sinne nach aus Veröffentlichungen entnommen habe, als solche kenntlich gemacht habe, mich auch keiner anderen als der angegebenen Literatur oder sonstiger Hilfsmittel bedient habe und die zu Prüfungszwecken beigelegte elektronische Version (PDF) der Dissertation mit der abgegebenen gedruckten Version identisch ist. / *With my signature I affirm in lieu of an oath that I prepared the submitted dissertation independently and without illicit assistance from third parties, that I appropriately referenced any text or content from other sources, that I used only literature and resources listed in the dissertation, and that the electronic (PDF) and printed versions of the dissertation are identical.*

Ich versichere an Eides Statt, dass ich die vorgenannten Angaben nach bestem Wissen und Gewissen gemacht habe und dass die Angaben der Wahrheit entsprechen und ich nichts verschwiegen habe. / *I affirm in lieu of an oath that the information provided herein to the best of my knowledge is true and complete.*

Die Strafbarkeit einer falschen eidesstattlichen Versicherung ist mir bekannt, namentlich die Strafandrohung gemäß § 156 StGB bis zu drei Jahren Freiheitsstrafe oder Geldstrafe bei vorsätzlicher Begehung der Tat bzw. gemäß § 161 Abs. 1 StGB bis zu einem Jahr Freiheitsstrafe oder Geldstrafe bei fahrlässiger Begehung. / *I am aware that a false affidavit is a criminal offence which is punishable by law in accordance with § 156 of the German Criminal Code (StGB) with up to three years imprisonment or a fine in case of intention, or in accordance with § 161 (1) of the German Criminal Code with up to one year imprisonment or a fine in case of negligence.*

_____   _____

Ort / *Place*, Datum / *Date*   Unterschrift / *Signature*

Abstract

The preservation of terrestrial organic carbon (OC) in marine sediments is a crucial component of global carbon cycle on geological timescale. Characterizing the origins and compositions of the terrestrial OC is critical for understanding the fate of terrestrial OC in marine sediments and constraining the terrestrial OC cycling. The amount of terrestrial OC discharged by the Amazon River to the Atlantic Ocean every year is about 8-10 % of the global annual input of terrestrial OC to oceans. Therefore, the terrestrial OC in the Amazon system has been extensively investigated. However, until now, many aspects regarding the origin and fate of terrestrial OC in the Amazon system are still ambiguous and need to be elucidated. Firstly, little is known about the disperse pattern of lignin (a major component of higher plants biomass and can serve as a biomarker of terrestrial OC) and the factors controlling the characteristics of terrestrial OC in the Amazon continental margin. Secondly, it is questionable whether the Amazon continental margin can efficiently store terrestrial OC or serve as a sedimentary OC incinerator. Thirdly, the response of vegetation to climate change during late Pleistocene is debated. To fill these knowledge gaps, lignin and its isotope compositions (^{13}C and ^{14}C) are used as the major tools to provide a better understanding of the origins, pattern of distribution, processing, composition and fate of terrestrial OC in the Amazon system.

In the first part, the biogeochemical characteristics of terrestrial OC in the fluvial sediments from the Amazon drainage basin and in the adjacent marine sediments are compared. Total organic carbon (TOC) and lignin content exhibit positive correlations with aluminium to silicon ratios (Al/Si, indicative of the sediment grain size) implying that the grain size of sediment discharged by the Amazon River plays an important role in the preservation of TOC and leads to preferential preservation of lignin phenols in fine particles. Low δ^{13}C values of bulk OC in the main tributaries consistently correspond with the dominance of C3 vegetation. Compositions of lignin, syringyl to vanillyl (S/V) and cinnamyl to vanillyl (C/V), suggest that non-woody angiosperm tissues are the dominant source of lignin in the Amazon basin. Although the Amazon basin hosts a rich diversity of vascular plant types, distinct regional lignin compositions are not observed. In the marine sediments, the distribution of δ^{13}C values of bulk OC and lignin contents implies that terrestrial OC discharged by the Amazon River is transported north-westward by the North Brazil Current and mostly deposited on the inner shelf. The lignin compositions in offshore sediments under the influence of the Amazon plume are consistent with the riverbed samples suggesting that processing of terrestrial OC during offshore transport does not change the encoded source information. Therefore, the lignin compositions preserved in these offshore sediments can reliably reflect the vegetation in the Amazon River catchment. In sediments from the Amazon Fan, low lignin content, relatively low δ^{13}C values of bulk OC and high degradation degree of lignin demonstrate that a significant fraction of the deposited terrestrial OC is derived from petrogenic (sourced from ancient rocks) sources.

In the second part, a new method of assessing procedural blank for compound-specific ^{14}C analysis is developed with a Bayesian model. This method is successfully used in the third part of this thesis, which is about radiocarbon dating of source-specific biomarkers (*n*-alkanoic acids and lignin phenols) in riverbed sediments from the lowland Amazon basin and offshore sediments. The results show that Δ^{14}C values of terrestrial OC on the Amazon continental margin are substantially influenced by matrix association effects, where terrestrial OC associated with the finer-grained particles is better preserved and more resistant to decomposition during residence in intermediate reservoirs. The compound-specific Δ^{14}C values imply that as expected short-chain *n*-alkanoic acids represent recently biosynthesized organic matter from riverine or marine primary production whereas both long-chain *n*-alkanoic acids and lignin phenols used as markers for land vegetation have pre-aged in soils where they resided attached to mineral surfaces. By using a ternary mixing model, a well-constrained quantitative estimate of the composition of sedimentary OC in riverbed and marine sediments is obtained. Despite the variable composition of sedimentary OC in the Amazon system, the burial of fossil rock-derived OC is relatively constant. Based on the absolute content of bulk terrestrial OC, lignin, and long-chain *n*-alkanoic acids and their ^{14}C ages, half-lives of bulk terrestrial OC, lignin and long-chain *n*-alkanoic acids during transport are estimated to be about 2310 years, 13860 and 470 years, respectively. This suggests that the preservation of terrestrial OC in the mud belt on the Amazon shelf is more efficient than previously assumed.

In the fourth part, the δ^{13}C analysis of lignin phenols are applied in marine surface sediments from the Amazon shelf and sediment core GeoB16224-1 recovered from the continental margin NW of the Amazon mouth. The weighted average δ^{13}C values of lignin indicate that the modern terrestrial OC on the Amazon shelf is dominated by C3 plants and the vegetation source remained constant over the past 12.8-50 kyr, in agreement with previous studies. A general pattern of phenolic δ^{13}C values is observed with the acid monomers of V and S phenols displaying lower δ^{13}C values than their aldehyde counterparts, while C phenols are always more enriched in ^{13}C than V and S phenols. The lignin content and composition paired with δ^{13}C of lignin are used to reconstruct the characteristics of terrestrial OC deposited on the continental margin NW of the Amazon mouth over the period 12.8-50 kyr. Lignin composition, δ^{13}C values of lignin, BIT index, δ^{13}C and δD values plant-wax lipids show clear in-phase variation. Therefore, it can be proposed that next to vegetation change, the variation of δ^{13}C values of lignin and plant-wax lipids during HS could reflect either enhanced discharge of more degraded terrestrial OC and/or more contributions of terrestrial from high altitude regions. These two possible scenarios suggest that the Amazon basin was still a stable ecological system dominated by C3 forest and the increases of δ^{13}C values of lignin and plant-wax lipids were actually the consequence of changes of sources of terrestrial OC through the late Pleistocene.

Kurzfassung

Die Erhaltung von terrestrischem organischen Kohlenstoff (OC, engl.: organic carbon) in ma-rinen Sedimenten stellt über geologische Zeiträume eine wichtige Komponente im globalen Kohlenstoffkreislauf dar. Um den Verbleib von terrestrischem OC in marinen Sedimenten zu verstehen, sind die Charakterisierung der Quellen und der Zusammensetzung des terrestri-schen OC entscheidend und bilden einen wichtigen Grundbaustein zum Verständnis des Kreislaufs von terrestrischem OC. Die Menge an terrestrischem OC, die jährlich mit der Sedi-mentfracht des Amazonas in den Atlantik eingetragen wird, beträgt 8-10% der globalen Zu-fuhr in die Ozeane. Aus diesem Grund ist die organische Sedimentfracht des Amazonas inten-siv in wissenschaftlichen Studien untersucht worden. Dennoch sind bis heute zahlreiche As-pekte bezüglich der Herkunft und des Verbleibs von terrestrischem OC im Amazonas Fluss-system und den angrenzenden marinen Sedimenten noch immer nicht eindeutig verstanden und bedürfen weiterer Forschung. Erstens ist über das Verteilungs-verhalten von Lignin (einer wichtigen organischen Verbindung terrestrischer Pflanzen und signifikanter Teil des terrestri-schen OCs in Flusssystemen) am Kontinentalhang und der zugrundeliegenden Prozesse wenig bekannt. Zweitens ist es fraglich, ob der Kontinentalhang vorm Amazonas effizient terrestri-schen OC erhalten und lagern kann oder, ob der OC primär abgebaut, bzw. remineralisiert wird. Drittens ist bisher nicht vollständig geklärt, wie die Vegetation im Amazonasbecken auf pleistozäne Klimaschwankungen reagiert hat. Um diese Wissenslücken zu füllen, werden in dieser Dissertation Lignin-Phenole und deren isotopische Zusammensetzung (^{13}C, ^{14}C) als In-dikatoren für Ursprung, Verteilungsmuster und Zusammensetzung des terrestrischen OC im Amazonassystem angewandt. Dies soll einen Beitrag leisten, die sedimentologischen, hydro-logischen und biogeochemischen Prozesse, denen der terrestrische OC im System ausgesetzt ist, besser zu verstehen.

Im ersten Teil der Arbeit werden die biogeochemischen Charakteristika des terrestrischen OC in fluviatilen Sedimenten aus dem Einzugsgebiet des Amazonas mit denen aus marinen Sedi-menten im Flussmündungsbereich verglichen. Die Gesamtgehalte organischen Kohlenstoffs (TOC, engl.: total organic carbon) und Ligningehalte sind positiv mit Alumini-um/Silicium Verhältnissen (Al/Si; ein Anzeiger für Korngrößen im Sediment) korreliert. Das impliziert, dass die Korngrößenverteilung der Sedimentfracht des Amazonas eine wichtige Rolle für die Erhaltung von TOC spielt und zur bevorzugten Erhaltung einzelner Lignin-Phenole in der Feinfraktion führt. Niedrige δ^{13}C-Werte des organischen Kohlenstoffs ($\delta^{13}C_{bulk}$) aus den Hauptarmen des Flusses reflektieren die Dominanz von C3-Pflanzen im Einzugsgebiet. Die Zusammensetzung von Lignin, (d.h. Syringyl/Vanillyl (S/V) und Cinnamyl/Vanillyl (C/V) Verhältnisse) suggerieren, dass holzfreie Angiospermen die dominierende Quelle für Lignin im Amazonasbecken sind. Obwohl vaskuläre Pflanzen im Einzugsgebiet des Flusssystems eine hohe Diversität aufweisen, zeigen die Daten aus den verschiedenen Flussarmen keine regionalen Unterschiede in der Ligninzusammensetzung. In den marinen Sedimenten impli-zieren die

Ligningehalte und die Verteilung der $\delta^{13}C_{bulk}$-Werte, dass der terrestrische OC aus der Amazonasfracht durch den Nordbrasilien-Strom nordwestlich transportiert und hauptsäch-lich auf dem inneren Schelf abgelagert wird. Die Ligninzusammensetzung in Offshore-Sedi-menten, welche unter dem Einfluss der Amazonassediment-fracht stehen, entspricht der Zu-sammensetzung in den Flussbettproben. Dies zeigt, dass sedimentologische und biogeochemi-sche Prozesse während des Transports die ursprünglichen Informationen bezüglich der Quel-len, die in der Phenolverteilung enthalten sind, nicht verändern. Daher kann die Ligninzu-sammensetzung in den marinen Sedimenten als verlässlicher Indikator für die Vegetationszu-sammensetzung im Amazonasbecken herangezogen werden. In den Sedimenten des Amazo-nas-Sedimentfächers, zeigen niedrige Ligningehalte zusammen mit relativ geringen $\delta^{13}C_{bulk}$-Werten und hohen Degradationsgraden von Lignin, dass eine signifikante Fraktion des abge-lagerten terrestrischen OC petrogen ist.

Im zweiten Teil der Arbeit wird eine neue Methode zur Bestimmung des Blindwertes in der komponenten-spezifischen ^{14}C Analyse mit Hilfe bayesscher Statistik entwickelt. Dieser An-satz wird im dritten Teil der Dissertation benötigt, um komponentenspezifische ^{14}C-Datie-rungen an Pflanzenbiomarkern (*n*-Alkansäuren und Lignin-Phenole), die an Flussbettsedimen-ten des Flachlandes und an offshore Sedimenten durchgeführt werden, für den Blindwert zu korrigieren. Die Ergebnisse der komponentenspezifischen Datierung zeigen, dass $\Delta^{14}C$-Werte von terrestrischem OC substanziell von matrixgebundenen Effekten beeinflusst werden. So wird an der Feinfraktion anhaftender terrestrischer OC generell besser erhalten. Die Flussbett-sedimente zeigen, dass terrestrischer OC während seiner Residenzzeit in intermediären Reser-voiren resistenter gegenüber Abbauprozessen ist. Die komponentenspezifischen $\Delta^{14}C$-Werte implizieren, dass kurzkettige *n*-Alkansäuren rezent biosynthetisiertes organisches Material aus fluviatiler oder mariner Primärproduktion repräsentieren. Die beiden Vegetationsbiomarker, langkettige *n*-Alkansäuren und Lignin-Phenole, sind dagegen vorgealtert, was auf Anhaften der Komponenten an Mineraloberflächen in Böden und der daraus resultierenden zwischen-zeitlichen Lagerung zurückzuführen ist. Mit Hilfe eines ternären Mischungsmodells kann eine quantitative Abschätzung der Zusammensetzung des sedimentären OC in Flussbettsedimenten und marinen Sedimenten gemacht werden. Trotz der variablen Zusammensetzung des sedi-mentären Materials im Amazonassystem, ist die Ablagerung von fossilem, petrogenem Mate-rial relativ konstant. Um die Halbwertszeiten für den exponentiellen Abbau von terrestri-schem OC, Lignin und langkettigen *n*-Alkansäuren im Amazonas-system zu berechnen, wer-den die Gesamtgehalte der drei Komponenten und deren ^{14}C-Alter herangezogen. Die Halb-wertszeiten können auf 2310, 13860 und 470 Jahre eingegrenzt werden. Diese Ergebnisse zei-gen, dass die Erhaltung von terrestrischem OC im Schlammgürtel des Amazonasschelfs effi-zienter ist, als in vorherigen Studien angenommen.

Im vierten Teil der Dissertation werden $\delta^{13}C$-Analysen von Lignin-Phenolen sowohl in Ober-flächensedimenten vom Schelf als auch in einem marinen Sedimentkern vom Kontinental-hang

südwestlich der Amazonasmündung gemessen. Der gewichtete Mittelwert der δ^{13}C-Werte aus den Schelfsedimenten zeigt, dass C3-Pflanzen die dominante Quelle des terrestri-schen OCs im heutigen System darstellen. Generell haben die Säuremonomere der V- und S-Phenole niedrigere δ^{13}C-Werte als ihre jeweiligen Aldehyd-Äquivalente. Dagegen sind C-Phenole grundsätzlich stärker an ^{13}C angereichert, als V- und S- Phenole. Der Ligningehalt und die -zusammensetzung werden mit den ^{13}C-Werten von Lignin kombiniert, um die Eigen-schaften des terrestrischen OCs im Zeitraum zwischen 12,8-50 ka BP zu rekonstruieren. Die Ergebnisse zeigen, dass die dominante Quelle des terrestrischen OCs auch zwischen 12,8-50 ka BP konstant aus C3-Pflanzen bestanden hat, was mit früheren Studien übereinstimmt. Die Variationen in der Lignin-Zusammensetzung, den δ^{13}C-Werte von Lignin, im BIT-index (engl.: Branched and Isoprenoid Tetraether index) und in den δ^{13}C und δD-Werten von Pflan-zenwachslipiden sind in Phase und zeigen Veränderungen im terrestrischen OC während der Heinrich Stadiale (HS). Diese Schwankungen deuten entweder auf vermehrten Transport von relativ stark degradiertem terrestrischen OC oder/und auf verstärkten Eintrag von terrestri-schem OC aus größeren Höhenlagen. Aus den Daten lässt sich insgesamt ableiten, dass das Amazonasbecken ein stabiles ökologisches System gewesen ist, dessen Vegetation primär aus C3-Pflanzenwäldern bestanden hat. Die Variabilität in den δ^{13}C-Werten von Lignin und den Pflanzenwachslipiden im späten Pleistozän resultieren primär aus Quellenverschiebungen des terrestrischen OCs während der HS.

Table of contents

1. Introduction

1.1. The importance of terrestrial organic carbon

Terrestrial organic carbon (OC) includes large amounts of carbon stored in various continental reservoirs, such as plants, soils, fluvial sediments, and sedimentary rocks. Compared to the carbon in atmospheric CO_2, the amount of terrestrial OC is greatly larger (Galy and Eglinton, 2011). Over geological timescales, the exchange of carbon between the continental and atmospheric reservoirs can cause variations of the atmospheric CO_2 concentration (Galy and Eglinton, 2011), which may affect the climate change. Globally, rivers transport about 200 Tg particulate OC from continental reservoirs to the ocean each year (Galy et al., 2007; Ludwig et al., 1996; Schlünz and Schneider, 2000; Galy et al., 2015). The accumulation of the river-delivered terrestrial OC in modern marine sediments occurs mostly at continental margins, despite that continental margins occupy only around 10 % of ocean surface area (Hedges and Keil, 1995). Terrestrial OC deposited in the continental margins records valuable information with regard to environmental conditions in the continents, which can be used to reconstruct paleo-environmental conditions and provide knowledge about processes and fate on terrestrial OC (Galy et al., 2011; Hedges, et al., 1997). Therefore, terrestrial OC buried in the marine sediments is a crucial component of global carbon cycle and plays an important role in controlling atmospheric gases, e.g., CO_2 and CH_4 and regulating the global climate over geological time scales (Drenzek et al., 2009). Quantitative knowledge of processing and fate of terrestrial OC is fundamental for understanding the dynamic state of terrestrial OC in global carbon cycle and comprehending the response and influence of terrestrial OC on climate change (Bloom et al., 2015).

Although many studies have been conducted on different aspects about terrestrial OC in marine sediments (Bianchi, 2011; Hedges et al., 1997; Keil et al., 1997; Schmidt et al., 2010; Tesi et al., 2014), it is currently still the least constrained component of the global carbon cycle (Bloom et al., 2015). For example, the missing carbon mystery has not been resolved that the burial of terrestrial OC in the continental margins account for less than 50 % of terrestrial OC exported by rivers to the ocean suggesting a substantial loss of a large fraction of terrestrial OC in the marine sediments (Hedges and Keil, 1995; Hedges et al., 1997; Bianchi, 2011). The difficulty in constraining the processing and fate of terrestrial OC in the marine sediments relies in many aspects, such as the complicate compositions of terrestrial OC, complexities of sedimentological regimes and geochemical process of accumulation (Schmidt et al., 2010). Terrestrial OC contains components from different provenances, with different stabilities, at various stages of degradation and having different pre-depositional histories. Different compositions of terrestrial OC might exhibit variant behaviour under the same environmental conditions, e.g., differential decomposition rates and reactivities to diagenetic processes (Blair and Aller, 2012). When terrestrial OC is composed mainly of compounds with simple structures and readily available for

degradation, it has fast turnover times (days to years). If terrestrial OC is dominated by fractions with complex structures and refractory to degradation, it has long turnover times of decades to millenniums or even longer. The composition of terrestrial OC can therefore to some extent define the fate of terrestrial OC in marine sediments (Burdige, 2005). During the transport and preservation, terrestrial OC is subjected to complex interplay of many physical and biological processes, e.g., sediment accumulation, association with mineral surfaces, oxygen exposure time, and chemical and biological alteration. These processes have large influence on the preservation of terrestrial OC in marine sediments. For instance, previous studies have suggested that association with mineral surfaces protects terrestrial OC from remineralization (Mayer, 1994; Hedges and Keil, 1995), high sediment accumulation rate and low oxygen availability can improve the preservation of terrestrial OC (Blair and Aller, 2012; Galy et al., 2007). The integrated effects of these processes can regulate the distribution and preservation of terrestrial OC in marine sediments. Thus, understanding of the mechanism in how these processes operate is vital for assessing the fate of terrestrial OC in marine sediments. The composition of terrestrial OC and the influential processes are in response to different environmental conditions at different settings, such as temperature, hydrology and topography, and during the last few thousands of years, are affected by human disturbance (i.e., land use) (Schuur et al., 2015).

Given that the current knowledge about processing and fate of terrestrial OC in marine sediments remains incomplete, exhaustive studies with various geochemical indicators are needed to provide a comprehensive understanding of diverse factors controlling the fate of terrestrial OC in marine sediments from different regions. This is important for deciphering the role of terrestrial OC for global carbon cycle (Zonneveld et al., 2009).

1.2. General introduction of the Amazon system

The Amazon River originates from the Ucayali River and the Marañón River in the Andean region in southwestern Peru (Goulding et al., 2003). The Amazon River is the largest river in terms of water discharge as it supplies estimated 15-20 % of the freshwater river flow on Earth. (Meybeck, 1982; Richey et al., 1986). The Amazon River mainstream receives about 1000 tributaries draining vast and heterogenous regions of the northern South America (Salati and Vose, 1984), which integrate the largest drainage basin in the world, the Amazon basin (Fig. 1.1). The Amazon basin covers a continental-scale region of about $6.1 \times 10^6 \, km^2$ (Guyot et al., 2007). It borders the Andes mountain range to the west and southwest, extends to the Guiana shield in the north, and to the Brazilian shield in the southern and eastern parts (Cordani and Sato, 1999) (Fig. 1.1). As the tributaries of the Amazon River drain such a large basin with various environments, they inevitably present different characteristics. They can be generally classified into three types according to their colours, which are white water rivers, black water rivers and clear water rivers. The Solimões River and the Madeira River are the typical white water rivers. Because they originate from the mountain environment (Peruvian and Bolivian Andean region)

and drain steep slope and intense weather areas (Gibbs, 1967), they are characterized by high concentrations of dissolved nutrients and enriched in suspended sediments, which is responsible for the white colour. The Negro River is a typical black water river that drains almost exclusively lowland tropical environment and have high content of dissolved humic substances, from which its dark tea-colour comes. The clear water rivers, such as the Xingu River, are nearly devoid of suspended sediment loads and depleted in dissolved organic matter. Due to their water clarity, the clear water rivers are also characterized by high phytoplankton production (Junk, 1997; Richey et al., 1990).

Figure 1.1. A general map of the Amazon system showing the sources and major tributaries of the Amazon River, the Amazon basin, and offshore area. The range of the Amazon basin is indicated by the black line. The Amazon-Guianas mud belt is marked by dark blue dots and the Amazon Fan is indicated by dashed fan-shaped sector. The colour bar shows altitudes.

The rainfall over the Amazon basin varies spatially with high annual rainfall in the north-western part but relatively lower rainfall in southern and eastern parts (Sombroek, 2001). In total, the Amazon basin receives a mean annual rainfall of about 2500 mm year^{-1}, which leads to a water discharge of 2×10^5 m^{3}s^{-1} (Callede et al., 2000; Guyot et al., 2007). The vegetation and ecosystems in the Amazon basin are mainly dependent on the distribution pattern of rainfall. In wet non-flooded regions with higher rainfall, the predominant vegetation is the rainforest, which has diverse species of evergreen broad-leaf trees with closed canopy cover and has high tree density and biodiversity rates (Saatchi et al., 2000). The relatively drier regions, where there is a six-month dry season, are dominated by deciduous and/or

3

semideciduous vegetation that have smaller canopy and larger proportion of root biomass (Saatchi et al., 2000). The savannah prevails mainly in the south and south-eastern part of the Amazon basin due to both dry climatic conditions and deforestation (Houghton et al., 2001).

The other important component of the Amazon system is the Amazon offshore region including the Amazon shelf and fan, which is the important sink of the Amazon River discharge (Fig.1.1). The Amazon shelf is an energetic regime and involves several physical processes such as tides, waves, and along-shore North Brazil Current (NBC), etc. These processes act in concert to control the dispersion of the Amazon-derived plume of water and suspended sediment. Once entering the ocean, the sediment-charged Amazon plume is advected northwestwards along the northern South American coastline. The suspended sediments move progressively and form highly turbid mud belt dispersal system, which extends 1600 km along the Amazon-Guianas coast (Geyer et al., 1996; Nittrouer and DeMaster, 1996). The Amazon Fan is one of the largest submarine fans in the world covering about 3.3×10^5 km^2 (Damuth and Kumar, 1975). It is located off the northern coast of Brazil (approximately 322 km from the mouth of the Amazon River) and extends 700 km down slope from the shelf break reaching a maximum width of about 650 km (Damuth and Kumar, 1984). In contrast to interglacial periods with high sea levels like today, the Amazon Fan receives most of the sediment loads derived from the Amazon River during glacial periods with low sea levels such as the Last Glacial Maximum (Schlünz et al., 1999). Generally, the function of the Amazon Fan as the receiver of Amazon River-derived discharge is interrupted by the glacial-interglacial sea level variation.

1.3. Scientific background of terrestrial OC in the Amazon system

The estimated average annual discharge of terrestrial OC by the Amazon River to the Atlantic Ocean is 40 Tg C, which accounts for around 8-10 % of the global annual amount of terrestrial OC transported into oceans by rivers (Moreira-Turcq et al., 2003; Spitzy and Ittekkot, 1991). Therefore, the Amazon system is a critical component of the global carbon cycling in source-to-sink sedimentary system. The sources, transportation and fate of terrestrial particulate OC in the Amazon system is of particular interest and important for disentangling terrestrial OC dynamics (Blair and Aller, 2012).

The characteristics of terrestrial OC in the Amazon system have been extensively investigated with various biomarkers and parameters of bulk OC. It has been found that organic matter (OM) transported by the Amazon River is mainly sourced from the lowland Amazon basin, whereas the suspended sediments are predominantly derived from the Andes (Meade et al., 1985; Bouchez et al., 2014). Most of the OM is transported associated with mineral particles along the Amazon River mainstream and grain size plays a crucial role in regulating the composition of terrestrial OM in the Amazon system (Hedges et al., 1986; Bouchez et al., 2010). For instance, the content of OC is higher in coarse particulate OM (CPOM, >63 μm) than in fine particulate OM (FPOM, 0.1-63 μm). The degradation degree of CPOM is lower than that of FPOM, and dissolved OM (DOM, <0.1 μm) shows the highest

degradation degree (Hedges et al., 1986). Within the same size fraction (CPOM or FPOM), the composition of OM in the Amazon system is nearly constant along the downstream transport (Hedges et al., 1986). However, this implication was challenged by the observed fast alteration of the OC, evidenced by lignin signatures, from the lower reach of the Amazon River to the mouth (Ward et al., 2015). This apparent anomaly highlights the necessity of improving our knowledge about the processing of terrestrial particulate OC during the transport in the Amazon system. The stable carbon isotopic compositions (δ^{13}C) of bulk OC in the Amazon basin revealed that terrestrial OM in the Amazon system is mainly sourced from C3 plants with only a small contribution of C4 plants (Hedges et al., 1986; Bouchez et al., 2010). This has been corroborated by compound-specific δ^{13}C analyissis of long-chain n-alkanes in the Amazon system (Häggi et al., 2016). The distribution of crenarchaeol and branched glycerol dialkyl glycerol tetraethers (GDGTs) in the riverine suspended sediments from the Amazon basin also indicated a mixture source of C3 plant-derived soil OC and aquatic-derived OC (Kim et al., 2012). The source and transport of OC in the Amazon basin have been constrained with radiocarbon analysis (Δ^{14}C) of bulk OC, which reflected that rock-derived OC is a significant component and contributes a constant proportion of the POC in the Amazon basin (Bouchez et al., 2010, 2011).

In the Amazon offshore area, the distribution of δ^{13}C of bulk OC and terrigenous biomarkers have been successfully used to trace the transport and fate of terrestrial OC (Aller and Blair, 2006; Feng et al., 2016; Häggi et al., 2016; Schlünz et al., 1999; Williams et al., 2015; Zell et al., 2014). Increasingly higher δ^{13}C values of bulk OC along the coast towards northwest support the hypothesis that terrestrial OC from the Amazon River is advected northwestwards with Amazon-derived plume under the influence of NBC. The drastic decreases of OC loads along the Amazon-Guianas dispersal system indicated a net loss of terrestrial OC, which suggest the Amazon-Guianas is an effective incinerator of sedimentary OC (Aller and Blair, 2006). The rapid loss of terrestrial OC was explained by the energetic conditions in the Amazon-Guianas mud belt, where terrestrial OC experiences deposition-resuspension cycles leading to relatively long cumulative oxygen exposure time (Blair and Aller, 2012). It has been estimated that decay rate of terrestrial OC during the transport along the Amazon-Guianas mud belt is around 0.2 yr^{-1}, which suggests that most terrestrial OC is remineralized within a few years (Aller and Blair 2006). In contrast, ramped pyrolysis Δ^{14}C values of sedimentary OC revealed more efficient preservation of refractory terrestrial OC in the Amazon-Guianas mud belt (Williams et al., 2015). Thus, insightful constraints on the ages and components of terrestrial OC are required to better understand the processing and fate of terrestrial OC in the Amazon system. Apart from the characterization of terrestrial OC, isotopic compositions (δD and δ^{13}C) of terrigenous biomarkers have been used to reconstruct past vegetation and environmental conditions (Crivellari et al., 2017; Häggi et al., 2017; Kastner and Goñi, 2003). Both δ^{13}C of long-chain n-alkanes and lignin compositions suggested that the vegetation remains relatively stable and dominated by C3 plants during late Pleistocene (Häggi et al., 2017; Kastner and Goñi, 2003). These evidences from terrigenous biomarkers apparently question the 'refugia hypothesis'

that the expansion of savannahs during the LGM leads to contraction of the Amazon rainforest to isolated fragments. Therefore, multiple biogeochemical indicators are needed to reconstruct the response of vegetation and discharge of terrestrial OM to past climate variation.

1.4. Biomarkers and isotopic compositions

1.4.1. Lignin

Lignin is a major component of cell walls in vascular plants and is the second most abundant biopolymer after cellulose on Earth (Adler, 1977; Hedges et al., 1979a). It accounts for about 15-35 % of the dry biomass, depending on types of plants (Galbe and Zacchi, 2007), for example, 20-35 % in woody tissues and 15-20 % in grass tissues (Faravelli et al., 2010; Perez-Pimienta et al., 2013). Lignin is exclusively biosynthesized by vascular plants and can be found in various natural environments, such as soils and sediments. Compared to other biopolymers, lignin is more recalcitrant to microbial degradation and enzymatic actions (Killops and Killops, 2005). The transport of lignin from lands to oceans is mainly by rivers. Due to these natural characteristics, lignin can serve as a biomarker of terrestrial OC and the quality and quantity of lignin can provide important information on sources, pathways and sinks of terrestrial OC (Ingalls et al., 2010; Opsahl and Benner, 1995).
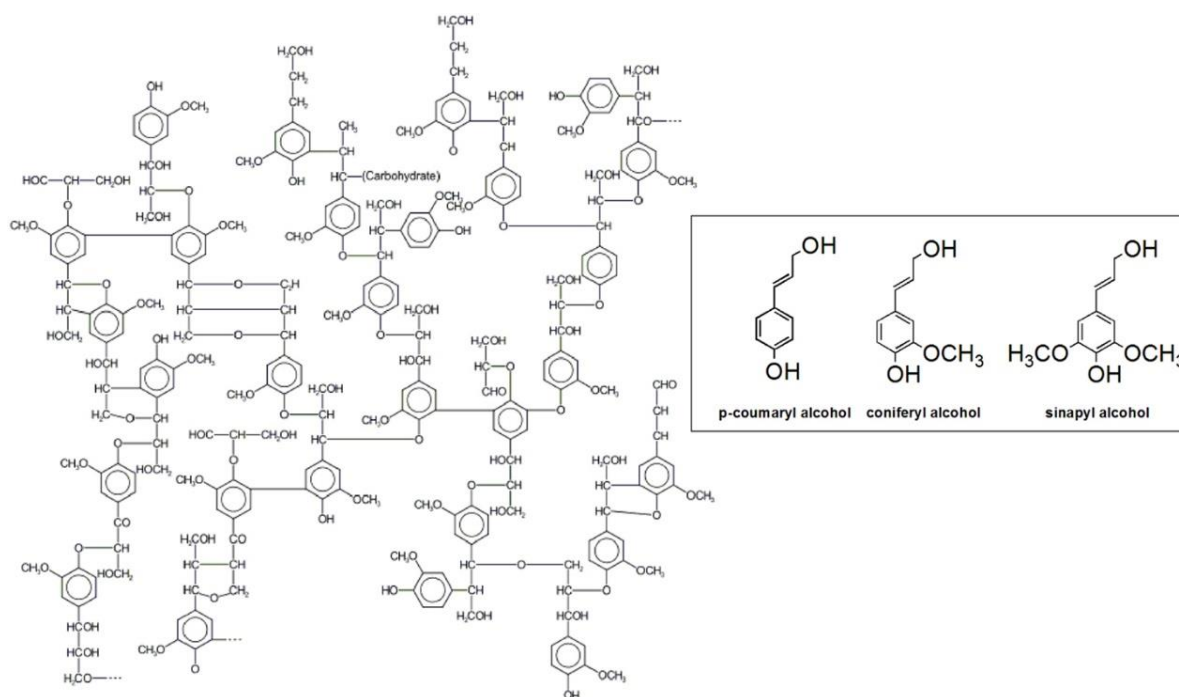
Figure 1.2. A random part of lignin polymer illustrating its schematic structure. The structural formulas of the three basic building blocks are shown in the rectangle (Christopher et al., 2014).

Lignin is mainly composed of phenylpropanoid units with different numbers of methoxyl group, which are linked together randomly by carbon-carbon and carbon-oxygen bonds (Adler, 1977, Karhunen et al., 1995) (Fig. 1.2). Three main phenylpropanoid units are *p*-coumaryl alcohol, coniferyl alcohol and sinapyl alcohol (Fig. 1.2). Therefore, lignin has high molecular weight and structural complexity, which

limits our ability to identify and quantify lignin polymers directly. Whereas, after oxidation with copper oxide (CuO), lignin polymers can produce several characteristic methoxylated phenols that can be analysed by gas chromatography. The most commonly used eleven phenolic monomers are shown in Fig. 1.3. According to their structure, these phenolic monomers can be divided into different groups (Fig. 1.3). The vanillyl phenols (V) include vanillin (Vl), acetovanillone (Vn), and vanillic acid (Vd). Syringyl phenols (S) include syringaldehyde (Sl), ancetosyringone (Sn), and syringic acid (Sd). Cinnamyl phenols (C) include p-coumaric acid (p-Cd) and ferulic acid (Fd). These eight phenolic monomers derive only from lignin. The para-hydroxybenzenes (P), which include *p*-hydroxybenzaldehyde (Pl), *p*-hydroxybenzophenone (Pn), and *p*-hydroxybenzoic acid (Pd), might also be yielded by non-lignin precursor, e.g., amino acid (Hedges et al., 1976). The compositions of these phenolic monomers vary in different plant types. Vanillyl phenols can be obtained in all vascular plants, but syringyl phenols exit only in angiosperms. Cinnamyl phenols are exclusively present in non-woody tissues of vascular plants. Hence, the C/V and S/V ratios can distinguish lignin between woody and nonwoody tissues of angiosperm and gymnosperms (Hedges and Mann, 1979a). Because microbial degradation of lignin increase the relative abundance of phenolic acids of V and S phenols, the ratios of vanillic acid to vanillin $(Ad/Al)_V$ and syringic acid to syringaldehyde $(Ad/Al)_S$ can indicate the degradation degree of lignin (Ertel and Hedges, 1984). The carbon- and sediment-normalized contents of the V, S, and C phenols ($\Lambda 8$, mg/100 mg OC and $\Sigma 8$, mg/10 g dry sediment) can reflect the content of lignin (Hedges and Mann, 1979b).
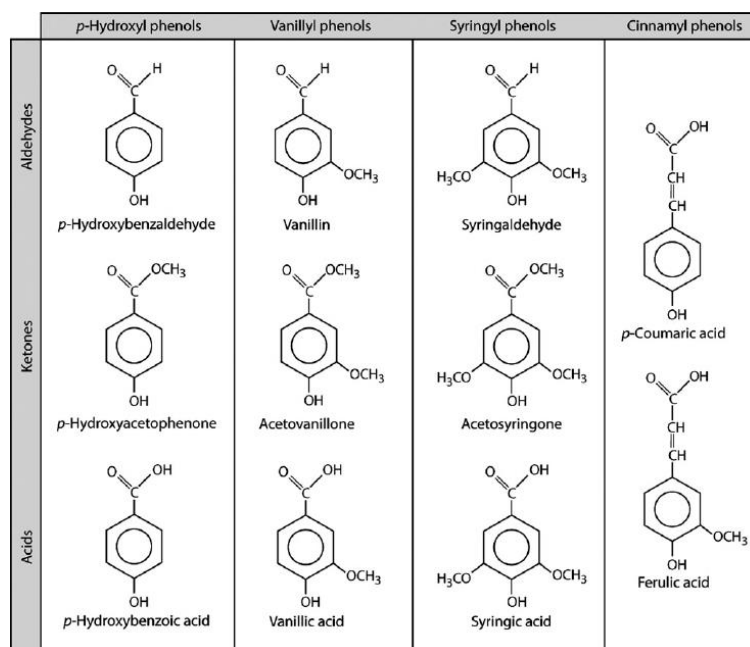

Figure 1.3. The structural formulas of eleven characteristic lignin phenolic monomers produced after the alkaline CuO oxidation (Thevenot et al., 2010).

1.4.2. *n*-alkanoic acids

Lipids are a class of source-specific compounds that have been extensively employed as biomarkers for terrigenous and planktonic OM in various environments (Eglinton and Eglinton, 2008; Meyers, 1997). The primary lipid compounds used in this thesis are long-chain and short-chain *n*-alkanoic acids. Long-chain *n*-alkanoic acids are the major constitutes of leaf-wax lipids that are uniquely from the waxy coatings of land plants. They have predominantly even carbon numbers (C_{24}-C_{36}). Because of the long chain structure, they are insoluble in water and have low volatility, which make them chemically stable and resist to biodegradation during long distance transport and after deposition in sediments. Therefore, long-chain *n*-alkanoic acids can function as a biomarker to detect variations in terrestrial inputs and preservation (Blair and Aller, 2012).

Short-chain (C_{16} and C_{18}) *n*-alkanoic acids also exist in all plants but only account for small proportion compared to their long-chain homologues. In contrast, short-chain *n*-alkanoic acids are dominantly produced by algae (Meyers, 1997). Thus, the short-chain *n*-alkanoic acids can serve as biomarkers for the aquatic produced OM. Compared to the long-chain homologues, short-chain *n*-alkanoic acids are labile and selectively decomposed. Thus, short-chain *n*-alkanoic acids can be used to reflect marine and terrestrial modern autochthonous OC inputs.

1.4.3. Branched and Isoprenoid Tetraether (BIT) index

The BIT index is a newly developed proxy based on the abundance ratio of branched glycerol dialkyl glycerol tetraether (GDGTs) to isoprenoid GDGTs (Hopmans et al., 2004). The structural formulas of branched and isoprenoid GDGTs are shown in Fig. 1.4. The branched GDGTs derive mainly from anaerobic or heterotrophic bacterial thriving in terrestrial environments such as peats and soils (Kim et al., 2006; Weijers et al., 2004, 2006a,b, 2010) and the isoprenoid GDGT 'crenarchaeol' is predominantly produced by marine planktonic Crenarchaeota (Sinninghe Damste et al., 2002). Because of their similar chemical structures, the branched and isoprenoid GDGTs have the same recalcitrance towards degradation (Kim et al., 2006). This makes the BIT index less subjected to diagenetic overprinting that can bias their source information (Kim et al., 2006). Therefore, the BIT index can be used to reflect contribution of soil OC in marine sediments (Sinninghe Damsté et al., 2002).
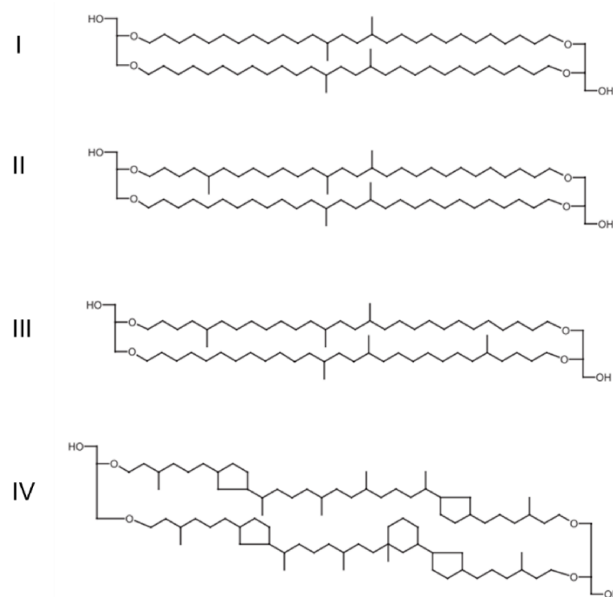
Figure 1.4. Structural formulas of branched GDGTs (I-III) and crenarchaeol (IV) (Zell et al., 2014).

The BIT index is calculated as BIT=([I]+[II]+[III])/([I]+[II]+[III]+[IV]). [I], [II], and [III] refer to the concentrations of branched GDGTs and [IV] refers to the concentration of the isoprenoid GDGT 'crenarchaeol' (Fig. 1.4) (Hopmans et al., 2004). According to the calculation, the BIT index varies between 0 and 1 with values close to 1 indicating a dominant proportion of terrestrial soil OC and values close to 0 suggesting limited contribution of terrestrial soil OC in the marine environments.

1.4.4. ^{13}C and ^{14}C compositions of bulk OC and biomarkers

The stable carbon isotopic composition (δ^{13}C value) can be used to distinguish the sources of OC in marine sediments, because marine and terrestrial plants biosynthesize OM by assimilating carbon from different sources with different pathways of carbon fixation (Meyers, 1997). The marine OM is produced by utilizing marine dissolved inorganic carbon so that the δ^{13}C values of marine OC are about -22 ‰ to -19 ‰ (Fontugne and Jouanneau, 1987). In contrast, the δ^{13}C values of OC of freshwater plankton range from -30 ‰ to -25 ‰ (Meyers, 1994). The OC biosynthesized by terrestrial vascular plants uptake atmospheric CO_2 using the C3 pathway has an average δ^{13}C value of around -27 ‰ with a full range of -32 ‰ to -20 ‰ (Mackie et al., 2005). While OC produced by C4 and CAM (Crassulacean Acid Metabolism) plants are characterized by a higher average δ^{13}C value of approximately -14 ‰ with the range of -15 ‰ to -12 ‰ (Meyers, 1997; Smith and Epstein, 1971; O'Leary, 1988). The 7 ‰ difference between δ^{13}C values of C3 plants-derived OC and marine OC allows identifying and quantifying terrestrial vs. marine contributions in marine sedimentary OC, if the terrestrial OC discharged to adjacent coasts are dominated by C3 plants. However, if the terrestrial OC receive substantial contribution from C4 plants, the δ^{13}C value of a mixture of C3 and C4 plants (e.g.,-20 ‰ with equal contribution from C3 and C4 plants) could mimic marine OC. This will invalidate the estimate of terrestrial OC using δ^{13}C value of sedimentary OC in marine sediments. This issue can be

9

circumvented by applying compound-specific $\delta^{13}C$ analysis of biomarkers of vascular plants. The $\delta^{13}C$ of lignin phenols are used in this thesis. Due to different synthesis pathways of various compounds during photosynthesis, the isotope compositions of major compounds are influenced by the isotope fractionation effect and exhibit different abundances in ^{13}C, e.g., the $\delta^{13}C$ values of lignin are slightly depleted in ^{13}C than the corresponding bulk OC. For example, $\delta^{13}C$ values of lignin from C3 plants show an average of about -30 ‰, while lignin from C4 plants have a higher average of around -17 ‰ (Goñi and Eglinton, 1996). The $\delta^{13}C$ values of lignin can be used to estimate C3 vs. C4 plants contributions to terrestrial OC, which can be further applied to assess terrestrial OC in marine sediments. The downcore record of $\delta^{13}C$ values of lignin can reveal the change of dominant vegetation type, which is helpful for reconstructing paleoclimate.

Radiocarbon (^{14}C) is a radioactive isotope that is used for determining the age of carbon (Ziokowski et al., 2009). ^{14}C compositions of bulk OC can indicate the residence time after the synthesis process of the OM stop, i.e., the death of an organism. ^{14}C compositions reveal additional information on the sources of OC that could not be obtained by $\delta^{13}C$ values. For example, ^{14}C compositions can distinguish freshly synthesized OC from pre-aged soil OC, although they have similar $\delta^{13}C$ values. Therefore, ^{14}C compositions of bulk OC is a powerful tool to constrain sources and turnover times of OC, which is important for understanding the pre-depositional history of OC (Marwick et al., 2015). Because bulk OC consists of a complex mixture of compounds from different sources and with different residence times and distinct fates, such as pre-aged terrestrial OC of vascular plant origin and relict OC (kerogen) inputs from erosion of sedimentary rocks. ^{14}C compositions on bulk OC level are not enough for characterizing the provenances and ages of the major components. Thus, ^{14}C compositions of source-specific compounds are needed to provide insights into turnover of the OC at molecular level. The compound-specific ^{14}C composition analyses of *n*-alkanoic acids and lignin were carried out in this thesis. As short-chain *n*-alkanoic acids derived mainly from aquatic production, their ^{14}C compositions can reflect the turnover of freshly produced OC pools. ^{14}C compositions of long-chain *n*-alkanoic acids and lignin can represent the cycling of pre-aged terrestrial OC as they are of vascular plant origin and might have undergone long-term turnover in soils before transport to oceans and deposition in sediments.

1.5. Objectives of this thesis

Although substantial research efforts have been made in investigating terrestrial particulate OC in the Amazon system, several issues are still unexplored and/or of debate as reviewed above. These issues include the following aspects:

I: Despite that lignin has been used to characterize terrestrial OC in the Amazon basin, little is known about the transport and distribution of lignin in the adjacent offshore region especially in the Amazon-Guianas mud belt sediments, where receives most of the terrestrial OC inputs. It is also unclear what

factors play critical role in controlling the transport, distribution and deposition of terrestrial OC in the Amazon system.

II: Up to now, the preservation of terrestrial OC in the Amazon system still debated, especially in the Amazon shelf area. Only few studies applied both ^{13}C and ^{14}C compositions of bulk OC to investigate the source and turnover of OC in the Amazon system. The compound-specific ^{14}C analysis of terrestrial OC biomarkers is needed to better constrain the major components of terrestrial OC and their specific residence time and fate in the Amazon system.

III: As a major biomarker of terrestrial vascular plants, the ^{13}C composition of lignin can provide new evidences to resolve the debate on whether the vegetation of the Amazon basin changed significantly during the late Pleistocene.

In order to address these problems, the major objectives of this thesis are

Objective 1: to investigate the origins and processing of terrestrial OC based on the δ^{13}C of bulk OC and content and composition of lignin in riverbed sediments of the Amazon basin and marine surface sediments on the Amazon shelf area;

Objective 2: to develop insights into the influence of grain size on the preservation and fates of terrestrial OC in the Amazon system;

Objective 3: to quantify contributions of OC from different pools and to reveal the pre-depositional histories of terrestrial OC;

Objective 4: to reconstruct the past vegetation change of the Amazon basin during the late Pleistocene.

1.6. Outline of the thesis

This thesis is composed of four manuscripts (chapter 2-5) aiming at achieving the raised objectives. These four manuscripts are either published, submitted, or in preparation for submission to international peer-reviewed journals. The first manuscript (chapter 2) (focused on objective 1 and 2) employed the content and composition of lignin to reflect the characteristics of terrestrial OC and the influence of grain size on lignin composition. In the second manuscript (chapter 3), a novel method of assessing procedural blank during compound-specific ^{14}C composition analysis was developed to prepare for accurate ^{14}C composition analyses of *n*-alkanoic acids and lignin. In the third manuscript (chapter 4, aiming at objective 2 and 3), a dual-carbon-isotope (^{13}C and ^{14}C) mixing model and compound-specific ^{14}C analyses of *n*-alkanoic acids and lignin were carried out to provide constraints on the origins of sedimentary OC and estimate the decay rate of terrestrial OC in the Amazon system. In the fourth manuscript (chapter 5, dealing with objective 4), compound-specific ^{13}C analysis of lignin was conducted to explore the vegetation change in the Amazon basin and the variation in discharge of

terrestrial OC from the Amazon basin to the offshore area. The major findings and conclusions of this thesis are summarized in the chapter 6.

1.7. Description of own contributions

All the samples used in this thesis were collected by André O. Sawakuchi, Cristiano M. Chiessi, Enno Schefuß, Paul A. Baker, and Stefan Mulitza. Enno Schefuß, Gesine Mollenhauer and I designed this study.

For the first manuscript, I prepared the marine surface sediments labelled with GeoB for δ^{13}C analysis of bulk OC. The preparation for δ^{13}C analysis of bulk OC of other samples are conducted by Stefanie Buchheister and measured by Monika Segl. The weight ratio of Al/Si was measured by Matthias Zabel. Grain size analysis was performed by Jürgen Titschack. The extraction and measurement of lignin were conducted by myself with technical support from Jens Hefter and Maria Winterfeld. I wrote the manuscript with comments and contributions from co-authors.

For the second manuscript, the idea of the method was drafted by Gesine Mollenhauer. Vera Meyer and I wrote the manuscript together with comments and contributions from co-authors. Vera Meyer and I contribute equally to this manuscript and share the first authorship. I prepared the extraction and purification of all the lignin standards and part of the n-alkanoic acids standards. Vera Meyer conducted the extraction and isolation of most of the other n-alkanoic acids standards. Maria Winterfeld and Wolf Dummann processed some n-alkanoic acids standards as well. The preparation of the standards was performed under supervision and help of Daniel Montluçon, Jens Hefter and Tessa van der Voort. The measurement of the F^{14}C values was conducted by Cameron McIntyre, Lukas Wacker, Negar Haghipour and Torben Gentz. Andrew Dolman provided the R and Stan code for the Bayesian model and performed the statistical analysis.

For the third manuscript, I wrote the manuscript with comments and contributions from co-authors. I extracted n-alkanoic acids and lignin, and purified individual compounds with preparative capillary gas chromatography (PCGC) and preparative high-performance liquid chromatography (prep-HPLC), and prepared the samples on vacuum line with help from Daniel Montluçon, Tessa van der Voort, and Jens Hefter. The F^{14}C values of n-alkanoic acids and lignin were measured by Negar Haghipour. The marine surface sediment samples for F^{14}C analysis of bulk OC were pre-treated and measured by Negar Haghipour.

For the fourth manuscript, the extraction of lignin was conducted by myself. The measurement of δ^{13}C values of lignin phenols were performed by myself under supervision of Enno Schefuß and Ralf Kreutz. The extraction of branched and isoprenoid GDGTs were conducted by Christoph Häggi and measured by Jens Hefter. I wrote the manuscript with comments and contributions from co-authors.

2. Manuscript I:

Origin and processing of terrestrial organic carbon in the Amazon system: lignin phenols in river, shelf, and fan sediments

Shuwen Sun[1,2,7], Enno Schefuß[2], Stefan Mulitza[2], Cristiano M. Chiessi[3], André O. Sawakuchi[4], Matthias Zabel[2], Paul A. Baker[5,6], Jens Hefter[7], Gesine Mollenhauer[1,2,7]

[1]Department of Geosciences, University of Bremen, Bremen, 28359, Germany

[2]MARUM-Center for Marine Environmental Sciences, University of Bremen, Bremen, 28359, Germany

[3]School of Arts, Sciences and Humanities, University of São Paulo, 03828-000 São Paulo, Brazil

[4]Institute of Geosciences, Department of Sedimentary and Environmental Geology, University of São Paulo, 05508-080 São Paulo, Brazil

[5]Duke University, Nicolas School of the Environment, 301 Old Chemistry, Box 90227, Durham, NC 27708, USA

[6]School of Geological Sciences and Engineering, Yachay Tech, Yachay City of Knowledge, 100650 Urcuqui, Ecuador

[7]Alfred Wegener Institute, Helmholtz Centre for Polar and Marine Research, Bremerhaven, 25570, Germany

Abstract. The Amazon River transports large amounts of terrestrial organic carbon (OC_{terr}) from the Andean and Amazon neotropical forests to the Atlantic Ocean. In order to compare the biogeochemical characteristics of OC_{terr} in the fluvial sediments from the Amazon drainage basin and in the adjacent marine sediments, we analysed riverbed sediments from the Amazon mainstream and its main tributaries as well as marine surface sediments from the Amazon shelf and fan for total organic carbon (TOC) content, organic carbon isotopic composition ($\delta^{13}C_{TOC}$), and lignin phenol compositions. TOC and lignin content exhibit positive correlations with Al/Si ratios (indicative of the sediment grain size) implying that the grain size of sediment discharged by the Amazon River plays an important role in the preservation of TOC and leads to preferential preservation of lignin phenols in fine particles. Depleted $\delta^{13}C_{TOC}$ values (-26.1 ‰ to -29.9 ‰) in the main tributaries consistently correspond with the dominance of C3 vegetation. Ratios of syringyl to vanillyl (S/V) and cinnamyl to vanillyl (C/V) lignin phenols suggest that non-woody angiosperm tissues are the dominant source of lignin in the Amazon basin. Although the Amazon basin hosts a rich diversity of vascular plant types, distinct regional lignin compositions are not observed. In the marine sediments, the distribution of $\delta^{13}C_{TOC}$ and $\Lambda 8$ (sum of eight lignin phenols in organic carbon (OC), expressed as mg/100mg OC) values implies that OC_{terr} discharged by the Amazon River is transported north-westward by the North Brazil Current and mostly

deposited on the inner shelf. The lignin compositions in offshore sediments under the influence of the Amazon plume are consistent with the riverbed samples suggesting that processing of OC_{terr} during offshore transport does not change the encoded source information. Therefore, the lignin compositions preserved in these offshore sediments can reliably reflect the vegetation in the Amazon River catchment. In sediments from the Amazon Fan, low lignin content, relatively depleted $\delta^{13}C_{TOC}$ values and high $(Ad/Al)_V$ ratios indicating highly degraded lignin imply that a significant fraction of the deposited OC_{terr} is derived from petrogenic (sourced from ancient rocks) sources.

2.1. Introduction

Rivers deliver annually about 200 Tg of particulate organic carbon (POC) to the oceans (Galy et al., 2007; Ludwig et al., 1996; Schlünz and Schneider, 2000; Galy et al., 2015), which is predominantly deposited on continental shelves and slopes (Hedges and Keil, 1995). Terrestrial organic carbon (OC_{terr}) buried in marine sediments has been intensely studied in order to reconstruct climate and environmental conditions on land (Bendle et al., 2010; Collins et al., 2014; Vogts et al., 2012) with rivers playing a role not only as conduits between terrestrial and marine reservoirs but also as efficient reactors of the OC_{terr} (Aufdenkampe et al., 2011; Battin et al., 2009). During transport in fluvial systems, OC_{terr} is subject to various natural processes, such as selective preservation within the watershed and microbial degradation, as well as anthropogenic processes associated to land-use change (Jung et al., 2015; Wang et al., 2015; Wu et al., 2007). In marine environments, OC_{terr} mixes with marine organic carbon and experiences further diagenetic alteration (Aller and Blair, 2006). The refractory fractions of OC_{terr}, which survive these processes, are preserved at sites of sediment deposition. As a result of this extensive processing, the climatic and environmental information recorded by OC_{terr} in marine sediments may be subject to temporal and spatial offsets. Hence, a comparison between the characteristics of OC_{terr} in drainage basins and adjacent continental margins is helpful to decipher which depositional sites can provide reliable marine sedimentary archives and to what extent they reflect climatic and environmental changes within the catchment.

The Amazon River is of special interest due to its large drainage basin size and discharge of OC_{terr} to the ocean. Previous studies that assessed the fate of OC_{terr} transported and discharged by the Amazon mainly relied on bulk organic parameters, isotope compositions of total organic carbon ($\delta^{13}C_{TOC}$ and $\Delta^{14}C_{TOC}$) (Bouchez et al., 2014) as well as on analyses of various biomarkers (e.g., lignin, plant-waxes and tetraether lipids) (Zell et al., 2014). Based on the correlation between TOC contents and Al/Si ratios, the latter being indicative of grain-size variations, Bouchez et al. (2014) showed a distinct mineral and size class association of particulate organic matter (POM), which in turn affects its transport in the fluvial system. Moreover, the $\delta^{13}C_{TOC}$ and $\Delta^{14}C_{TOC}$ of POM indicated that rock-derived POM accounts for a significant proportion of riverbed sediments. Hedges et al. (1986) reported lignin compositions of

typical plant tissues in the Amazon basin and found that POM has distinct lignin compositions in different grain size fractions.

Offshore the Amazon River mouth, the predominant depo-center of terrestrial organic matter has been shown to change between glacial and interglacial periods (Schlünz et al., 1999). During glacials (i.e., low sea-level), most of the Amazon derived OC_{terr} is deposited on the Amazon Fan, while during interglacials (i.e., high sea-level), along-shore currents result in deposition of OC_{terr} on the continental shelf northwest of the Amazon River mouth. Terrestrial climate and vegetation from the last glacial period has thus been reconstructed by analysing molecular biomarkers, such as lignin, plant-wax lipids, and branched glycerol dialkyl glycerol tetraethers (GDGTs) in sediment cores recovered from the Amazon Fan (Bendle et al., 2010; Boot et al., 2006; Goñi et al, 1997; Kastner and Goñi, 2003).

Lignin is a useful tracer for OC_{terr} because it is exclusively produced by vascular plants and accounts for about 20-30 % of dry biomass in woody plants (Zhu and Pan, 2010) and 15-20 % in grasses (Perez-Pimienta et al., 2013). It is relatively resistant to microbial degradation (Killops and Killops, 2005) and abundant in many environments (e.g. Kuzyk et al., 2008; Loh et al., 2012; Winterfeld et al., 2015). To date, little is known about the factors influencing lignin composition in the Amazon basin and adjacent marine sediments, its transport pathways in the Amazon continental margin, and the potential of lignin in offshore sedimentary archives to constrain sources and compositions of OC_{terr}.

Here we determined lignin contents and composition in riverbed sediments of the Amazon River and its lowland tributaries as well as in surface sediments of the Amazon shelf and slope. By doing so, we provide evidence on the spatial distribution of OC_{terr}, its plant sources, its origin within the catchment, and its dispersal patterns on the Amazon continental margin.

2.2. Study area

The Amazon River originates from the confluence of the Ucayali and Marañon Rivers in the Andean region in southwestern Peru and receives numerous tributaries that form the largest hydrographic basin in the world (Goulding et al., 2003). It covers an area of about $6.1 \times 10^6 \, km^2$ extending from the Guiana Highlands in the north to the Central Brazil Highlands in the south, and is bordered by the Andes mountain range in the west (Guyot et al., 2007). The Peruvian and Bolivian Andean tributaries Solimões (upper stretch of the Amazon River from its confluence with the Negro River) and Madeira are typical white water rivers. Because they drain the steep slope and rapidly weathering Andean region, they are characterized by high concentrations of suspended sediments and dissolved nutrients (Gibbs, 1967). The other major tributaries in the Amazon basin drain lowland regions and are classified as either black or clear water rivers. The black water rivers, such as the Negro River, are rich in dissolved humic substances derived from podzols and depleted in suspended sediments (Mounier et al., 1999). The clear water rivers (e.g., the Xingu River) have low concentrations of suspended sediments and dissolved

organic matter compared to the white and black water rivers, and their clarity allows high phytoplankton productivity (Junk, 1997; Richey et al., 1990). Although the deforested area of the Amazon basin is increasing significantly in the eastern and south-eastern portions, the remainder of the lowland Amazon basin is largely forested except for some small areas dominated by savannah (Houghton et al., 2001). Elsewhere, some grasses grow along the shoreline regions of white water rivers (Guyot et al., 2007; Hedges et al., 1986).

The Amazon basin annually receives an average of about 2500 mm rainfall and has the world's largest water discharge of about $2 \times 10^5 \, m^3 s^{-1}$ (Callede et al., 2000; Guyot et al., 2007). Up to 40 Tg of carbon are discharged along with $8\text{-}12 \times 10^{11}$ kg suspended sediment load each year by the Amazon River into the Atlantic Ocean, which makes the Amazon the largest fluvial source of OC_{terr} to the ocean (Dunne et al., 1998; Moreira-Turcq et al., 2003). The Amazon-derived plume of water and suspended sediment is advected northwestward along the northern South American coastline by the North Brazil Current, eventually forming the Amazon subaqueous delta-Guianas mud belt extending 1600 km along the northeastern coast of South America (Geyer et al., 1996; Nittrouer and DeMaster, 1996). The Amazon Fan is located off the northern coast of Brazil centered around 4 °N, extending 700 km from the shelf break seaward reaching a maximum width of about 650 km. The Amazon Fan is largely inactive today, but during past periods of low sea level such as the Last Glacial Maximum, large amount of suspended sediment and bed load were transported via submarine canyons and deposited on the Fan (Schlünz et al., 1999).

2.3. Materials and methods

2.3.1. Sample collection

Riverbed sediments were collected from the Amazon River mainstream and its main tributaries during two sampling campaigns in November 2011 and May 2012, corresponding respectively to the dry and wet seasons. Sediment samples were retrieved from sites with different channel depths to reflect their range of grain size variability. A Van Veen grab sampler was used for sampling, and the station locations are shown in Table 2.1 and Fig. 2.1A.
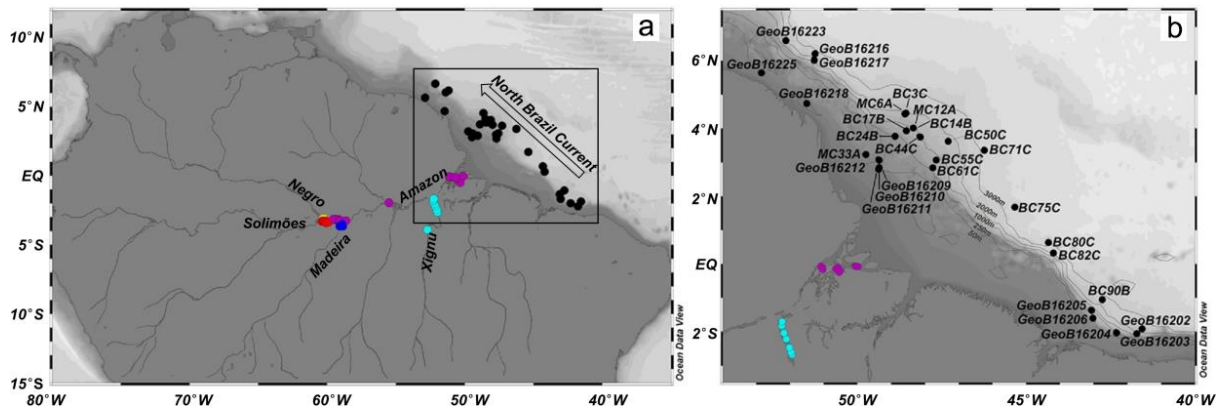
Figure 2.1. A) Map of the Amazon basin with the sample locations in individual tributaries and offshore area indicated by colored dots (red dots=Solimões, yellow dots=Negro, blue dots=Madeira, aqua dots=Xingu, violet dots=Amazon mainstream, black dots=offshore), the black rectangle indicates the area of map B and B) Map of the Amazon continental margin with the sample locations indicated by black dots. Maps were created using Ocean Data View 4.7.8 (Schlitzer, 2016).

Marine surface sediments from the Amazon shelf and fan were collected during two cruises (Table 2.2, Fig. 2.1B). The GeoB samples were recovered with a multicorer in February/March 2012 during the R/V Maria S. Merian cruise MSM 20/3, while the other marine surface sediments were taken in February/March 2010 with a box corer deployed from R/V Knorr during cruise KNR197-4. All samples were kept frozen at -20 °C before analysis and were subsampled into 1-cm intervals. The uppermost 2 cm of GeoB multicore samples and slices of 1 cm from intervals between 5 and 8 cm sediment depth of cores taken during cruise KNR197-4 were used in this study.

The GeoB surface sediments were oven dried at 50 °C, while the riverbed and the other marine surface sediments were freeze dried in a Christ Alpha 1-4 LD plus freeze dryer. After drying, all samples were homogenized for further analysis.

2.3.2. Grain size analysis

Grain size analysis was only conducted for marine sediments, because the riverbed sediment samples had already been ground before sub-sampling. For grain size measurement of the terrigenous fraction, bulk marine sediments were pre-treated as follows. Samples of about 0.5 g were successively boiled with H_2O_2 (35 %), HCl (10 %) and NaOH to remove respectively organic matter, carbonate and biogenic silica. To prevent potential aggregation, 10 ml of dissolved sodium pyrophosphate ($Na_4P_2O_7 \cdot 10H_2O$) was added immediately prior to grain size analysis. Samples were measured using a Laser Diffraction Particle Size Analyser (Beckman Coulter laser particle sizer LS-13320) in 116 size classes ranging from 0.04 to 2000 μm. All measurements were performed in demineralized and degassed water to avoid interference of gas bubbles.

2.3.3. Elemental and bulk isotopic analysis

About 4 g dry sediment was used to measure the Al and Si elemental concentrations by energy dispersive polarization X-ray fluorescence (EDP-XRF) spectroscopy. The device was operated with the software Spectro X-Lab Pro (Version 2.4) using the Turboquant method. Analytical quality of measurements was assessed by repeated analyses of the certified standard reference material MAG-1, and the standard deviation of replicate measurement of sediment samples was better than 0.5%.

After removal of carbonates with 12.5 % HCl and drying, the total organic carbon content (TOC) of all samples was determined by a LECO CS 200 CS-Analyzing System. The relative standard deviation of duplicate analyses was better than 1%.

Stable carbon isotopic ratios of TOC ($\delta^{13}C_{TOC}$) were analyzed on a Finnigan MAT Delta plus coupled with a CE elemental analyzer and a Con-Flo II interface. Samples were pre-treated by the same method as used for the TOC measurement. $\delta^{13}C_{TOC}$ values are reported using the standard notation relative to the Vienna Pee Dee Belemnite (VPDB) standard. The uncertainty was less than ±0.1‰, as calculated by long-term repeated analyses of the internal reference sediment (WST2).

2.3.4. Lignin-phenol analysis

Alkaline CuO oxidation was used to obtain eight lignin-derived phenols (vanillyl phenols, syringyl phenols and cinnamyl phenols) and three para-hydroxybenzenes. A CEM MARS5 microwave accelerated reaction system was used to perform alkaline CuO oxidation of lignin based on the approach described by Goñi and Montgomery (2000). Dried sediment samples (containing about 2-5 mg of TOC) were oxidized with CuO (500 mg) and ferrous ammonium sulfate (50 mg) in de-aerated 2 N NaOH at 150 °C for 90 min under a nitrogen atmosphere. After the oxidation, known amounts of recovery standards (ethyl vanillin and *trans*-cinnamic acid) were added to each reaction tube. The alkaline supernatant was transferred and acidified to pH 1 by addition of concentrated HCl. Reaction products were extracted twice with ethyl acetate and water in the ethyl acetate solution was removed by addition of Na_2SO_4. Ethyl acetate was evaporated under a continuous nitrogen flow. Once dry, 400 μl of pyridine was added immediately to re-dissolve the reaction products. Lignin phenols were analyzed by gas chromatography-mass spectrometry (GC-MS). Prior to the injection to the GC-MS, compounds in pyridine were derivatized with bis-trimethylsilyl-trifluoroacetamide (BSTFA) +1 % trimethylchlorosilane (TMCS) to silylate exchangeable hydrogen. Chromatographic separation was achieved by a 30 m×0.25 mm (i.d.) DB-1MS (0.25 μm film thickness) capillary GC column. The temperature program was 100 °C initial temperature, 4 °Cmin^{-1} ramp and 300 °C final temperature with a hold of 10 minutes.

The eight lignin-derived phenols obtained by alkaline CuO oxidation are subdivided into the following groups: the vanillyl (V) phenols include vanillin (Vl), acetovanillone (Vn), and vanillic acid (Vd);

syringyl (S) phenols are syringaldehyde (Sl), acetosyringone (Sn) and syringic acid (Sd); and cinnamyl (C) phenols consist of *p*-coumaric acid (*p*-Cd) and ferulic acid (Fd). The para-hydroxybenzenes include *p*-hydroxybenzaldehyde (Pl), *p*-hydroxybenzophenone (Pn) and *p*-hydroxybenzoic acid (Pd). The C phenols are only present in non-woody tissues of vascular plants while the S phenols are unique to angiosperms and V phenols exist in all vascular plants. Therefore, the ratios of S/V and C/V divide the plant sources of lignin into four types, non-woody and woody tissues of gymnosperms and angiosperms (Hedges and Mann., 1979a). $(Ad/Al)_V$ and $(Ad/Al)_S$ refers to the acid to aldehyde ratios of V and S phenols, which indicate the degradation of lignin (Ertel and Hedges, 1985).

The lignin phenols and identified compounds were quantified by individual response factors calculated from mixtures of commercially available standards analyzed periodically. The yields of Pl, Vl and Sl were calculated by the recovery rate of ethyl vanillin and the recovery rate of trans-cinnamic acid was applied for the yield estimation of other lignin-derived compounds (Kuzyk et al., 2008).

Carbon-and sediment-normalized lignin yields are respectively reported as $\Lambda 8$ (mg/100mg OC) and $\Sigma 8$ (mg/10g dry sediment). These measures indicate respectively the relative contributions of vascular plant material to the TOC, and to the total samples, and were respectively calculated as the sum of S, V and C phenols in 100 mg organic carbon and 10 g dried sample (Hedges and Mann, 1979b).

2.4. Results

2.4.1. Riverbed sediments

2.4.1.1. TOC and stable carbon isotopic composition

Part of the TOC and Al/Si data were previously published in Häggi et al. (2016). Riverbed sediments contain between 0.13 % and 3.99 % dry weight (wt) TOC (Table 2.1, Fig. 2.2A). Negro River and Xingu River sediments have similar TOC contents (0.53 %-3.99 %, mean=2.08±1.15 %, *n*=7 and 0.52 %-3.82 %, mean=2.44±1.37 %, *n*=8, respectively), which are higher than the TOC contents in other main tributaries. Consistently low TOC contents are observed in the Madeira River varying from 0.14 % to 0.52 % (mean=0.36±0.17 %, *n*=6). Solimões River sediments display TOC contents ranging from 0.28 % to 0.90 % with an average of 0.62±0.20 % (*n*=7). Amazon River mainstream sediments have intermediate TOC contents ranging from 0.13 % to 1.44 % (mean=0.73±0.36 %, *n*=19).

The range of $\delta^{13}C_{TOC}$ values of all riverbed samples is from -26.1 ‰ to -29.9 ‰ (Table 2.1, Fig. 2.2B). The most enriched (-26.1 ‰) and depleted (-29.9 ‰) $\delta^{13}C_{TOC}$ values are both observed in Solimões River sediments, which have an average value of -28.2±1.2 ‰ (*n*=6). A similar scatter of $\delta^{13}C_{TOC}$ values is obtained from sediments of the Negro River varying between -26.5 ‰ and -29.8 ‰ (mean=-28.7±1.3 ‰, *n*=7). In comparison, narrower ranges are found in the other tributaries and the Amazon River mainstream, with values ranging from -27.8 ‰ to -28.4 ‰ (mean=-28.0±0.3 ‰, *n*=3) for the

Madeira River, from -27.9 ‰ to -29.8 ‰ (mean=-29.2±0.8 ‰, n=8) for the Xingu River, and from -27.5 ‰ to -29.4 ‰ (mean=-28.2±0.5 ‰, n=15) for the Amazon River mainstream.

2.4.1.2. Lignin phenols

The Λ8 values in riverbed sediments vary from 0.73 mg/100mg OC in the Madeira River to 9.27 mg/100mg OC in the northern channel of the Amazon River mouth (Table 2.1, Fig. 2.2C). The highest average Λ8 of 4.92±1.44 mg/100mg OC (n=8) is observed in the Xingu River with values ranging between 3.30 and 6.91 mg/100mg OC. In contrast, Madeira River sediments display the lowest average Λ8 value of 2.61±1.30 mg/100mg OC (n=6; 0.73 to 4.42 mg/100mg OC). The Λ8 values of samples in the Negro River and the Solimões River vary respectively between 3.55 and 4.89 mg/100mg OC (mean=4.38±0.51 mg/100mg OC, n=7) and 3.49 and 6.44 mg/100mg OC (mean=4.59±0.96 mg/100mg OC, n=7). The Λ8 values of the mainstream sediments have the largest variability, from 0.75 to 9.27 mg/100mg OC (mean=4.88±1.93 mg/100mg OC, n=19).

Negro River and Xingu River sediments have higher Σ8 values and greater variability, ranging respectively from 1.89 to 19.52 mg/10g dry sediment (mean=9.50±5.90 mg/10g dry sediment, n=7) and from 2.73 to 17.97 mg/10g dry sediment (mean=11.18±5.93 mg/10g dry sediment, n=8). In contrast, the samples from the other tributaries and the Amazon mainstream display lower Σ8 values, 0.99-4.94 mg/10g dry sediment (mean=2.91±1.22 mg/10g dry sediment, n=7) for the Solimões River, 0.10-2.30 mg/10g dry sediment (mean=1.11±0.85 mg/10g dry sediment, n=6) for the Madeira River and 0.10-11.05 mg/10g dry sediment (mean=3.96±2.93 mg/10g dry sediment, n=19) for the Amazon River mainstream. Apart from the Xingu River, the Σ8 values and Λ8 values in individual tributaries are well correlated (r^2 from 0.64 to 0.96, p<0.05).

S/V and C/V of all riverbed samples range respectively from 0.70 to 1.51 and 0.08 to 0.47 (Table 2.1, Fig. 2.3). Negro River and Xingu River sediments show slightly lower average S/V ratios (0.88 and 1.00) than samples from the Solimões River, the Madeira River and the Amazon mainstream (1.08, 1.10, and 1.09, respectively). The range of average C/V ratios of all tributaries is from 0.16 to 0.24 and the highest mean C/V ratio was observed in the Madeira River. Except for the highest P/V ratio in the Madeira River (0.38), the P/V ratios in the other tributaries vary only slightly (0.24-0.27). $(Ad/Al)_V$ values in all riverbed samples (Table 2.1, Fig. 2.2D) vary from 0.26 to 0.71 with an average of 0.42, and $(Ad/Al)_S$ values range from 0.15 to 0.57 with an average of 0.28. The $(Ad/Al)_V$ and $(Ad/Al)_S$ are correlated ($r2$=0.76, p<0.05, n=47), but all $(Ad/Al)_S$ values are lower than the respective $(Ad/Al)_V$ values.

2.4.1.3. Al/Si

In riverbed sediments, the Al/Si varies from 0.11 to 0.56 (Fig. 2.4A), which is larger than the Al/Si range of riverbed sediments reported by Bouchez et al. (2011). Solimões River sediments have a narrow Al/Si range (0.27-0.37) with an average of 0.33±0.04. The samples in the Madeira River and the

Amazon River mainstream display lower Al/Si values (0.17-0.37, mean=0.26±0.08, n=6 and 0.11-0.38, mean=0.29±0.07, n=19, respectively). On the contrary, Negro River and Xingu River sediments have larger variations and higher average Al/Si ratios (0.17-0.51, mean=0.37±0.15, n=7 and 0.14-0.56, mean=0.40±0.15, n=8, respectively).

Table 2.1. Sample information, results of bulk OC and lignin analyses of riverbed sediment samples from the Amazon basin presented in this study.

Sample code	River	Long	Lat	TOC (%)	$\delta^{13}C_{TOC}$ (‰)	Λ8 (mg/100mgOC)	C/V	S/V	P/V	(Ad/Al)v	(Ad/Al)s	Σ8 (mg/10g dry sediment)	Al/Si (weight ratio)
MAO02d	Negro	-60.36	-3.07	1.44	-29.5	3.79	0.26	0.82	0.34	0.59	0.44	5.44	0.19
MAO02e	Negro	-60.35	-3.06	2.93	-29.3	4.62	0.13	0.85	0.24	0.43	0.30	13.53	0.51
MAO02f	Negro	-60.35	-3.05	1.22	-27.3	4.46	0.13	0.97	0.25	0.59	0.32	5.44	0.43
MAO1	Negro	-60.30	-3.06	3.99	-29.3	4.89	0.14	1.09	0.23	0.61	0.30	19.52	0.50
MAO03a	Negro	-60.20	-3.05	2.13	-26.5	4.73	0.10	0.70	0.25	0.56	0.26	10.08	0.49
MAO03h	Negro	-60.20	-3.05	0.53	-29.6	3.55	0.18	0.91	0.31	0.71	0.36	1.89	0.17
MAO4	Negro	-60.15	-3.11	2.31	-29.8	4.59	0.18	0.81	0.28	0.35	0.24	10.59	0.31
MAO11c	Solimões	-60.38	-3.30	0.90	-29.9	3.86	0.20	1.12	0.24	0.32	0.20	3.48	0.37
MAO09b	Solimões	-60.29	-3.27	0.28	n.a.	3.49	0.17	1.19	0.30	0.28	0.15	0.99	0.30
MAO08b	Solimões	-60.21	-3.30	0.59	-27.9	4.97	0.21	0.99	0.25	0.33	0.28	2.93	0.37
MAO08a	Solimões	-60.20	-3.29	0.74	-28.4	4.34	0.24	1.13	0.22	0.32	0.23	3.19	0.34
MAO05a	Solimões	-60.03	-3.27	0.50	-26.1	4.30	0.28	1.10	0.23	0.52	0.34	2.13	0.27
MAO05d	Solimões	-60.02	-3.29	0.57	-28.4	4.71	0.14	0.94	0.17	0.35	0.26	2.69	0.33
MAO13c	Solimões	-59.88	-3.20	0.77	-28.4	6.44	0.17	1.06	0.24	0.28	0.19	4.94	0.37
MAO23a	Madeira	-59.08	-3.68	0.52	-28.4	4.42	0.14	0.96	0.21	0.29	0.23	2.30	0.37
MAO25e	Madeira	-58.91	-3.52	0.47	-27.8	3.29	0.21	1.21	0.26	0.35	0.22	1.55	0.31
MAO28d	Madeira	-58.80	-3.44	0.52	-27.9	3.10	0.24	1.17	0.25	0.39	0.25	1.61	0.23
MAO23c	Madeira	-59.08	-3.67	0.16	n.a.	1.69	0.29	1.04	0.44	0.49	0.40	0.28	0.17
MAO25d	Madeira	-58.91	-3.53	0.14	n.a.	0.73	0.36	1.07	0.63	0.67	0.57	0.10	0.17

MAO25b	Madeira	-58.91	-3.53	0.35	n.a.	2.42	0.23	1.16	0.48	0.71	0.38	0.84	0.31
MAO15e	Amazon	-59.38	-3.19	0.25	n.a.	2.84	0.20	1.14	0.18	0.31	0.21	0.70	0.24
MAO15a	Amazon	-59.38	-3.15	0.80	-27.9	4.01	0.14	0.91	0.20	0.40	0.24	3.21	0.36
MAO17	Amazon	-59.29	-3.15	0.59	-28.9	3.51	0.14	1.16	0.34	0.37	0.20	2.06	0.26
MAO19	Amazon	-59.13	-3.18	1.00	-29.4	4.22	0.14	0.92	0.23	0.48	0.32	4.22	0.37
MAO21f	Amazon	-59.03	-3.23	0.99	-28.7	5.04	0.12	0.96	0.26	0.29	0.21	5.01	0.38
MAO36	Amazon	-58.62	-3.25	1.44	-28.1	4.76	0.21	0.84	0.24	0.45	0.26	6.85	0.31
OB1	Amazon	-55.56	-1.89	0.61	-28.4	3.79	0.21	1.10	0.30	0.48	0.28	2.33	0.32
MC11	Amazon	-51.09	-0.06	0.13	n.a.	0.75	0.47	1.01	0.64	0.61	0.56	0.10	0.11
MC12-2	Amazon	-51.05	-0.08	1.19	-28.3	9.27	0.11	0.88	0.17	0.28	0.25	11.05	0.37
MC12-1	Amazon	-51.05	-0.08	1.01	-28.1	7.20	0.13	1.05	0.19	0.42	0.29	7.29	0.36
MC8	Amazon	-50.66	-0.13	0.62	-27.5	5.30	0.13	1.20	0.37	0.30	0.19	3.27	0.31
MC1	Amazon	-50.65	-0.12	0.60	-28.0	3.83	0.16	1.51	0.35	0.35	0.15	2.29	0.30
MC2	Amazon	-50.64	-0.13	0.40	-28.0	3.82	0.15	1.14	0.20	0.36	0.22	1.53	0.26
MC3	Amazon	-50.62	-0.15	0.26	n.a.	6.36	0.15	1.17	0.19	0.26	0.22	1.67	0.18
MC4	Amazon	-50.61	-0.17	0.72	-28.0	5.06	0.16	1.14	0.20	0.27	0.19	3.64	0.30
MC7	Amazon	-50.59	-0.21	0.37	n.a.	3.51	0.13	1.08	0.29	0.38	0.22	1.29	0.27
MC5	Amazon	-50.58	-0.20	1.29	-28.0	7.11	0.11	1.01	0.18	0.30	0.31	9.18	0.23
MC6	Amazon	-50.56	-0.19	0.80	-27.8	5.13	0.21	1.31	0.33	0.57	0.25	4.10	0.29
MC10	Amazon	-50.09	-0.05	0.76	-28.4	7.18	0.11	1.22	0.35	0.30	0.23	5.49	0.26
XA14L	Xingu	-52.69	-3.88	3.37	-29.7	5.33	0.16	0.98	0.20	0.55	0.36	17.97	0.29
XA30	Xingu	-52.24	-1.69	0.83	-27.9	3.30	0.16	1.23	0.28	0.31	0.18	2.73	0.33
XA36	Xingu	-52.13	-2.22	3.24	-29.8	3.33	0.08	0.90	0.24	0.43	0.26	10.81	0.55

XA25	Xingu	-51.97	-2.64	3.82	-29.4	3.90	0.19	1.12	0.25	0.42	0.27	14.90	0.54
XA38	Xingu	-52.02	-2.47	3.52	-29.6	4.47	0.15	1.05	0.25	0.55	0.28	15.73	0.49
XA31	Xingu	-52.25	-1.79	1.11	-28.4	6.91	0.19	0.91	0.19	0.34	0.26	7.70	0.30
XA34	Xingu	-52.26	-1.79	0.52	-28.3	6.88	0.19	0.75	0.40	0.38	0.27	3.55	0.14
XA35	Xingu	-52.19	-2.04	3.07	-29.8	5.22	0.16	1.03	0.36	0.53	0.37	16.04	0.56

n.a.: not available

2.4.2. Marine sediments

2.4.2.1. TOC and stable carbon isotopic composition

TOC content in the marine surface sediments on the Amazon shelf varies from 0.11 % to 0.91 % (Table 2.2, Fig. 2.5A). Three samples near the Amazon River mouth exhibit low TOC contents of less than 0.2 % (0.13±0.04 %, GeoB16209-2, GeoB16210-2 and GeoB16211-2). The highest TOC content is obtained for GeoB16204-1, the sample from the south-east region to the Amazon River mouth. The $\delta^{13}C_{TOC}$ values for marine surface sediments range from -18.6 ‰ at station GeoB16202-1, which is located southeast of the river mouth (SE sector), to -26.7 ‰ at station MC33A (near the river mouth) (Table 2.1 and Fig. 2.5B). The samples from the SE sector reveal the most enriched $\delta^{13}C_{TOC}$ values between -18.6 ‰ and -21.6 ‰ (-19.6±1.1 ‰, n=6). The samples collected off the Amazon River mouth exhibit the most depleted $\delta^{13}C_{TOC}$ values (-24.8±1.4‰, n=5). $\delta^{13}C_{TOC}$ values increase along the shelf towards the northwest from the Amazon River mouth to around -20.4 ‰ at the north-westernmost stations deeper than 2000m. Apart from the relatively depleted $\delta^{13}C_{TOC}$ value of -24.5 ‰ at station BC61C, the $\delta^{13}C_{TOC}$ values on the Amazon Fan range between -21.4 ‰ and -23.0 ‰.

2.4.2.2. Lignin phenols

The $\Lambda8$ values in marine surface sediments vary from 0.04 to 2.01 mg/100 mg OC (Table 2.2, Fig. 2.5C). The samples in the SE sector display very low $\Lambda8$ values (0.04-0.17 mg/100mg OC), which increase slightly with distance from the Amazon River mouth. Apart from the higher lignin content at station BC61C (0.57 mg/100mg OC), the samples in the Amazon Fan (Fan sector) also have low $\Lambda8$ values ranging from 0.05 to 0.22 mg/100mg OC with a decreasing trend with distance from the Amazon River mouth. The distribution pattern of lignin content in the northwest area (NW sector) is similar to that shown by $\delta^{13}C$ values. In the NW sector, $\Lambda8$ values increase first from 0.19 to 2.01 mg/100mg OC at stations closest to the Amazon River mouth, decrease north-westward and reach rather constant low values of 0.18 mg/100mg OC on the offshore slope of the NW sector. The $\Sigma8$ values in marine surface sediments vary from 0.01 to 1.49 mg/10g dry sediment and are highly correlated with $\Lambda8$ values (r^2=0.85, p<0.05, n=30).

Ranges of S/V and C/V ratios in marine sediments are similar to those observed in riverbed sediments. S/V and C/V ratios vary respectively from 0.59 to 1.62 and from 0.10 to 0.43 (Table 2.2, Fig. 2.3). Sediments in the SE sector have higher C/V ratios (mean=0.30±0.11, n=9). The $(Ad/Al)_V$ and $(Ad/Al)_S$ values in marine samples vary respectively from 0.37 to 1.16 (Table 2.2, Fig. 2.5D) and from 0.32 to 0.97 (Table 2.2). However, our marine samples show no correlation between $(Ad/Al)_V$ and $(Ad/Al)_S$ values. Samples from the Amazon Fan exhibit the highest average $(Ad/Al)_{V,S}$ values of 0.81 and 0.71. Samples in the SE and NW sectors have similar average $(Ad/Al)_V$ values (0.62 and 0.61, respectively), but samples from the NW region exhibit larger variation.

2.4.2.3. Al/Si and grain size

In marine sediments, the Al/Si varies from 0.14 to 0.47. The SE and Fan sectors have narrow Al/Si ranges, which are respectively 0.37-0.41 with an average of 0.39±0.01 and 0.40-0.46 with an average of 0.43±0.02 (Table 2.2). In contrast, the samples in the NW sector display large Al/Si variance (0.14-0.47, mean=0.32±0.14).

Grain size of marine sediments is reported as mean grain size and varies between 3.23-92.90 μm (Table 2.2). Coincident with the Al/Si ratio distribution, samples in the SE and Fan sectors respectively have narrow grain size ranges, which are 4.44-11.79 μm with an average of 8.07±2.75 μm and 3.23-14.50 μm with an average of 5.84±3.38 μm. On the contrary, sediments in the NW sector display wide range grain sizes (4.74-92.90 μm, mean=31.23±35.19 μm). The correlation between grain size and Al/Si ratio (r^2=0.85, p<0.05, n=28) indicates that the Al/Si ratio is a reliable proxy for the grain size of terrestrial sediments.

Table 1. Sample information, results of bulk OC and lignin analyses of marine surface sediment samples from the Amazon continental margin presented in this study.

Sample code	Long	Lat	TOC (%)	$\delta^{13}C_{TOC}$ (‰)	Λ8 (mg/100mg OC)	S/V	C/V	(Ad/Al)v	(Ad/Al)s	Σ8 (mg/10g sediment)	Al/Si (weigt ratio)	Mean grain size (μm)
The Amazon Fan sector (Fan)												
BC14B	-48.35	4.04	0.46	-23.0	0.09	0.81	0.15	0.91	0.81	0.04	0.42	5.2
BC17B	-48.54	3.96	0.44	-21.8	0.14	1.33	0.13	0.99	0.65	0.06	0.42	6.2
BC24B	-48.89	3.80	0.49	-22.2	0.22	1.62	0.18	0.88	0.49	0.11	0.40	14.5
BC3C	-48.61	4.46	0.60	-21.9	0.19	1.33	0.35	0.65	0.71	0.11	0.45	3.9
BC44C	-48.17	3.78	0.44	-21.8	0.10	0.59	0.11	0.75	0.70	0.04	0.41	4.7
BC50C	-47.31	3.65	0.57	-22.3	0.09	0.78	0.22	0.87	0.80	0.05	0.45	3.8
BC55C	-47.64	3.07	0.46	-21.7	0.13	0.76	0.14	0.81	0.70	0.06	0.40	8.2
BC61C	-47.74	2.85	0.64	-24.5	0.57	1.28	0.24	0.92	0.61	0.37	0.46	3.2
BC71C	-46.25	3.39	0.50	-21.4	0.06	1.28	0.35	0.70	0.77	0.03	0.46	n.a.
MC12A	-48.34	4.04	0.67	-22.6	0.13	1.61	0.27	0.56	0.78	0.09	0.43	5.1
MC6A	-48.62	4.46	0.77	-22.2	0.06	1.04	0.26	0.92	0.76	0.05	0.45	3.5
The southeast sector (SE)												
BC75C	-45.35	1.68	0.31	n.a.	0.04	0.81	0.25	0.86	0.92	0.01	0.40	n.a.
BC80C	-44.35	0.66	0.21	n.a.	0.10	0.80	0.11	0.49	0.42	0.02	0.38	4.8
BC82C	-44.21	0.34	0.35	-21.6	0.05	0.91	0.31	0.80	0.77	0.02	0.40	4.4
BC90B	-42.74	-1.03	0.43	n.a.	0.08	1.25	0.20	0.76	0.48	0.04	0.40	6.0
GeoB16202-1	-41.59	-1.91	0.47	-18.6	0.06	0.86	0.27	0.50	0.64	0.05	0.37	9.3
GeoB16203-2	-41.72	-2.04	0.75	-19.1	0.08	0.98	0.43	0.51	0.67	0.07	0.41	8.3

GeoB16204-1	-42.34	-2.00	0.91	-19.6	0.09	1.05	0.43	0.52	0.68	0.10	0.39	11.8
GeoB16205-3	-43.10	-1.35	0.50	-19.7	0.17	0.70	0.23	0.54	0.53	0.12	0.40	10.9
GeoB16206-2	-43.02	-1.58	0.55	-18.9	0.07	0.87	0.43	0.59	0.85	0.05	0.39	9.1
The northwest sector (NW)												
MC33A	-49.79	3.23	0.74	-26.7	2.01	1.23	0.16	0.73	0.54	1.49	0.46	5.0
GeoB16209-2	-49.37	2.83	0.11	-23.2	0.19	0.83	0.20	0.64	0.97	0.03	0.15	88.4
GeoB16210-2	-49.36	2.87	0.11	-24.1	0.39	1.06	0.29	0.50	0.48	0.04	0.17	48.7
GeoB16211-2	-49.35	2.88	0.18	-24.1	1.08	0.84	0.12	0.46	0.35	0.22	0.22	41.9
GeoB16212-2	-49.39	3.10	0.73	-25.7	1.55	1.01	0.16	0.51	0.35	1.05	0.46	5.7
GeoB16216-2	-51.26	6.24	0.79	-20.4	0.18	1.17	0.31	0.66	0.90	0.17	0.41	5.7
GeoB16217-1	-51.29	6.07	0.50	-20.3	0.18	1.10	0.25	1.16	0.76	0.10	0.30	13.1
GeoB16218-3	-51.52	4.77	0.76	-23.7	1.18	0.99	0.16	0.47	0.32	0.95	0.47	4.7
GeoB16223-1	-52.12	6.63	0.79	-20.5	0.19	1.11	0.29	0.65	0.86	0.17	0.38	6.1
GeoB16225-2	-52.86	5.67	0.27	-21.7	1.05	0.63	0.10	0.37	0.32	0.33	0.14	92.9

n.a.: not available

2.5. Discussion

2.5.1. Lowland Amazon River system

2.5.1.1. Spatial distribution and isotopic composition of OC_{terr}

The TOC contents of our riverbed sediments in individual tributaries are larger than values of bedload sediments reported by Bouchez et al. (2014) (mean=0.23±0.42 % in the Solimões and Madeira rivers and the Amazon mainstream), but lower than the values of suspended materials (e.g. mean=1.14±0.33 % in the Solimões and Madeira rivers and the Amazon mainstream) in the Amazon lowland basin (Hedges et al., 1986; Moreira-Turcq et al., 2003; Bouchez et al. , 2014). The distribution of TOC contents basically reflects the characteristics of the tributaries, which are mainly influenced by the content of dissolved organic matter and suspended sediment (Fig. 2.2A). The relatively high TOC contents in the Negro River are due to the low suspended sediment content and high content of humic substances (Ertel et al., 1986). The Xingu river is characterized by low suspended sediment content and high phytoplankton production, which lead to the high TOC contents in riverbed sediments (Moreira-Turcq et al., 2003). In contrast, the Solimões River and the Madeira River being the primary contributors of the suspended sediment to the Amazon River mainstream, have large suspended sediment load (Moreira-Turcq et al., 2003). Consequently, the low TOC contents in the riverbed sediments in these tributaries are due to dilution by lithogenic material. The lower-intermediate TOC contents for the Amazon River mainstream results from the mixing of different signals from these tributaries with a greater influence from the Solimões and the Madeira Rivers.
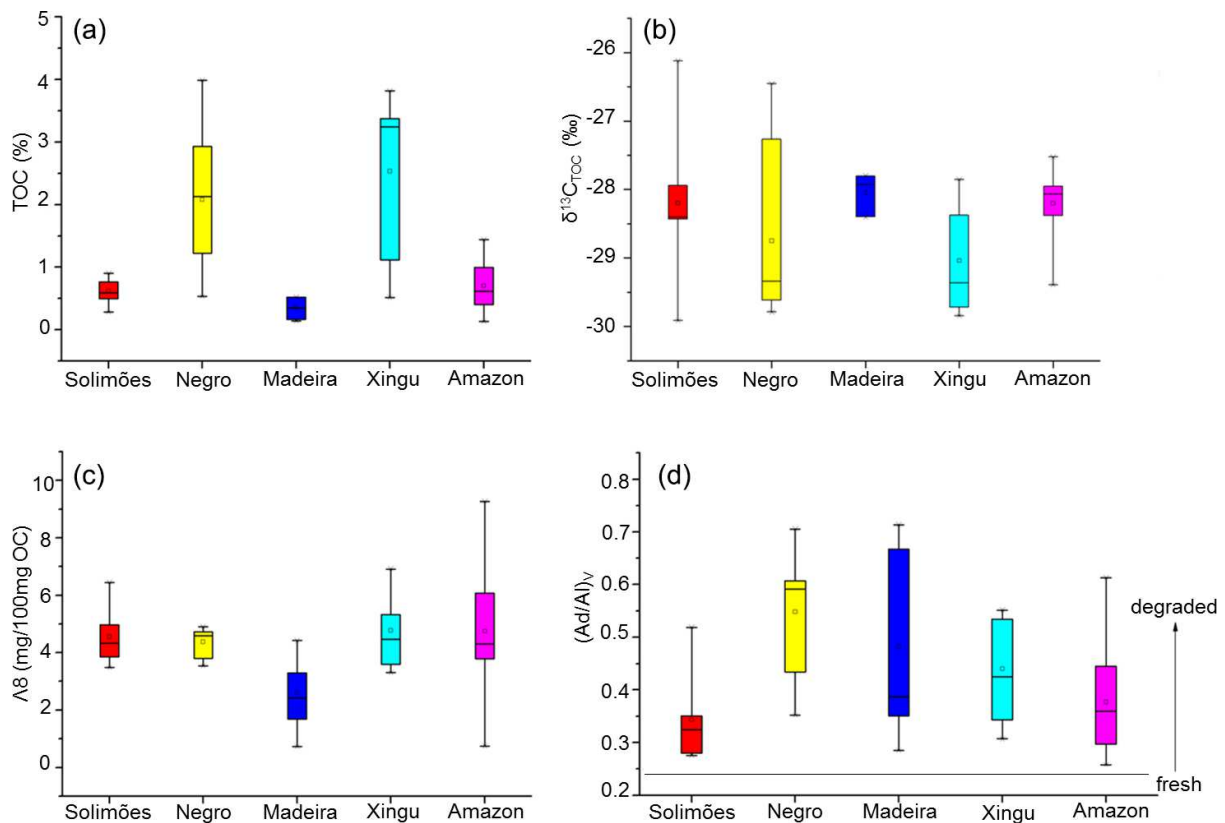
Figure 2.2. A) Total organic carbon (TOC) content, B) stable carbon isotopic composition of total organic carbon ($\delta^{13}C_{TOC}$), C) carbon-normalized lignin content ($\Lambda 8$) and D) degradation index of lignin (Ad/Al)$_V$ in different tributaries and in the Amazon mainstream. In D, (Ad/Al)$_V$ ≤0.24 suggests fresh vascular plant tissues, whereas (Ad/Al)$_V$ >0.24 reveals degraded plant material. See Table 2.1 and Fig. 2.1 for the location of the samples.

The $\delta^{13}C_{TOC}$ values of our riverbed sediments (i.e., from -26.1 ‰ to -29.9 ‰) (Fig. 2.2B) are similar to the values reported for riverbed sediments (e.g. from -27.6 ‰ to -28.8 ‰) and suspended particulate matter (e.g. -28.3±1.1 ‰) in the Amazon River system in previous studies (Hedges et al., 1986; Cai et al., 1988; Kim et al., 2012; Bouchez et al., 2014). Hedges et al. (1986) studied $\delta^{13}C_{TOC}$ values of different organic carbon sources in samples from the Amazon River and found the respective average $\delta^{13}C_{TOC}$ values of C3 tree leaves, woods, macrophyte tissues and C4 grasses to be -30.1±0.9 ‰, -27.6±1.0 ‰, -21.4±8.4 ‰ and -12.2 ‰. The total average $\delta^{13}C_{TOC}$ value of riverbed sediments in this study (-28.5±0.9 ‰) confirms the dominant contribution from terrestrial C3 plants. There is no significant difference in the distribution of $\delta^{13}C_{TOC}$ values among the sampled tributaries.

2.5.1.2. Characteristics of lignin phenols

With the exception of the samples from the Xingu River (r^2=0.02, p=0.71), all riverbed sediments exhibit a good relation between $\Lambda 8$ values and $\Sigma 8$ values (average r^2=0.76, p<0.05, n=39). In the Xingu River, the high level of in situ primary production and low-turbidity conditions favour the settling of phytoplankton-derived organic matter from the water column (Moreira-Turcq et al., 2003). The deposited phytoplankton-derived organic matter dilutes the abundance of lignin in TOC ($\Lambda 8$) but has

only a small influence on sediment mass and, as a result, $\Sigma8$, resulting in divergence of $\Lambda8$ and $\Sigma8$ (Rezende et al., 2010). Based on previous studies, the $\Lambda8$ values of different organic matter fractions range from 0.45 to 2.40 mg/100 mg OC for fine particulate organic matter (FPOM, silt and clay fraction, <63 μm), and from 1.21 to 10.46 mg/100 mg OC for coarse particulate organic matter (CPOM, sand-size fraction, >63 μm) (Aufdenkampe et al., 2007; Hedges et al., 1986; Hedges et al., 2000). In this study, riverbed sediments (Fig. 2.2C), except for three samples with lignin contents lower than 2.0 mg/100 mg OC, had $\Lambda8$ values (2.42-9.27 mg/100 mg OC) similar to those of CPOM. Most of the $\Lambda8$ values of our samples are smaller than the average $\Lambda8$ values of tree wood tissues (19.3 mg/100 mg OC) and C4 grasses (9.1 mg/100 mg OC), and closer to the range of tree leaves and macrophytes (3.7 mg/100mg OC and 6.4 mg/100mg OC, respectively) (Hedges et al., 1986). This finding is also supported by the distribution of C/V and S/V ratios. The plot of S/V vs. C/V (Fig. 2.3) indicates that angiosperm leaves are the major origin of lignin in the lower Amazon basin. It is noteworthy that the range of typical C/V values for angiosperm leaf material in the Amazon basin is larger (i.e., including C/V values as low as 0.07) than in other regions (with lowest C/V values around 0.20) (Bianchi et al., 2011; Cathalot et al., 2013; Tesi et al., 2014). The resulting small difference between C/V ratios of non-woody and woody tissues of angiosperms in the Amazon region results in a larger uncertainty in inferring the plant sources of lignin. C/V values around 0.1 could be interpreted either as signals exclusively from leaves or as signals from a mixture of woody tissues and leaves. To circumvent this uncertainty, the P/V values are also used to identify the lignin sources. P phenols in our samples are derived from lignin, as supported from the significant correlation of the content of P phenols and lignin content (r^2=0.50, p<0.05, n=47). All P/V values of our samples (0.17-0.64) are higher than the average P/V ratio of woods (0.05) and similar to the range observed for leaves (0.16-6.9) (Hedges et al., 1986). Considering all parameters, non-woody angiosperms are the most likely major source of lignin in the lowland Amazon basin. The slightly higher C/V ratios in the Solimões River (0.20) and the Madeira River (0.24) suggest a small contribution of grass-derived material (C/V>1) probably from the Andean highlands (Aufdenkampe et al., 2007; Hedges et al., 2000).
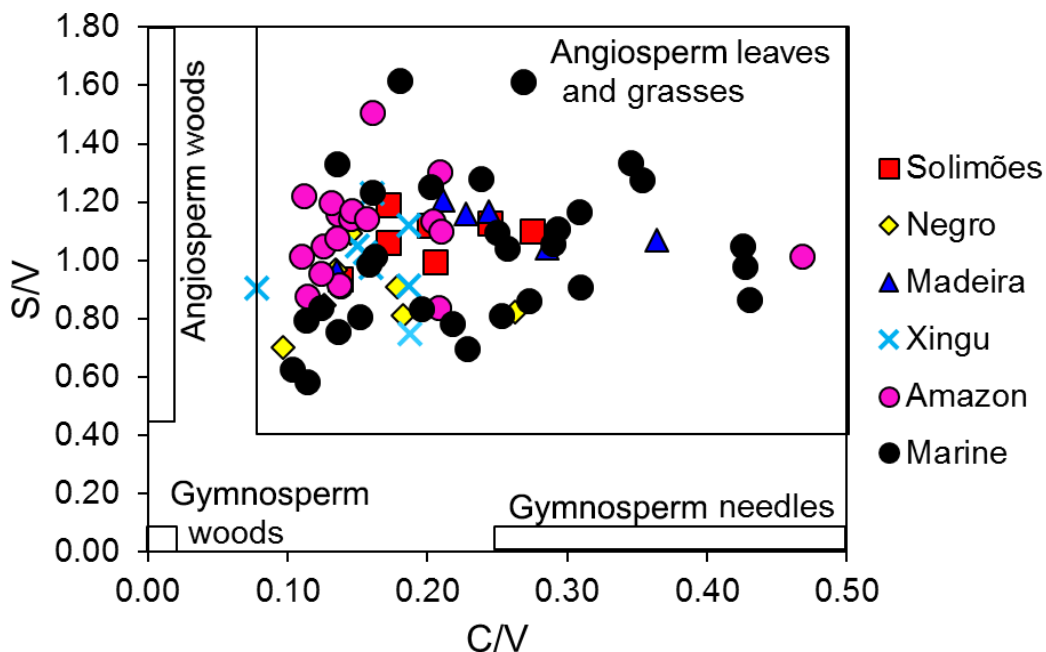
Figure 2.3. Syringyl:vanillyl (S/V) vs. cinnamyl:vanillyl (C/V) ratios of lignin from Amazon basin river bed sediments and marine surface sediments from the adjacent continental margin. The black boxes show typical ranges for different vascular plant tissues from the Amazon basin (Hedges et al., 1986, Goñi et al.,1998). See Tables 2.1 and 2.2, and Fig. 2.1 for the location of the samples.

The degradation extent of OC_{terr} can be assessed by $(Ad/Al)_V$ and $(Ad/Al)_S$ ratios as more degraded lignin yields elevated $(Ad/Al)_V$ and $(Ad/Al)_S$ values (Hedges et al., 1988; Opsahl and Benner, 1995). In the case of the Amazon basin, the $(Ad/Al)_V$ and $(Ad/Al)_S$ ratios of typical fresh woods and tree leaves both range from 0.11 to 0.24 (Hedges et al., 1986). All of our samples exhibiting values between 0.26 and 0.71 for $(Ad/Al)_V$ (Fig. 2.2D) and between 0.15 and 0.57 for $(Ad/Al)_S$ are outside of the range of fresh plant materials, suggesting degraded OC_{terr} in all samples. Instead, the $(Ad/Al)_{V,S}$ ratios observed in our samples are within the ranges of suspended particulate solids obtained in the lower Amazon basin and Bolivian headwaters $((Ad/Al)_{V,S}$ of 0.21-0.39 and 0.13-0.22 for CPOM and $(Ad/Al)_{V,S}$ of 0.38-0.79 and 0.22-0.41 for FPOM (Hedges et al., 1986; Hedges et al., 2000)). The Negro River displayed the highest average $(Ad/Al)_V$ ratio (0.55), reflecting a greater degree of degradation. This might be indicative of more efficient degradation in the podzols of the lateritic landscapes in the Negro River watershed (Bardy et al., 2011). The $(Ad/Al)_V$ ratios in the Solimões and the Madeira Rivers increase with increasing C/V values (r^2=0.50, p<0.05, n=13), which implies that the plant tissues with higher C/V values (higher grass contributions) are more degraded. This further supports the inference that the Solimões and the Madeira Rivers receive POC from grass sources from high-altitude watersheds, where deeper soil erosion of more degraded OC_{terr} could occur. The degradation status of lignin in riverbed sediments does not display a downstream increasing trend and is similar to previous studies on suspended POC of different size fractions. This leads to the conclusion that OC_{terr} processing during transport through the Amazon river system probably has limited influence on the composition of lignin recorded in the riverbed sediments and the degradation information likely reflects source characteristics

of OC_{terr} prior to fluvial transport (Hedges et al., 1986; Hedges et al., 1994). This finding contradicts the conclusion of Ward et al. (2013) that lignin is rapidly degraded within the Amazon River. Ward et al. (2013) studied particulate and dissolved lignin in the water column, which is exposed to degradative environments. In contrast, our study focuses on the lignin associated with mineral particles, which are deposited and protected from degradation. This discrepancy highlights the important role of matrix association effects in the preservation of organic matter.

2.5.1.3. Sedimentological control on OC_{terr} characteristics

As grain size data could not be obtained directly on the riverbed sediment samples, we inferred grain size information based on the relationship between the Al/Si ratio and grain size of riverbed sediments observed by Bouchez et al. (2011) in samples from the Amazon basin. High Al/Si indicates aluminium-rich fine-grained sediment, whereas low Al/Si suggests silicon-rich particles of larger grain size (Bouchez et al., 2011; Galy et al., 2008).

As expected, the TOC contents increase with Al/Si (Fig. 2.4A), indicating that fine particles, associated with larger specific surface areas and likely rich in clay, carry more TOC than coarser particles. The Negro and the Xingu Rivers have larger Al/Si and TOC variations, and for a given Al/Si ratio, the Negro and the Xingu Rivers show higher TOC contents compared to the other tributaries. As these rivers have distinct chemical characteristics and clay mineral composition (e.g., lower pH in the waters of the Negro River and higher kaolinite content in the sediments of the Negro and the Xingu Rivers than in other tributaries; Guyot et al., 2007), the adsorption affinities of OC_{terr} on different clay minerals or under different chemical conditions may be distinct.

Different grain size classes may not only have different TOC content but also the composition of their OC_{terr} might vary. For example, previous studies on POM in the Amazon basin found that CPOM has a higher content of lignin phenols than FPOM and that CPOM is composed of fresher lignin with lower C/V ratios (Hedges et al., 1986). Nevertheless, contradictory results were observed in our riverbed sediments. The $\Lambda 8$ values in the Madeira River, the Solimões River and the mainstream Amazon River show a remarkable increase with decreasing grain size (indicated by increasing Al/Si ratios) (Fig. 2.4B). This rise in lignin content in organic matter associated with finer minerals implies preferential preservation of lignin on finer particles compared with other components. A similar trend has been observed in other environments, such as in surficial sediments of the East China Sea (Wu et al., 2013) and the Iberian margin (Schmidt et al., 2010). However, opposite distribution patterns with lignin enriched in coarser size-classes and low density fractions have been found in sediments from the Washington margin (Keil et al., 1998) and the Laptev Sea (Tesi et al., 2016). This is likely because codeposited plant debris preferentially accumulates within coarser and low density fractions. Thus the apparent discrepancy between these studies may derive from the different methods employed, i.e. partitioning sediments into discrete size and density fractions (Keil et al., 1998, Tesi et al., 2016) versus

characterizing the mean grain size of bulk sediments, respectively (Wu et al., 2013, Schmidt et al., 2010, and our study). On the other hand, the distinct environmental settings in which these studies were conducted, may influence the grain size distribution of lignin. The Amazon River drains tropical lowlands where degradation on land is efficient, and the turbid waters of the Amazon River might limit the settling of plant fragments. Consequently, in our riverbed samples sedimentary organic matter likely contains only a small contribution of plant debris, whereas less efficient degradation on land in the colder climates of the higher latitudes will result in deposition of more coarse plant debris. In the Negro River, there is only a slight increase in Λ8 values as mineral particles become finer, probably as a result of the large amount of sediment-associated chemically stable humic substances (Hedges et al., 1986), in which the lignin content is relatively constant. However, Xingu River sediments exhibit decreasing Λ8 values with decreasing grain size probably because the lignin content in finer particles from the Xingu River is diluted by other non-lignin organic components. With respect to the indicator of plant sources (Fig. 2.4C), the C/V ratios for samples from the Madeira River, the Solimões River and the Negro River decrease with decreasing grain size, which implies that lignin with higher C/V ratios is typically enriched in coarser particles. This suggests that the non-woody tissues with higher proportions of cinnamyl phenols are enriched in coarse-grained sediments. Xingu River and Amazon River mainstream sediments present no pronounced trend between C/V ratios and Al/Si values.
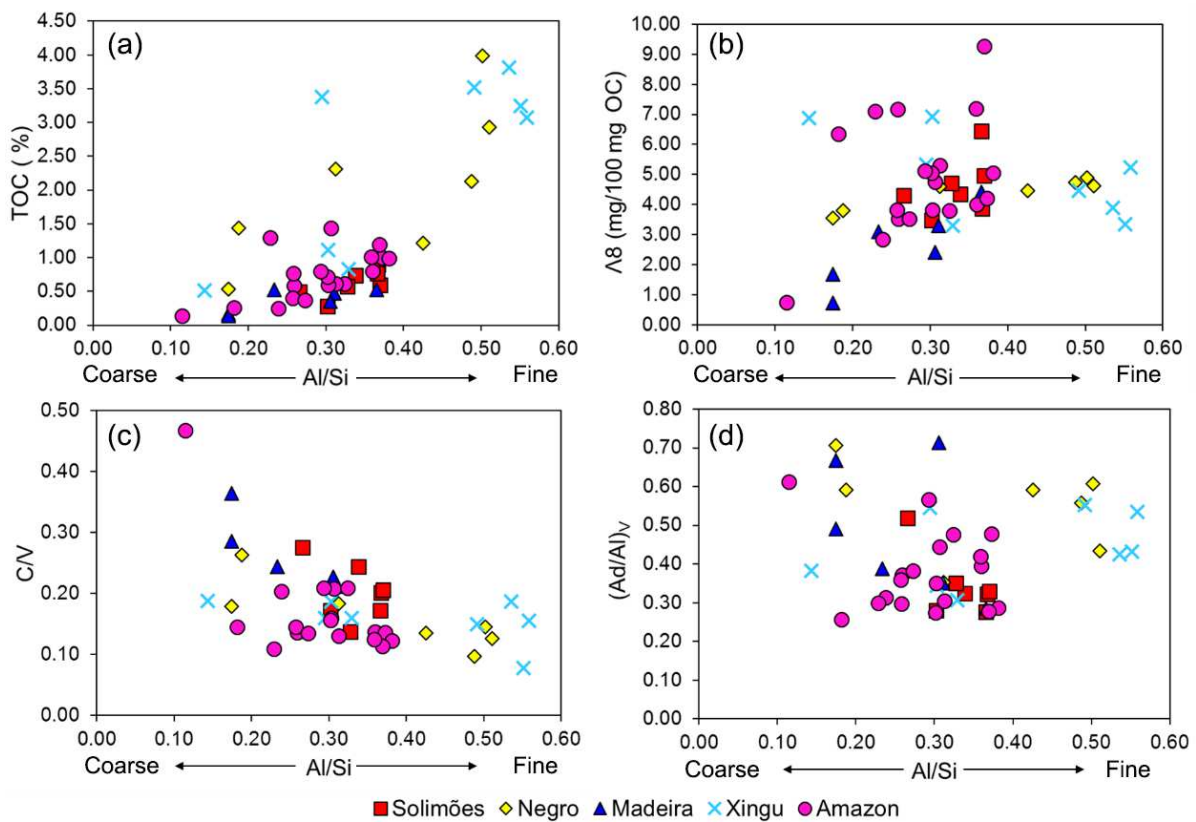
Figure 2.4. A) Total organic carbon (TOC) content vs. Al/Si, B) carbon-normalized lignin content (Λ8) vs. Al/Si, C) cinnamyl:vanillyl (C/V) ratio vs. Al/Si, and D) degradation index of lignin ((Ad/Al)v) vs. Al/Si from Amazon basin riverbed sediments. See Table 2.1 and Fig. 2.1 for the location of the samples.

34

(Ad/Al)$_V$ values for all riverbed sediments do not show any obvious relationship with Al/Si (Fig. 2.4D). Only Madeira River and Solimões River sediments exhibit decreasing (Ad/Al)$_V$ values with increasing Al/Si, which suggests that lignin associated to larger mineral particles is more degraded. This observation implies preferential preservation of lignin in finer-grained sediments due to better protection against oxidative degradation (Killops and Killops, 2005). Like the correlation between Λ8 values and Al/Si, our observation on (Ad/Al)$_V$ values is different to the trends found by Keil et al. (1998) and Tesi et al. (2016), where lower (Ad/Al)$_V$ values have been found in coarser fractions. Again, this is likely due to the fact that these studies investigated individual grain size and density fractions, and that they were conducted in higher latitudes with less efficient processing of plant remains prior to deposition. As a result, fresh plant tissue would be found in the coarse fractions leading to low (Ad/Al)$_V$ values (see discussion above). Because our sediments likely contain limited amounts of plant debris, the (Ad/Al)$_V$ are lower in finer sediments implying that lignin is better preserved in finer grained particles. In previous studies on suspended sediments, lignin in the coarse fractions is more abundant and less degraded compared to the counterpart in fine fractions (e.g. Hedges et al., 1986). In contrast, our results for riverbed sediments suggest that lignin is preferentially preserved and better protected against degradation on fine-grained material. The different grain size effects on OC$_{terr}$ composition between suspended and riverbed sediments suggest that there are other processes working on OC$_{terr}$ in suspended sediments and riverbed sediments which cause post-depositional changes in the OC$_{terr}$ characteristics.

In summary, our data indicate that lignin derives mainly from non-woody tissues of angiosperms in the lowland Amazon basin, and there is little evidence for contribution from C4 plants to riverbed sediments. Grain size plays an important role in OC$_{terr}$ preservation and lignin composition in the Amazon River. Fine inorganic particles have high adsorption affinity for OC$_{terr}$, especially for lignin compared to other OC$_{terr}$ components and efficiently protect lignin from degradation.

2.5.2. Amazon shelf and fan

2.5.2.1. Spatial distribution and characteristics of OC$_{terr}$ and lignin phenols

Because of the depleted average $\delta^{13}C_{TOC}$ values of the riverbed sediments (-28.5±0.9 ‰), contribution of C4 plants is not expected in the offshore sediments affected by the Amazon outflow. Therefore, enriched $^{13}C_{TOC}$ values in the SE sector (-18.6 ‰ to -21.6 ‰) likely indicate organic matter predominantly of marine origin. $\delta^{13}C_{TOC}$ values in the Amazon Fan sector ranging from -21.4 ‰ to -24.5 ‰, (Fig. 2.5B) also reflect dominantly marine organic matter. These values are within the range of published values for high sea-level periods (Schlünz et al., 1999), when most terrestrial POM discharged from the Amazon River is transported to the north-western shelf. In the NW sector, increasing $\delta^{13}C_{TOC}$ values with distance from the Amazon River mouth indicate that the terrestrial POM input from the Amazon River transported to the NW by the North Brazil Current is increasingly diluted

by marine organic matter. OC$_{terr}$ is dominant on the continental shelf, corroborating previous results (e.g., Schlünz et al., 1999).
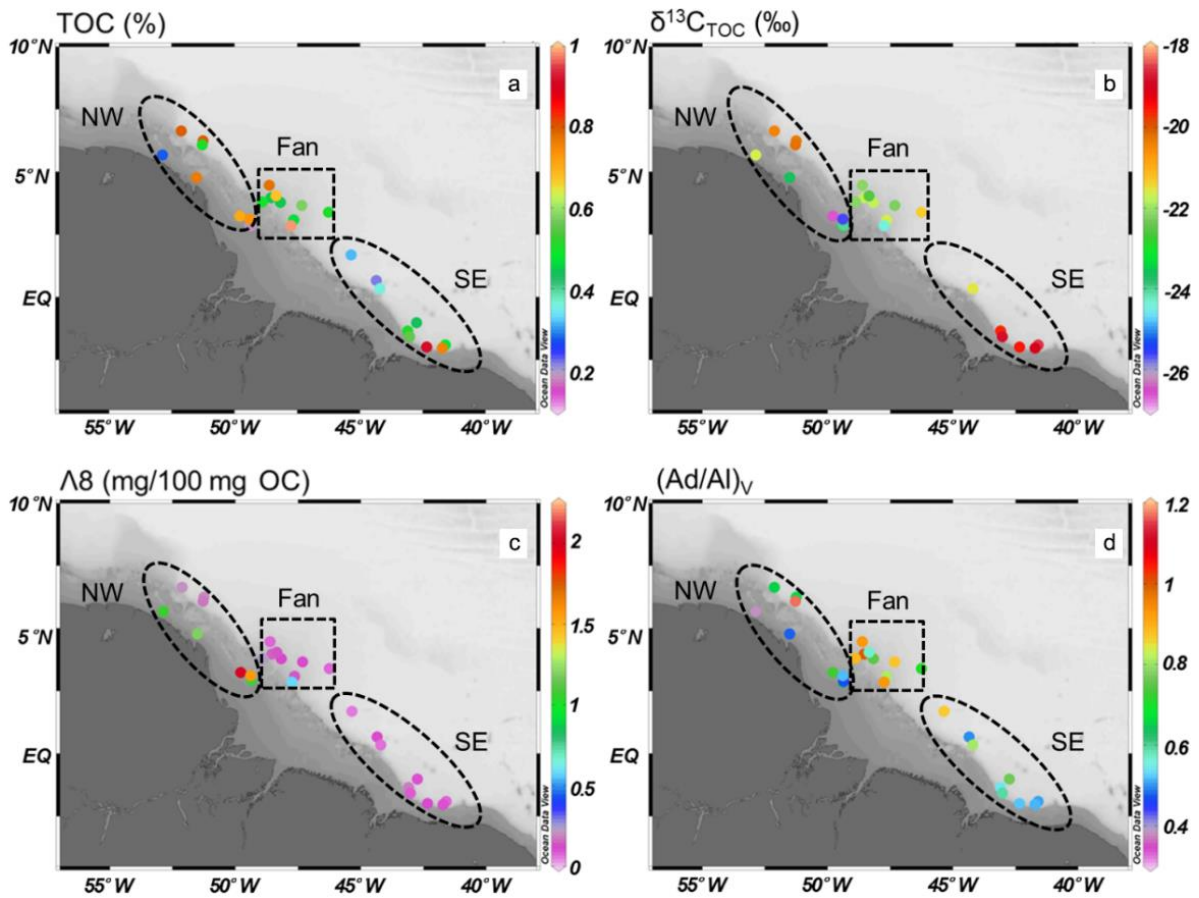

Figure 2.5. Spatial distribution of A) total organic carbon (TOC) content, B) stable carbon isotopic composition of total organic carbon (δ^{13}C$_{TOC}$), C) carbon-normalized lignin content (Λ8), and D) degradation index of lignin ((Ad/Al)$_V$) in marine surface sediment samples from the Amazon continental margin. The dashed ellipses and the rectangle represent the northwest sector (NW), the Amazon Fan sector (Fan) and southeast sector (SE).

Sediments in the SE sector exhibit much lower Λ8 values than observed in the Fan and NW sectors. Here, slightly increasing Λ8 values with distance from the Amazon River mouth suggest that this terrestrial material is predominantly supplied by rivers to the southeast of the Amazon mouth and not by the Amazon River itself. The Λ8 values in sediments near the Amazon River mouth are highly variable and decrease with distance from the river mouth to the Fan and NW sectors, reaching very low Λ8 values in the slope of the NW sector. Lower lignin contents (0.05-0.32 mg/mg OC) have been observed in the deep sea fan sediments measured in the study of Feng et al. (2016), which means there is increasing loss of lignin during the transport seawards to the Fan and NW sectors. Λ8 and δ^{13}C$_{TOC}$ values show similar spatial distribution and are positively correlated (r^2=0.53, p<0.05, n=27) (Fig. 2.6). The agreement in the spatial patterns of lignin content and isotope composition of organic matter suggest that lignin is a reliable tracer of OC$_{terr}$ in the Amazon shelf and fan, and that the SE sector receives little OC$_{terr}$ contribution from the Amazon River. The intercept of the correlation between Λ8

and $\delta^{13}C_{TOC}$ of NW and Fan sediments (r^2=0.58, p<0.05, n=21) is at -20.8 ‰, which corresponds to conditions with minimal OC_{terr} input to the marine sediments. It should be noted that the samples from the Amazon Fan have the same low lignin contents as in the SE sector, which indicates low contribution of OC_{terr} from terrestrial vascular plants under modern conditions. However, the Fan sediments show more depleted $\delta^{13}C_{TOC}$ than sediments from the SE sector, which implies that a small terrestrial fraction is contained in the organic matter of the modern Fan sediments. Potentially, the OC_{terr} from vascular plants deposited in the Amazon Fan is readily degraded as indicated, e.g., by the high $(Ad/Al)_{V,S}$ ratios, while the relict OC_{terr} is predominantly rock-derived (with estimated $\delta^{13}C_{TOC}$ between -24.3 ‰ and -25.7 ‰) (Bouchez et al., 2014) and responsible for the depleted $\delta^{13}C_{TOC}$. Petrogenic organic matter is thus likely a significant component in the offshore sediments because of its refractory nature and resulting high preservation potential.
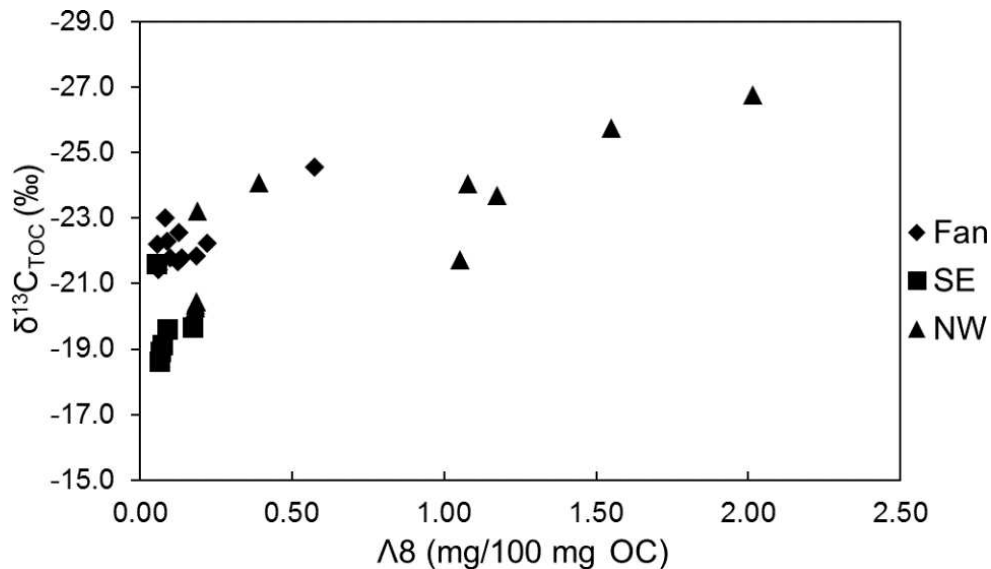
Figure 2.6. Stable carbon isotopic composition of total organic carbon ($\delta^{13}C_{TOC}$) vs. carbon-normalized lignin content ($\Lambda8$) for marine surface sediment samples from the Amazon continental margin.

C/V and S/V ratios (0.08-0.47 and 0.70-1.57, respectively; Fig. 2.3) in the entire Amazon shelf and fan are comparable to those in the riverbed sediments of the lowland Amazon basin, which indicates the same predominant source of non-woody angiosperm tissues. This also implies no further alteration of Amazon-derived lignin after it is discharged into the ocean and deposited in marine sediments. Lignin in offshore marine sediments thus can provide reliable evidence for the reconstruction of the vegetation cover in the Amazon basin.

The distribution of the degradation state of lignin based on $(Ad/Al)_V$ is shown in Fig. 2.5D. The strikingly elevated $(Ad/Al)_V$ values in the Amazon Fan are probably caused by longer exposure to oxygen (Blair and Aller, 2012) at the sediment-water interface under low sedimentation rates, corroborating our previous interpretation of the low $\Lambda8$ values but intermediate $\delta^{13}C_{TOC}$ values in the Fan sediments (Fig. 2.6). In the NW sector, there is no obvious decreasing trend of the $(Ad/Al)_V$ values

with the distance from the river mouth. Low $(Ad/Al)_V$ values found at shallow nearshore sites far from the Amazon River mouth (e.g., GeoB16218-3 and GeoB16225-2) may be due to rapid transport and deposition of the material discharged from the Amazon River (Nittrouer et al., 1995) or contributions from local small rivers which may carry an indistinguishable lignin signature from the Amazon River. In the study of Feng et al. (2016), the sampling locations in the Amazon deep sea fan are in deeper water depths than our samples (>4000 m). Despite, very low $(Ad/Al)_{V,S}$ (0.04-1.3 and 0.03-0.8 for V and S phenols, respectively) were observed. Neither S/V nor C/V ratios decrease with $(Ad/Al)_{V,S}$ in the marine sediments, which would be expected because cinammyl and syringyl pheonls are preferentially degraded compared to vanillyl phenols (Benner et al., 1990; Opsahl and Benner, 1995). Despite the fact that the degradation of lignin preserved in marine sediments is slightly higher than that preserved in riverbed sediments, degradation has no major impact on the lignin composition.

2.5.2.2. Influence of grain size on OC$_{terr}$ deposition in marine sediments

The grain size and Al/Si in the Amazon Fan and SE sectors vary within a rather small range. The grain size and Al/Si relationship in the NW sector is in accordance with the results obtained by Bouchez et al. (2011). The sediments in the NW sector have similar Al/Si ratios as our riverbed sediments (Table 2.2) which are correlated with grain size. We use grain size data for the following discussion of the sedimentological control on the distribution pattern of OC$_{terr}$ in the NW sector and refer to the relationship between TOC and Al/Si as observed in the riverbed sediments.
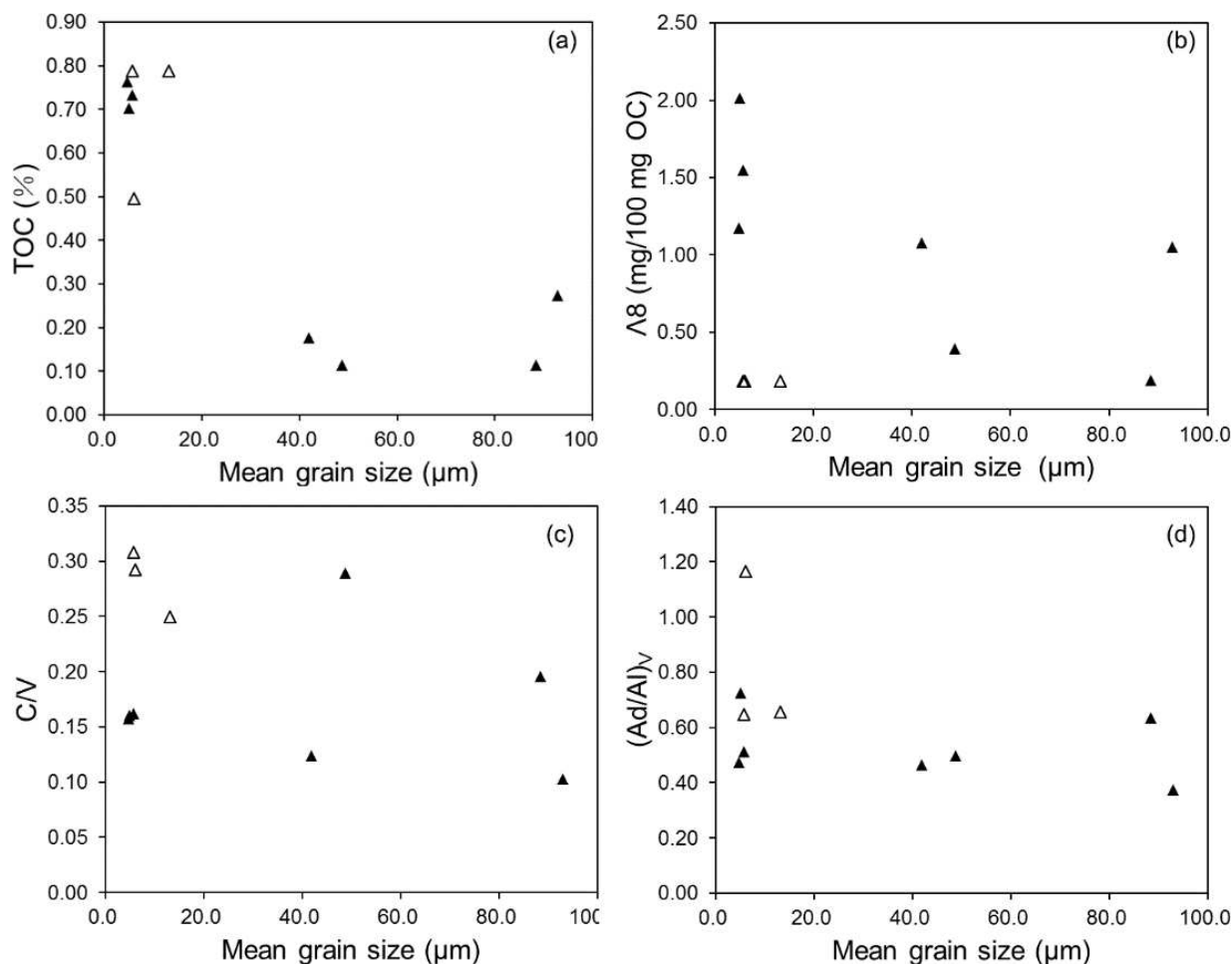
Figure 2.7. A), B), C) and D) indicate total organic carbon (TOC) content, carbon-normalized lignin content (Λ8), cinnamyl:vanillyl (C/V) ratio and lignin degradation index ((Ad/Al)ᵥ) for marine surface sediment samples from the NW sector vs. mean grain size, respectively. Empty triangles represent the three deepest sites (>2000 m) far from the coast, and filled triangles represent the other sites in the NW sector with water depth shallower than 100 m. See Table 2.2 and Fig. 2.5 for the location of the NW sector.

Fine sand sediments were observed at the position closest to the Amazon River mouth (GeoB16209-2) and at site GeoB16225-2, which is far from the Amazon River mouth (about 700 km) but near the coast in a water depth of 34 m. The sample GeoB16225-2 probably receives additional input from local smaller rivers, from which coarser sediments are discharged. Considering that the characteristics of organic matter in the lowland Amazon basin are almost uniform, the local contributions deposited in GeoB16225-2 cannot reliably be distinguished from the material from the Amazon River system. The trend of increasing TOC contents with decreasing grain size (Fig. 2.7A) parallels the one demonstrated for the riverbed sediments (Fig. 2.4A) and in other marine sediments (Keil et al, 1997; Mayer 1994). The lignin content in organic matter (Λ8) and grain size are not significantly related likely because the OC_{terr} is mixed with marine-derived organic matter in marine environments (Fig. 2.7B). For example, according to the enriched $\delta^{13}C_{TOC}$ values (mean=-20.4±0.1 ‰), sites GeoB16216-2, GeoB16217-1 and GeoB16223-1, which are the sites located farthest offshore, contain the largest fractions of marine organic matter, which reduces their Λ8 values to about 0.18 despite their small mean grain size (<14

μm). Except for these three locations, the $\Lambda 8$ values are higher in finer grained sediments than in sandy sediments. This suggests that in marine sediments, as in the riverbed sediments, sorption of lignin on finer sediment is the dominant control on its distribution.

C/V and (Ad/Al)$_V$ values are not related to the grain size in the NW sector (Fig. 2.7C, D), which suggests that the influence of grain size on lignin composition and degradation is not as important as in the riverbed sediments. The control on the degradation of lignin on the inner Brazil-French Guiana shelf and slope is probably complex and influenced by many factors, including oxygen exposure time, contribution of material by coastal rivers, and sedimentation rate. Compared with riverbed sediments, offshore sediments also exhibit better preservation of organic matter and selective preservation of lignin in finer grain size particles, but grain size has limited impact on the lignin composition and degradation status.

In summary, the spatial patterns of lignin content and isotope compositions of organic matter corroborates earlier findings (Geyer et al., 1996; Nittrouer and DeMaster, 1996; Schlünz et al., 1999) that material discharged by the Amazon River is transported north-westward by the North Brazil Current. The modern Amazon Fan area receives more marine organic matter, and petrogenic organic matter is a significant component of OC$_{terr}$ in the Amazon Fan sediments. The similarity of lignin composition (C/V and S/V) of marine and riverbed sediments suggests that lignin is a reliable tracer reflecting the plant source of terrestrial organic matter in the Amazon basin and can be applied to reconstruct vegetation changes and paleoclimate conditions. Organic matter and lignin content furthermore vary with sediment grain size in the Amazon shelf and slope area and show the same preservation trend, better preservation in finer grained sediments, as in riverbed sediments. However, lignin composition is rather uniform in sediments of different grain sizes.

2.6. Conclusions

In this study, we use TOC content, stable carbon isotopic composition of organic matter, lignin phenol concentrations, sediment grain size and Al/Si ratios (as indicator of grain size) to investigate the characteristics of OC$_{terr}$ in the lowland Amazon basin and its fate on the adjacent continental margin. Depleted δ^{13}C$_{TOC}$ of all riverbed sediments prove that there are limited contributions from C4 plants to the OC$_{terr}$ in the lowland Amazon basin. As evidenced by lignin compositions and stable carbon isotopes of organic matter, the most important plant sources of organic matter in the lowland Amazon basin are non-woody angiosperm C3 plants. There are no distinct regional lignin compositional signatures in the lowland Amazon basin, although the Amazon River receives contributions from tributaries draining different watersheds. Both the bulk organic matter parameters and the lignin compositions were observed to be related to the grain size of the riverbed sediments. Fine inorganic particles in the Amazon River carry more organic matter, preferentially preserving lignin against degradation. Lignin with higher C/V ratio is inclined to be adsorbed to coarse inorganic particles.

In marine surface sediments, the bulk parameters and lignin compositions indicate that the continental shelf southeast of the Amazon River mouth receives little OC_{terr} from the Amazon River. Most of the OC_{terr} discharged from the Amazon River is transported by the North Brazil Current to the northwest and deposited on the continental shelf close to the coast. Modern organic matter in the Amazon Fan is composed predominantly of marine-derived organic matter and the terrestrial organic matter undergoes extensive diagenetic alteration before deposition. On the Amazon shelf, the OC_{terr} and lignin are both associated preferentially with fine-grained sediments. Despite long-distance transport in the marine environment, the lignin composition found in the marine sediments retains its plant source information in accordance with riverbed sediments. Lignin can thus be used to reliably provide assessments on the integrated vegetation cover in the Amazon basin.

Data availability. The data presented here are available on the Pangaea database (https://doi.pangaea.de/10.1594/PANGAEA. 875162).

3. Manuscript II:

^{14}C blank assessment in small-scale compound-specific radiocarbon analysis of lipid biomarkers and lignin phenols

Shuwen Sun[1,2,3], Vera Meyer[3], Andrew M. Dolman[4], Maria Winterfeld[3], Jens Hefter[3], Wolf Dummann[5], Cameron McIntyre[6,7,8], Daniel B. Montluçon[6], Negar Haghipour[6,7], Lukas Wacker[7], Torben Gentz[3], Tessa van der Voort[6], Timothy I. Eglinton[6], Gesine Mollenhauer[1,2,3]

[1]Department of Geosciences, University of Bremen, 28359 Bremen, Germany

[2]MARUM-Center for Marine Environmental Sciences, University of Bremen, 28359 Bremen, Germany

[3]Alfred Wegener Institute, Helmholtz Centre for Polar and Marine Research, 25570 Bremerhaven, Germany

[4]Alfred Wegener Institute, Helmholtz Centre for Polar and Marine Research, 14473 Potsdam, Germany

[5]Institute of Geology and Mineralogy, University of Cologne, 50674 Cologne, Germany

[6]Geological Institute, Department of Earth Sciences, ETH Zürich, 8092 Zurich, Switzerland

[7]Laboratory of Ion Beam Physics (LIP), ETH, 8093 Zurich, Switzerland

[8]Current address: AMS laboratory, SUERC, G750QF East Kilbride, UK.

Abstract. Compound-specific radiocarbon dating often requires working with small samples of < 100 µg carbon (µgC). This makes the radiocarbon dates of biomarker compounds very sensitive to biases caused by extraneous carbon of unknown composition, a procedural blank, which is introduced to the samples during the steps necessary to prepare a sample for radiocarbon analysis by accelerator mass spectrometry (i.e., isolating single compounds from a heterogeneous mixture combustion, gas purification and graphitization). Reporting accurate radiocarbon dates thus requires a correction for the procedural blank. We present our approach to assess the fraction modern carbon ($F^{14}C$) and the mass of the procedural blanks introduced during the preparation procedures of lipid biomarkers (i.e. *n*-alkanoic acids) and lignin phenols. We isolated differently sized aliquots (6-151 µgC) of *n*-alkanoic acids and lignin phenols obtained from standard materials with known $F^{14}C$ values. Each compound class was extracted from two standard materials (one fossil, one modern) and purified using the same procedures as for natural samples of unknown $F^{14}C$. There was an inverse linear relationship between the measured

$F^{14}C$ values of the processed aliquots and their mass, which suggests constant contamination during processing of individual samples. We used Bayesian methods to fit linear regression lines between $F^{14}C$ and 1/mass for the fossil and modern standards. The intersection points of these lines were used to infer $F^{14}C_{blank}$ and m_{blank} and their associated uncertainties. We estimated 4.88 ± 0.69 µgC of procedural blank with $F^{14}C$ of 0.714 ± 0.077 for n-alkanoic acids, and 0.90 ± 0.23 µgC of procedural blank with $F^{14}C$ of 0.813 ± 0.155 for lignin phenols. These $F^{14}C_{blank}$ and m_{blank} can be used to correct AMS results of lipid and lignin samples by isotopic mass balance. This method may serve as a standardized procedure for blank assessment in small-scale radiocarbon analysis.

3.1. Introduction

Compound-specific radiocarbon analysis (CSRA) is an attractive tool for studying the carbon cycle as it provides information about the sources and transport mechanisms of biomarker molecules. A major challenge in CSRA of biomarkers is the low abundance of these specific compounds in natural matrices (e.g. sediments and water) from which they are commonly extracted. This often requires CSRA to work with samples of small sizes (< 100 µgC). Recent improvements in the technology of accelerator mass spectrometry (AMS) permit the radiocarbon analysis of samples as small as ~1 µgC (Santos et al., 2007). However, small samples are very sensitive to biases caused by blank carbon (carbon of unknown isotopic composition and from unknown sources) that enters the samples during processing in the laboratory. This makes it necessary to carefully assess and correct for the mass and ^{14}C content of the blank carbon.

The preparation of samples for CSRA usually requires a series of complex procedures. An unknown amount of contaminant carbon of unknown $F^{14}C$ value might be introduced into the sample at any of these steps, such as during chemical extraction, isolation of pure compounds with preparative capillary gas chromatography (PCGC) or preparative-high performance liquid chromatography (prep-HPLC), preparation on vacuum line systems, and, in some cases, graphitization. Potential contamination sources include solvents, column bleed (from PCGC, prep-HPLC), carry-over and atmospheric carbon during combustion and vacuum line handling. Combined, these procedural blanks might be large enough to contribute a significant proportion of the mass of purified compound samples or even outweigh the target compound for ultra-small mass samples (Shah and Pearson, 2007). The $F^{14}C$ value of the analysed samples will significantly deviate from the true values of the target compounds without the proper assessment and correction of procedural blank, which will potentially lead to erroneous interpretation of the biogeochemical characteristics or cycling of the biomarker compounds. Therefore, the assessment of procedural blanks, i.e. the determination of $F^{14}C$ and the mass of the procedural blank ($F^{14}C_{blank}$, m_{blank}), is critical for reporting accurate radiocarbon composition.

Several studies have used various approaches to quantify the procedural blank and have attempted to identify the sources of the blank carbon. Shah and Pearson (2007) measured the masses of procedural

blanks from different volumes of effluent from a prep-HPLC system (no sample added) and found masses of the procedural blank to be correlated to the prep-HPLC effluent volumes, which suggests that the procedural blank introduced during the isolation of compounds would vary in proportion to the mass of sample (the larger size samples require larger effluent volume). They also observed that the blank introduced from combustion is constant and there are some additional blanks introduced during other preparation steps in addition to prep-HPLC and combustion that are difficult to identify. Ziolkowski and Druffel (2009) have analyzed the mass and $F^{14}C$ of the eluted procedural blank from repeated dry injections (no solvent injected) on PCGC to directly evaluate the blank introduced from the PCGC separation step. An indirect method of determining the $F^{14}C$ of PCGC isolated size-series of paired standard compounds (one modern, one fossil) has also been used to calculate the masses of modern and fossil blanks introduced during the PCGC step. Ziolkowski and Druffel (2009) have shown that the direct and indirect methods agree in the assessment of the mass and $F^{14}C$ of procedureal blank and half of the procedural blank is introduced before PCGC isolation and likely from the chemical extraction step. In the study of Tao et al. (2015), the authors added modern and fossil standards of known $F^{14}C$ values into solvent blanks and used the deviation between the measured and known $F^{14}C$ values to indirectly assess the amount of modern and fossil blanks. Santos et al. (2010) proposed an approach to consider the amount of modern and fossil procedural blanks as integrated components which are a combination of all potential sources. Hanke et al. (2017) separated the procedural blank into ^{14}C-depleted and modern components and varied their masses to obtain the best value by chi-square fitting.

As stated above, preparing samples for CSRA involves many steps. Although it is theoretically possible to quantify the mass and $F^{14}C$ value of extraneous carbon from each step and potentially helpful when attempting to minimize the procedural blank, this work is very time consuming and further complicates the process for CSRA analysis. In addition, a detailed assessment of blank-carbon contributions from each step will further complicate the error propagation during the correction for blank carbon and introduces additional large uncertainties into the final $F^{14}C$ data. Therefore, a simplified but precise approach for blank assessment, which integrates over all preparation steps and avoids the detailed determination of individual contaminant sources, is highly needed for CSRA analysis - especially for small sized samples.

Here, we present a protocol for blank assessment that is relatively easy to achieve without complicated calculation or labour-intensive laboratory procedures. As a case study, we apply this method to two different biomarker compound classes (*n*-alkanoic acid and lignin phenols), both commonly targeted for CSRA, to test whether it is practical for different compounds and preparation procedurals.

3.2. Blank assessment

In our approach we neither focus on the extraneous carbon added through individual preparation steps, nor attempt to determine modern C and fossil C contamination separately. Instead, the procedural blank

is integrally considered. This approach is based on a hypothesis stated in the study of Santos et al. (2007) according to which the mass and $F^{14}C$ value of the integral procedural blank is generally constant per batch of samples handled with the same preparation protocol for a certain class of compounds. Relying on this assumption, the measured mass and $F^{14}C$ value of a processed sample consists of the pure compound of interest and the constant contaminant (blank). Thus, the measured mass (m) and $F^{14}C$ value of a processed sample can be described as equation (3.1) and (3.2), respectively.

$$m_{\text{sample}} = m_{\text{true}} + m_{\text{blank}} \qquad (3.1)$$

$$F^{14}C_{\text{sample}} = F^{14}C_{\text{true}} \times \left(\frac{m_{\text{true}}}{m_{\text{sample}}}\right) + F^{14}C_{\text{blank}} \times \left(\frac{m_{\text{blank}}}{m_{\text{sample}}}\right) \qquad (3.2)$$

Where m_{sample}, m_{ture} and m_{blank} refer to the mass of carbon of the processed sample, the pure compound and the procedural blank, respectively. $F^{14}C_{\text{sample}}$, $F^{14}C_{\text{true}}$ and $F^{14}C_{\text{blank}}$ are the $F^{14}C$ values of a processed sample, the pure compound and the procedural blank, respectively. Equation (3.2) can be rearranged to show the relation between $F^{14}C_{\text{sample}}$ and m_{sample}:

$$F^{14}C_{\text{sample}} = (F^{14}C_{\text{blank}} \times m_{\text{blank}} - F^{14}C_{\text{true}} \times m_{\text{blank}}) \times \frac{1}{m_{\text{sample}}} + F^{14}C_{\text{true}} \qquad (3.3)$$

Except for m_{sample}, the other terms in equation (3.3) are constant when using differently sized aliquots of the same material. Therefore, equation (3.3) shows a linear relation between $F^{14}C_{\text{sample}}$ and $1/m_{\text{sample}}$ (Shah and Pearson, 2007). The intercept ($F^{14}C_{\text{true}}$) is the $F^{14}C$ value of the pure compound and the slope (a) is defined as:

$$a = F^{14}C_{\text{blank}} \times m_{\text{blank}} - F^{14}C_{\text{true}} \times m_{\text{blank}} \qquad (3.4)$$

This shows the effect of the procedural blank on the measured $F^{14}C_{\text{sample}}$ as a function of the sample size (m_{sample}). It allows the procedural blank to be assessed graphically when determining the $F^{14}C_{\text{sample}}$ of several aliquots (of different size) of two standard materials, with known $F^{14}C_{\text{true}}$ values ($F^{14}C_{\text{true1}}$ and $F^{14}C_{\text{true2}}$), e.g. one modern and one fossil standard. We can correlate the $F^{14}C_{\text{sample}}$ to $1/m_{\text{sample}}$ resulting in two regression lines with two slopes (a_1 and a_2), which can be used to derive the m_{blank} from their point of intersection:

$$m_{\text{blank}} = \frac{a_1 - a_2}{(F^{14}C_{\text{true2}} - F^{14}C_{\text{true1}})} \qquad (3.5)$$

The $F^{14}C_{\text{blank}}$ can then be calculated as:

$$F^{14}C_{\text{blank}} = \frac{a_1}{m_{\text{blank}}} + F^{14}C_{\text{true1}} \quad \text{or} \quad F^{14}C_{\text{blank}} = \frac{a_2}{m_{\text{blank}}} + F^{14}C_{\text{true2}} \qquad (3.6)$$

The chosen standards should contain the same or at least similar biomarker compounds as the set of "real" samples which is intended to be blank corrected. The standards and "real" samples should be processed using identical protocols. The range of chosen sample sizes (m_{sample}) for the standards should include the mass-range covered by the real sample-set and extend to the high- and low- detection limits at the same time (e.g. 10-100μgC).

There are uncertainties in the measurements of the mass and $F^{14}C$ values of the different sized standards and both of these should be considered when fitting regression lines and calculating the intersection point. Accordingly, we applied a Bayesian model that included error models for both response and predictor variables. This method allows for easy numerical estimation of the bivariate distribution of the intersection of the two regression lines (from which m_{blank} and $F^{14}C_{blank}$ are inferred) using the posterior sample of the distribution of the model parameters. The statistical model was written in the Stan language (Carpenter et al. 2017) and was fitted using the RStan package (Stan Development Team, 2018) for R (R Core Team, 2017). The values of $1/m_{blank}$ and $F^{14}C_{blank}$ (the intersection point) were constrained to be positive. Weak half-normal priors (mean = 0, sd = 10) were placed on the regression slopes, with the fossil slope constrained to be positive and the modern slope negative. When available, $F^{14}C_{true}$ values for the standards were used to place an informative prior on the value of the intercept ($F^{14}C$ value at $1/m = 0$). Three chains of the fitting process were run for 5000 iterations and checked for convergence visually and with the Rhat statistic (Gelman and Rubin, 1992). The output from the Bayesian model is the 'posterior distribution', which consists of a matrix of parameter estimates based on 7500 iterations, 2500 from the second half of each chain. Each iteration provided one paired estimate of $F^{14}C_{blank}$ and $1/m_{blank}$. The median absolute deviation (MAD) is used as a robust measure of uncertainty for error propagation because the intersection is the ratio of the differences in slopes and intercepts, whose distribution has long tails. For normally distributed variables, the expected value of MAD is equal to the standard deviation. The script and the necessary Stan-code file are provided in the supplementary material along with diagnostic plots of the model fit.

3.3. Case studies

We applied this approach to two groups of biomarkers, i.e. *n*-alkanoic acids (lipid biomarkers) and lignin phenols. For the blank assessment of radiocarbon analysis on lipid biomarkers, *n*-hexadecanoic acid (*n*-$C_{16:0}$ alkanoic acid) from apple peel collected in 2013 ($F^{14}C$ value of bulk OC=1.031±0.001) was used as modern standard. A commercial *n*-triacontanoic acid (*n*-$C_{30:0}$ alkanoic acid; Sigma-Aldrich Prod. No. T3527-100MG, LOT 018K3760) of known $F^{14}C$ value (0.003±0.001) (Rethemeyer et al., 2013) as well as *n*-hexacosanoic acid (*n*-$C_{26:0}$ alkanoic acid) and *n*-octacosanoic acid (*n*-$C_{28:0}$ alkanoic acid) extracted from Messel Shale (immature Eocene oil shale, $F^{14}C$ value of bulk OC=0.000) were used as fossil standards.

For the blank assessment of radiocarbon analysis on lignin phenols, vanillin extracted from woodchips collected in the wood workshop of University of Bremen in 2010 was used as the modern standard and the commercial standard ferulic acid (Sig-Aldrich, Prod. No.12,870-8, Lot STBB6360) of known $F^{14}C$ value (0.000) was used as fossil standard.

The handling of purified standards for ^{14}C analysis was described in the study of Winterfeld et al (submitted for publication) and Sun et al. (manuscript in preparation). Briefly, the procedure involves flame-sealing the standards with CuO in a vacuum line system and combustion to CO_2 that was purified and transferred to glass ampoules in the next step on the same vacuum line system. The ^{14}C of these standards was analysed as gaseous samples using the miniaturized radiocarbon dating system (MICADAS) at the Laboratory of Ion Beam Physics, ETH Zürich (Ruff et al., 2007).

3.3.1. Case Study I: *n*-alkanoic Acid Samples – methods and results

To collect sufficient *n*-$C_{16:0}$ and *n*-$C_{28:0}$ alkanoic acid from standard material to permit isolation of multiple aliquots, about 2 g dried apple peel and about 10 g dried and homogenized Messel Shale were Soxhlet-extracted with dichloromethane (DCM): methanol (MeOH) 9:1 (v/v) at 60 °C for 48 hours and further processed by the method described in Mollenhauer and Eglinton (2007). Additionally, asphaltene precipitation was performed with the total lipid extract of the Messel Shale according to the protocol described in Weiss et al. (2000). The dried total lipid extracts were saponified with 0.1 N potassium hydroxide (KOH) in MeOH:H_2O 9:1 (v/v) at 80 °C for two hours. After the extraction of neutral compounds by *n*-hexane, the solution was acidified to pH=1. The acid fraction was extracted by DCM. Approximately 2 mg of the commercial standard *n*-$C_{30:0}$ alkanoic acid was processed following the same procedure as the extracted acid fraction from this step onwards. The acid fractions and *n*-$C_{30:0}$ alkanoic acid were then methylated with MeOH of known $F^{14}C$ value (0.001±0.000) to corresponding *n*-alkanoic acid methyl esters in 5 % HCl under N_2 atmosphere at 50 °C overnight. The *n*-alkanoic acid methyl esters were extracted into *n*-hexane and further eluted with DCM:*n*-hexane 2:1 (v/v) through silica gel column chromatography. The targeted *n*-$C_{16:0}$, *n*-$C_{26:0}$, *n*-$C_{28:0}$ and *n*-$C_{30:0}$ alkanoic acid methyl esters were purified and collected by preparative capillary gas chromatography (PCGC) following the methods described by Eglinton et al. (1996) and Kusch et al. (2010). The injection volume was 5 μl, and ~25-120 repeated injections were conducted to collect sufficient mass of individual standard approximately ~22-151 μgC. This covers a reasonable range of sample sizes, in which samples for CSRA may commonly occur (Table 3.1). The purity of these standards was checked by injecting a small aliquot of collected standards to a gas chromatograph coupled to a flame ionization detector (GC-FID).

Table 3.1. The measured m_{sample} and $F^{14}C_{sample}$ of standard compounds for the blank assessment for *n*-alkanoic acid methyl ester.

Standard compound	m_{sample} (μgC)	$F^{14}C_{sample}±σ(F^{14}C_{sample})$
fossil standard		

Unprocessed n-C$_{30:0}$ alkanoic acid methyl ester	n.a.	0.0003±0.0002
Processed n-C$_{30:0}$ alkanoic acid methyl ester	89.00±4.45[2015]	0.0400±0.0016[2015]
	63.00±3.15[2015]	0.0568±0.0028[2015]
	24.00±1.2[2014W]	0.1453±0.00338[2014W]
Processed n-C$_{28:0}$ alkanoic acid methyl ester	81.00±4.05[2017]	0.0220±0.0011[2017]
	32.00±1.60[2017]	0.0582±0.0018[2017]
	23.00±1.15[2017]	0.1833±0.0030[2017]
Processed n-C$_{26:0}$ alkanoic acid methyl ester	108.00±5.40[2017]	0.0685±0.0028[2017]
	75.00±3.75[2017]	0.0625±0.0019[2017]
modern standard		
Unprocessed n-C$_{16:0}$ alkanoic acid methyl ester	n.a.	0.9705±0.0036
	151.00±7.55[2014W]	0.9650±0.0078[2014W]
	136.00±6.80[2017]	0.9670±0.0061[2017]
Processed n-C$_{16:0}$ alkanoic acid methyl ester	119.00±5.95[2015]	0.9960±0.0015[2015]
	67.00±3.35[2015]	0.9442±0.0088[2015]
	44.00±2.20[2015]	0.9594±0.0068[2015]
	22.00±1.10[2014W]	0.9013±0.0083[2014W]

n.a.: not available. The superscript W refer to the data adopted from Winterfeld et al. (submitted for publication). The superscript numbers represent the years when the standards were prepared.

The measured m_{sample} and $F^{14}C_{sample}$ of the modern and fossil standards of this case study are listed in Table 3.1. The measured $F^{14}C_{sample}$ is plotted against $1/m_{sample}$ of the modern and fossil n-alkanoic acid methyl esters standards in Fig. 3.1. The true $F^{14}C$ values of modern and fossil n-alkanoic acid standards are assumed to be identical to the bulk organic carbon of apple peel and Messel Shale, respectively. In the course of the isolation procedure in the laboratory, n-alkanoic acids usually are methylated to n-alkanoic methyl esters in order to facilitate gas chromatography. Therefore, CSRA-data is obtained from the methyl esters and not from the pure n-alkanoic acids. This has to be acknowledged for the blank assessment. The methylation means that $F^{14}C_{sample}$ is affected by the $F^{14}C$ of the added methyl-group ($F^{14}C_{methyl}$) while the $F^{14}C_{true}$ (unprocessed equivalent, apple peel bulk, Messel Shale bulk values) is not. Hence, when determining the m_{blank} and $F^{14}C_{blank}$ as discussed above and shown in Fig. 3.1, the methyl group of the processed n-C$_{16:0}$ and n-C$_{26:0-30:0}$ methyl esters affects the slope of the regression lines. As a result, this would count towards the unknown blank. Combining the $F^{14}C_{methyl}$ value, with the $F^{14}C_{true}$ of the modern and fossil standard (bulk values of apple peel and Messel Shale) by isotopic mass balance yields the $F^{14}C_{true}$ of the respective methyl esters. The calculated value is set as the intercept for the regression lines as indicated in equation (3.3).
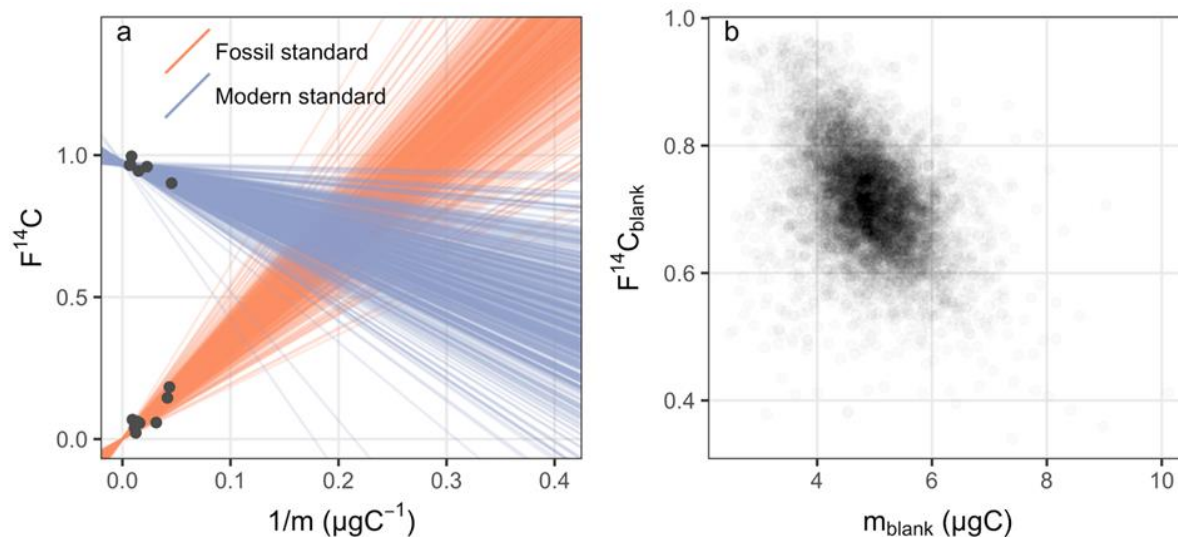
Figure 3.1. Procedural blank assessment for *n*-alkanoic acid methyl esters. (a) A sample of 500 regression lines from the posterior distribution give a visual check of the of the fitted Bayesian model. (b) The posterior distribution of masses and $F^{14}C$ values of the procedural blank.

It appears in Fig.3.1a that both standards display significant linear relationships between their measured $F^{14}C_{sample}$ and $1/m_{sample}$ as expected according to equation (3.3). Although the fossil standards include saturated *n*-alkanoic acid methyl esters with different chain lengths (n-C_{26}, n-C_{28} and n-C_{30}), their $F^{14}C_{sample}$ and $1/m_{sample}$ relationships are consistent. It is also worth noting that these fossil standards were actually processed at different times between 2014 and 2017. However, this did not influence the consistency in the linear relationship, which suggests that the procedural blank is relatively invariant with time. A sample from the posterior distribution of regression lines fitted with the Bayesian model are plotted in Fig. 3.1a. Fig. 3.1b shows the posterior distribution of masses and $F^{14}C$ values of the procedural blank, which are obtained from the pairwise intersection points of the regression lines. Using our Bayesian model, the m_{blank} and $F^{14}C_{blank}$ of the *n*-alkanoic acids and their uncertainties are estimated at $m_{blank}\pm\sigma(m_{blank})$ 4.88±0.69 μgC and $F^{14}C_{blank}\pm\sigma(F^{14}C_{blank})$ 0.714±0.077, respectively (Table 3.3).

3.3.2. Case Study II: Lignin Phenol Samples – methods and results

Vanillin from woodchips was extracted using the method of Goñi and Montgomery (2000). Briefly, about 10 g of woodchip were oxidized with copper oxide (CuO) and ferrous ammonium sulfate in de-aerated 2 N sodium hydroxide (NaOH) at 150 °C for 90 min under a nitrogen (N₂) atmosphere in CEM MARS5 microwave accelerated reaction system. After the oxidation, the supernatant was acidified to pH=1 and the reaction products were extracted into ethyl acetate. Approximately 3 mg of commercial standard ferulic acid were dissolved in ethyl acetate and processed as the extracted oxidation products according to the method of Feng et al. (2013).

Briefly, the extracts and the ferulic acid were both pre-cleaned with Supelclean ENVI-18 solid phase extraction (SPE) cartridges and eluted with acetonitrile. Subsequently, the vanillin from the extracts

and ferulic acid were further isolated by LC-NH$_2$ SPE cartridges and were eluted into MeOH and MeOH:12 N HCl 95:5 (v:v), respectively. The vanillin and ferulic acid were extracted from their elution with ethyl acetate and re-dissolved in MeOH for purification on prep-HPLC. The vanillin was then purified with a Phenomenex Synergi Polar-RP column followed by a ZORBAX Eclipse XDB-C18 column. The ferulic acid was purified with the same columns but in reverse order. The specific elution conditions on the prep-HPLC system can be found in Feng et al. (2013). ~ 20 repeated injections were conducted to collect sufficient mass of individual standard, which was divided into a range of sample sizes (Table 3.2). The purity of the collected standards was checked by injecting a small aliquot of the standard to GC-FID.

Table 3.2. The measured m_{sample} and F^{14}C$_{sample}$ of standard compounds for the blank assessment of lignin phenols (Sun et al., manuscript in preparation).

Standard compound	m_{sample} (μgC)	F^{14}C$_{sample}$±σ(F^{14}C$_{sample}$)
fossil standard		
Unprocessed ferulic acid	n.a.	0.0000
	83.00±4.15	0.0095±0.0013
	51.00±2.55	0.0076±0.0012
Processed ferulic acid	33.00±1.65	0.0110±0.0013
	13.00±0.65	0.0130±0.0016
	6.00±0.30	0.1446±0.0067
modern standard		
vanillin	70.00±3.50	1.2129±0.0115
vanillin	50.00±2.50	1.2007±0.0113
vanillin	29.00±1.45	1.2237±0.0120
vanillin	11.00±0.55	1.1875±0.0132
vanillin	6.00±0.30	1.1577±0.0234

n.a.: not available.

As is the case of blank assessment for n-alkanoic acid methyl esters, the measured m_{blank} and F^{14}C$_{blank}$ of a range of different sized modern and fossil lignin phenolic standards are listed in Table 3.2. The F^{14}C value of pure ferulic acid was measured as graphite target and assumed to be the F^{14}C$_{true}$, which is set as the intercept for the regression line of the fossil standard. Because the F^{14}C value of wood chips from which the vanillin was extracted is not available, the intercept of the regression line of modern standard (F^{14}C$_{true}$) is not set manually but produced statistically. The statistically produced value is assumed to be the F^{14}C$_{true}$ of vanillin. Similar to the lipid standards, the measured F^{14}C$_{sample}$ of both vanillin and ferulic acid are linearly related to the corresponding 1/m_{sample} (Fig. 3.2a). This suggest that the assumption of a constant procedural blank is also valid for the purification of lignin phenolic compounds. The posterior distribution of the masses and F^{14}C values of the procedural blank from the Bayesian model is shown in Fig. 3.2b. The m_{blank} and F^{14}C$_{blank}$ value of the procedural blank during CSRA of lignin phenolic compounds are estimated at 0.90±0.23 μgC and 0.813±0.155, respectively (Table 3.3).
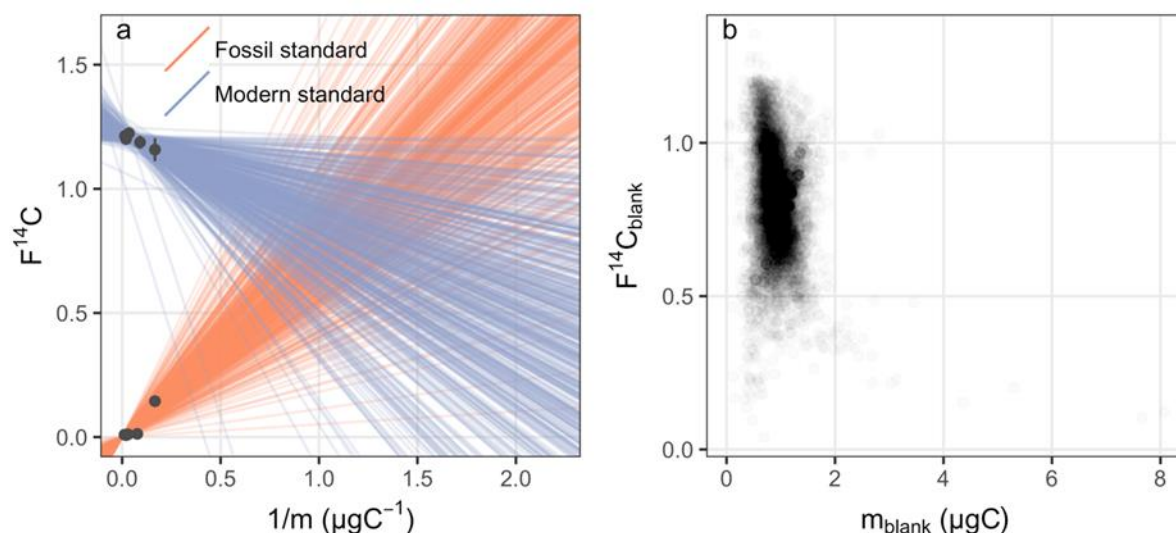
Figure 3.2. Procedural blank assessment for lignin phenols. (a) A sample of 500 regression lines from the posterior distribution give a visual check of the of the fitted Bayesian model. (b) The posterior distribution of masses and F^{14}C values of the procedural blank.

Table 3.3. Estimated values of m_{blank} and F^{14}C$_{blank}$

Blanks	Parameter	mean	sd	median	MAD
Blank of *n*-alkanoic acid	F^{14}C$_{blank}$	0.716	0.083	0.714	0.077
	m_{blank} (µgC)	4.898	0.746	4.881	0.691
Blank of lignin phenols	F^{14}C$_{blank}$	0.809	0.166	0.813	0.155
	m_{blank} (µgC)	0.927	0.291	0.905	0.229

3.4. Case studies-discussion

From our two case studies, it can be seen that we were able to obtain statistically robust estimates of the mass and F^{14}C value of the procedural blank (i.e. small uncertainties in both variables), despite requiring a long extrapolation of the regression lines to the intersection point. This also suggests that much smaller uncertainties could be obtained if small sized samples with masses close to the intersection point (mass of the blank) are available because this will shorten the extrapolation distance. Therefore, the smallest sample sizes of the set of standards should be go as small as possible to shorten the extrapolation distance, which will get better estimate of m_{blank} and F^{14}C$_{blank}$.

The mass and F^{14}C values of procedural blanks for *n*-alkanoic acid methyl esters and lignin phenolic compounds can be further applied to correct for the F^{14}C values of the real samples. The F^{14}C of the procedural blank (0.714±0.077 or Δ^{14}C=-292±71 ‰) for *n*-alkanoic acid methyl esters is similar to the procedural blank assessed in the study of Tao et al. (2015) (Δ^{14}C=-325±129 ‰), in which a similar sample preparation protocol was applied. In Tao et al. (2015), the mass of the combined procedural

51

blank was determined to be 1.3±0.2 μgC per 30 PCGC injections, which means that these authors assumed the procedural blank varies with the sample size rather than a constant procedural blank.

The larger procedural blank for *n*-alkanoic acid methyl esters (4.88±0.69 μgC) means for this case, the results of small size samples (e.g. <15 μgC) are meaningless due to a high proportion of contaminant carbon (~30 %). Compared to the preparation process of *n*-alkanoic acid methyl esters, our preparation of CSRA for lignin phenols introduced a lower amount of procedural blank (0.90±0.23 μgC). Although the masses of procedural blank in preparation of lignin phenols and *n*-alkanoic acid methyl esters are different, their $F^{14}C$ values are identical within errors. This implies that the blank introduced by the two different protocols has the same composition and source but varies in size.

We use the same vacuum line system for both *n*-alkanoic acid methyl esters compounds and lignin phenols. The difference in the preparation for these two types of compounds is the chemical extraction, cleaning and isolation methods prior to vacuum line handling, i.e. solvent extraction and PCGC for *n*-alkanoic acid methyl esters and alkaline CuO oxide digestion and solvent extraction followed by prep-HPLC for lignin phenols. The mass difference of the blank for these two compound classes might derive from any step or the combination effect of several steps.

According to the results of these two case studies, our approach of blank assessment is successfully applied for *n*-alkanoic acid methyl esters and lignin phenols that require different isolation methods. It demonstrates that this blank assessment method can further be applicable for other compounds and various preparation protocols. Unlike the methods considering modern or fossil procedural blank separately and assessing contamination introduced from different preparation steps, our method is not difficult to achieve and reduces the complexity in the calculation of uncertainty. Therefore, this method has the potential to serve as a simple and widely applied approach for blank assessment. We propose to routinely conduct blank assessment for different batches of samples and different compounds-classes to ensure the accuracy and precision of $F^{14}C$ values of real samples, especially of small sizes (<100 μgC).

3.5. Conclusion

Based on our methods of blank assessment, we observe that our preparation protocol of radiocarbon analysis of *n*-alkanoic acid and lignin phenols will produce 4.88±0.69 μg of extraneous carbon with $F^{14}C$ of 0.714±0.077 and 0.90±0.23 μg of extraneous carbon with $F^{14}C$ of 0.813±0.155, respectively. The $F^{14}C$ of the procedural blanks for both biomarkers are similar, but the mass of the procedural blank of *n*-alkanoic acid is five times larger than that for lignin. This discrepancy is probably due to different chemical cleaning and isolation methods prior to preparation on vacuum line system and highlights the necessity to conduct blank assessment for different compounds and preparation procedures. The method

proposed in this study is not time consuming or labour intensive, and it is worth extending to other biomarkers and may serve as a standardized method for blank assessment.

Data and supplementary material. The data and supplementary material presented here are available on the Pangaea database (https://doi.pangaea.de/10.1594/PANGAEA.892180).

Author contributions

Shuwen Sun and Vera Meyer performed most of the sample processing in the laboratory and on the vacuum line. They did the calculations for the blank assessment and wrote the manuscript with contributions from all co-authors. They contributed equally to the study and share the first authorship. Andrew Dolman provided the R and Stan code for the Bayesian model and performed the statistical analysis. All authors were involved in the discussions about the blank-assessment approach and contributed to writing the manuscript. Gesine Mollenhauer drafted the idea of this approach. Jens Hefter, Daniel B. Montluçon and Tessa van der Voort helped isolating the compounds on PCGC and prep HPLC. Maria Winterfeld and Wolf Dummann processed some samples and were involved in the calculations for the blank assessment. Cameron McIntyre, Lukas Wacker and Negar Haghipour conducted the AMS analysis at ETH Zürich. Torben Gentz measured the $F^{14}C$ of bulk OC of Messel Shale.

4. Manuscript III:

Processing and fate of terrestrial particulate organic carbon transported through the Amazon system: [14]C composition of higher plant biomarkers

Shuwen Sun[1, 2, 3], Enno Schefuß[2], Timothy I. Eglinton[4], Stefan Mulitza[2], Cristiano M. Chiessi[5], André. O. Sawakuchi[6], Christoph Häggi[2], Tessa S. van der Voort[4], Daniel B. Montluçon[4], Negar Haghipour[4,7], Jens Hefter[3], Gesine Mollenhauer[1, 2, 3]

[1]Department of Geosciences, University of Bremen, 28359 Bremen, Germany

[2]MARUM-Center for Marine Environmental Sciences, University of Bremen, 28359 Bremen, Germany

[3]Alfred Wegener Institute, Helmholtz Centre for Polar and Marine Research, 27570 Bremerhaven, Germany

[4]Geological Institute, Department of Earth Sciences, ETH Zürich, 8092 Zürich, Switzerland

[5]School of Arts, Sciences and Humanities, University of São Paulo, 03828-000 São Paulo, Brazil

[6]Institute of Geosciences, Department of Sedimentary and Environmental Geology, University of São Paulo, 05508-080 São Paulo, Brazil

[7]Department of Physics, Laboratory of Ion Beam Physics, ETH Zürich, 9083 Zürich, Switzerland

Abstract. Assessing the composition and age of terrestrial organic carbon (OC) buried in continental margins is essential for understanding its origin and transformations before deposition in marine sediments. In order to comprehensively characterize sources and pre-depositional histories of terrestrial OC in the Amazon system, we employ radiocarbon dating of bulk OC and source-specific biomarkers (*n*-alkanoic acids and lignin phenols) in riverbed sediments from the lowland Amazon basin and offshore sediments. We find that Δ14C values of terrestrial OC on the Amazon continental margin are substantially influenced by matrix association effects, where terrestrial OC associated with the finer-grained particles is better preserved and more resistant to decomposition during residence in intermediate reservoirs. The compound-specific Δ14C values imply that as expected short-chain *n*-alkanoic acids represent recently biosynthesized organic matter from riverine or marine primary production whereas both long-chain *n*-alkanoic acids and lignin phenols used as markers for land vegetation have pre-aged in soils where they resided attached to mineral surfaces. By using a ternary mixing model, we obtain a well-constrained quantitative estimate of the composition of sedimentary OC in riverbed and marine sediments. Despite the variable composition of sedimentary OC in the Amazon system, the burial of fossil rock-derived OC is relatively constant. Derived from the absolute content of bulk terrestrial OC, the sediment-normalized lignin yields, long-chain *n*-alkanoic acids and their 14C ages, we estimate the half-lives of bulk terrestrial OC, lignin and long-chain *n*-alkanoic acids during transport to be about 2310 years, 13860 and 470 years, respectively. This suggests that the

preservation of terrestrial OC in the mud belt on the Amazon shelf is more efficient than previously assumed.

4.1. Introduction

Rivers are major links between continental and oceanic carbon reservoirs. The annual contribution of river-borne terrestrial particulate organic carbon (POC) to the oceans is about 200 Tg (Galy et al., 2007, 2015; Ludwig et al., 1996; Schlünz and Schneider, 2000). During the transport from river catchments to the oceans, terrestrial organic carbon (OC) experiences various physical and biogeochemical processes before deposition together with autochthonous marine OC. It is estimated that about 55-80 % of the fluvially transported terrestrial OC is remineralized after being exported to the oceans (Burdige, 2005). The remaining terrestrial OC is primarily buried in the deltaic regions and on the inner continental shelves and becomes a critical component of the global carbon cycle (Hedges and Keil, 1995). Terrestrial OC contains OC originating from different sources (such as plant debris, soils and petrogenic OC), which vary in reactivity and age (Hedges and Keil, 1995). These constituents have their own pre-depositional histories and abilities to resist the multiple processes of sediment transport and early diagenesis until deposition. Thus, a quantitative assessment of the surviving and remineralized fractions of the terrestrial OC in continental drainage basins and adjacent marine sediments is crucial for understanding the fate of terrestrial OC.

Combinations of isotopic mass balance, radiocarbon (Δ^{14}C) and/or stable carbon (δ^{13}C) isotopic compositions have been used to provide source apportionments and temporal constraints on the sedimentary organic matter transport (Cathalot et al., 2013; Komada et al., 2005; Vonk et al., 2015; Wu et al., 2013). The development of compound-specific Δ^{14}C and δ^{13}C analysis of organic compound classes has provided a tool to better constrain the provenance and residence time of sedimentary OC at the molecular level. This is a more powerful and detailed method than the approach at the bulk level (Eglinton et al., 1996; Goñi and Eglinton, 1996). Compound-specific Δ^{14}C and/or δ^{13}C analysis have been successfully applied in several studies to characterize the composition of terrestrial OC in a variety of environments, such as rivers (e.g., Galy et al., 2011) and soils (van der Voort et al., 2017). For example, the compositions of OC in the Yellow River suspended load and the marine sediments in the Bohai Sea and Yellow Sea have been investigated based on the Δ^{14}C and δ^{13}C values of biomarkers specific to modern autochthonous OC, pre-aged soil OC, and petrogenic OC, respectively (Tao et al., 2015, 2016). Δ^{14}C values of various terrestrial biomarkers (e.g. plant wax lipids, cutin, lignin) have been measured in riverbed sediments of major rivers across Arctic watersheds to distinguish the sources and fates of terrestrial OC from various pools (Feng et al., 2015). By combining the initial ^{14}C ages of leaf-wax n-alkanes and n-alcohols and their hydrogen stable isotope compositions in a sedimentary archive offshore the Congo River, Schefuß et al. (2016) were able to show the effect of continental hydrologic changes on terrestrial OC release.

Better constraints on sources and ages of sedimentary OC not only provide knowledge about major components of the global carbon budget but are also important for quantifying the efficiency and understanding the diagenetic state of terrestrial carbon cycling. The rate and efficiency of terrestrial OC cycling differs between climatic regions. For instance, in the Amazon system, young and labile carbon pools were found to drive the outgassing of carbon dioxide, which suggests rapid cycling of contemporary OC pools (Mayorga et al., 2005). In contrast, old terrestrial OC was found to be the dominant source of respiration in temperate lakes and streams in Quebéc, which indicates fast degradation of old terrestrial OC (McCallister and Paul, 2012). From a global perspective, it has been demonstrated that the decay rate of OC during transport from land to ocean is negatively related to water retention times (Catalán et al., 2016). Despite numerous studies on the carbon dynamics, it is still difficult to define the efficiency of terrestrial OC cycling in different regions and systems, because the estimates of decay rate of terrestrial OC were based on different assumptions, used different quantitative approaches and time constraints. Therefore, improved estimates of losses of terrestrial OC and the corresponding time constraints are needed to develop a decay model for predicting the terrestrial OC cycling efficiency and identifying the main controlling parameters on terrestrial OC cycling.

Tropical ecosystems are of particular interest because they are the most productive ecosystems (about 15.3 Gt C yr^{-1}) on Earth and act as important reservoirs of terrestrial OC (Killops and Killops, 2005). Moreover, tropical rivers serve as the major pathways of terrestrial OC to the oceans (up to about 60 % of the global terrestrial OC discharge) and integrate various biogeochemical processing of terrestrial OC within river networks (Meybeck, 1982). In spite of their global relevance, a lack of knowledge on residence times of terrestrial OC and drivers of terrestrial OC cycling in tropical regions persists. As an important conduit between the Amazon tropical forest, flood plain lakes and the Atlantic Ocean OC reservoirs, the Amazon River is of global relevance for terrestrial OC cycling. The contribution of terrestrial OC transported by the Amazon River accounts for 8-10 % of the global terrestrial OC flux to the oceans (Kim et al., 2012; Moreira-Turcq et al., 2003). A variety of biomarkers (e.g. lignin, plant wax lipids and GDGTs) have been studied to investigate the origins and composition of terrestrial OC suggesting that C3 plants from the lowland Amazon basin are the major plant sources of the terrestrial OC in the Amazon system (Häggi et al., 2016; Kim et al., 2012; Sun et al., 2017). In addition to biomarkers, many previous studies have also applied Δ^{14}C and δ^{13}C analyses to characterize the terrestrial OC in the Amazon system. Δ^{14}C and δ^{13}C analyses of POC indicate that the absolute content of petrogenic carbon is invariant in the lowland Amazon basin, and may account for a substantial proportion of terrestrial OC in offshore sediments (Bouchez et al., 2010, 2014). Ramped pyrolysis Δ^{14}C analysis has been employed to constrain terrestrial OC on the Amazon shelf, which suggests efficient preservation of refractory pre-aged terrestrial OC in marine sediments (Williams et al., 2015). Several studies employing compound-specific radiocarbon analysis in other regions, e.g., Fiordland fjords in New Zealand and Eurasian Arctic river basins, have shown that lignin displays higher Δ^{14}C values than

long-chain n-alkanoic acids, although they both predominantly originate from the same initial source, i.e. terrestrial vascular plants (Cui et al., 2017; Feng et al., 2013b). This discrepancy is interpreted as the consequence of the contribution from different soil layers via various transport pathways. Specifically, lignin is dominantly supplied from young plant debris in surface layers and introduced into rivers by surface runoff. Unlike lignin, long-chain n-alkanoic acids are thought to be rather associated with mineral surfaces and leached from deeper soil layers (Cui et al., 2017; Feng et al., 2013b; van der Voort et al., 2017). As the Amazon River drains a large tropical hinterland with different hydroclimatic processes than the Fiordland fjords and the Eurasian Arctic river basins, the release and transport of terrestrial OC in the Amazon basin might exhibit its own pattern imprinted on the $\Delta^{14}C$ values of compounds deriving from specific origins. So far, however, $\Delta^{14}C$ analyses in most previous studies addressing OC cycling the Amazon system were based on bulk OC.

In order to determine residence times of specific compounds and obtain insights on the efficiency of the terrestrial OC cycling, we analyse compound-specific $\Delta^{14}C$ data of higher plant biomarkers in riverbed sediments from the lowland Amazon basin and in marine surface sediments from the adjacent offshore area along with $\Delta^{14}C$ of bulk OC. The sources and compositions of sedimentary OC in the Amazon system are quantitatively constrained based on diagnostic $\Delta^{14}C$ and $\delta^{13}C$ signatures deriving from different OC pools. In addition, we estimate the decay rate of terrestrial OC during the transport from the lowland Amazon basin to the offshore area based on the spatial distribution of $\Delta^{14}C$ values and absolute content of terrestrial OC.

4.2. Study area

The Amazon River is the largest river on Earth in terms of water discharge and drainage basin size, with an average annual water discharge of 2×10^5 m^{3}s^{-1} (Callède et al., 2000; Guyot et al., 2007) and a catchment area of about 6.1×10^6 km^2 (Guyot et al., 2007). Originating from the source tributaries (Ucayali and Marañon Rivers) in south-eastern Peru, the Amazon River flows eastward from the Andes through the lowland Amazon floodplain and finally discharges into the Atlantic Ocean (Guyot et al., 2007) (Fig. 4.1). The Amazon watershed consists of numerous tributaries that can be roughly classified into three types based on their colour, which correspond to physical and chemical water properties. The Solimões and the Madeira Rivers (draining the fast weathering Andean region) are typical white water rivers, characterized by high concentrations of suspended sediments and dissolved nutrients (Gibbs, 1967). Black water rivers (e.g. the Negro River) have high levels of chromophoric dissolved organic matter and are depleted in suspended sediments (Mounier et al., 1999). Clear water rivers (e.g. the Xingu River) typically have high phytoplankton productivity but low suspended sediment load and low content of dissolved chromophoric dissolved organic matter compared to the black and white water rivers (Junk, 1997; Richey et al., 1990). An annual discharge of about 40 Tg OC ranks the Amazon River the largest fluvial source of terrestrial OC to the ocean (Moreira-Turcq et al., 2003). When sea

level is high during interglacial periods (e.g., Holocene), the terrigenous sediments from the Amazon River are advected north-westward by the North Brazil Current (NBC) and predominantly deposited on the inner shelf along the northern South American coastline, forming the 1600-km long Amazon-Guianas subaqueous mud belt (Geyer et al., 1996; Nittrouer and DeMaster, 1996; Schlünz et al., 1999).

In regions beyond the inner shelf (i.e., on the continental margin), Amazonian sedimentation is low during interglacial periods. The fluid mud in the Amazon-Guianas subaqueous mud belt is continuously influenced by tides and waves, and the deposits are consequently constantly resuspended and remobilized. In this environment, the sedimentary OC is repetitively exposed to oxic or suboxic conditions that promote "incineration" of organic matter (Aller and Blair, 2006; Hedges and Keil, 1995).
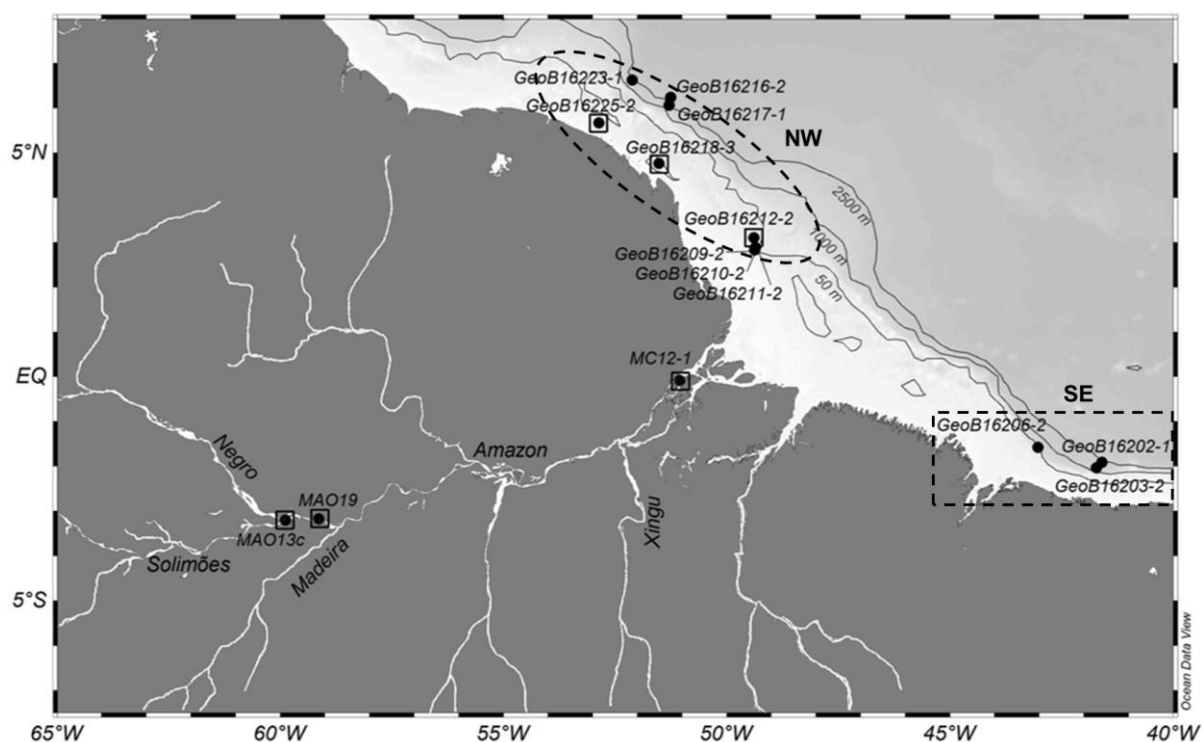
Figure 4.1. Map of the lowland Amazon basin and the offshore area with sample locations. Samples used for compound-specific Δ^{14}C analysis are indicated by rectangles. The map was created using Ocean Data View 4.7.10 (Schlitzer, 2017). The dashed ellipse and rectangle represent the north-west sector (NW) and the south-east sector (SE), respectively.

4.3. Material and analytical methods

4.3.1. Sample collection

Riverbed sediment samples were collected with a Van Veen grab sampler in November 2011 and May 2012. Marine surface sediments from the Amazon continental margin were recovered with a multicorer during the *R/V Maria S. Merian* cruise MSM 20/3 in February/March 2012 (Mulitza et al., 2013). Sampling sites are listed in Table 4.1 and displayed in Fig. 4.1. Detailed information about the sampling sites and processing of riverbed and marine surface sediments can be found in Häggi et al. (2016) and Sun et al. (2017). The results for contents of total organic carbon (TOC), stable carbon isotopic ratios

of TOC ($\delta^{13}C_{TOC}$), aluminium to silicon ratios (Al/Si), as well as concentrations and compositions of lignin have been reported and discussed in detail in Häggi et al. (2016) and Sun et al. (2017).

4.3.2. Extraction and purification of compounds for radiocarbon measurement

4.3.2.1. Extraction and purification of *n*-alkanoic acids

Dried and homogenized samples were processed for compound-specific radiocarbon measurement of *n*-alkanoic acids in accordance with the methods described by Mollenhauer and Eglinton (2007). MC12-1 (32 g), GeoB16212-2 (31 g), GeoB16218-3 (11 g) and GeoB16225-2 (55 g) were Soxhlet-extracted with dichloromethane (DCM): methanol (MeOH) 9:1 (v/v) at 60 °C for 48 hours. MAO19 (13 g) and MAO13c (15 g) were ultrasonically extracted three times for 15 minutes with DCM: MeOH 9:1 (v/v). After removing the solvent by rotary evaporation, the total extracts were saponified with 0.1 N potassium hydroxide (KOH) in MeOH: H_2O 9:1 (v/v) at 80 °C for two hours. The neutral fraction was liquid-liquid extracted into hexane. The remaining solution was acidified to pH=1 by adding Seralpure water and 12 N hydrochloric acid (HCl), and the acid fraction was extracted into DCM. MeOH of known ^{14}C composition and about 5 % HCl were added to the acid extracts and the *n*-alkanoic acids were methylated to corresponding *n*-alkanoic acid methyl esters under N_2 atmosphere at 50 °C overnight. After methylation, Seralpure water was added and the *n*-alkanoic acid methyl esters were extracted into hexane. The *n*-alkanoic acid methyl esters were further separated by silica gel column chromatography and eluted with DCM: hexane 2:1 (v/v).

In order to purify the target compounds, the extracted *n*-alkanoic acid methyl esters were isolated and collected by preparative capillary gas chromatography (PCGC). Aliquots of 5 µL of the FAME-fraction in hexane were repeatedly (24-38 times) injected via a Gerstel CIS 4 in solvent vent mode and into an Agilent 6890N gas chromatograph. The inlet was equipped with a deactivated, baffled glass liner (70 mm x 1.6 mm i.d.), set to an initial temperature of 60°C and heated to 320°C at 12°C s^{-1} and a final hold time of 2 min. For compound separation, the GC was equipped with a Restek Rxi-XLB capillary column (30 m, 0.53 mm i.d., 0.5 µm film thickness). The GC was operated using Helium as carrier gas at a constant flow of 4 mL min^{-1}. After an initial time of 2 min at 60°C, the oven was heated with 20° min^{-1} to 150°C and with 8°C min^{-1} to 320°C, with a final hold time of 6 min. A zero dead volume splitter diverted 1 % of the column effluent via a restriction control capillary to a flame ionization detector (FID), whereas the remaining 99 % were transferred to a Gerstel preparative fraction collector (PFC). The PFC was connected via a heated fused silica transfer capillary to the GC and set to 320°C. The switching device, directing the column effluent into seven time-programmable individual traps, was also set to 320°C. After trapping, the target compounds were recovered by rinsing the traps with 5 x 500 µL hexane.

From our samples, *n*-C_{16}, *n*-C_{18}, *n*-C_{24}, *n*-C_{26}, *n*-C_{28}, and *n*-C_{30} alkanoic acid methyl esters were collected. A split of collected *n*-alkanoic acid methyl esters was injected to an Agilent 7890A GC-FID equipped

with Agilent J&W DB-5ms column (60 m×0.25 mm i.d., 0.25 μm film thickness) to quantify and check the purity. The *n*-alkanoic acid methyl esters were recombined to short-chain (n-C_{16+18}) and long-chain (n-$C_{24+26+28+30}$) alkanoic acid methyl esters groups to obtain sufficient carbon for radiocarbon analysis. The combined short-chain (n-C_{16+18}) and long-chain (n-$C_{24+26+28+30}$) alkanoic acid methyl esters are used to reflect aquatic and vascular plant inputs, respectively.

4.3.2.2. Extraction and purification of lignin phenols

The extraction and purification of lignin phenols for radiocarbon analysis followed the method described by Feng et al. (2013a). The solvent extracted sediment residues (see above) were dried and hydrolysed with 1 N KOH in MeOH at 100 °C for three hours to remove hydrolysable lipids (Otto and Simpson, 2005, 2006). The remaining sediments after the hydrolysis were divided equally to one to five vessels (6-12 g sediments in each vessel) and oxidized with copper oxide (CuO) (4 g) and ferrous ammonium sulfate (0.6 g) in de-aerated 2 N sodium hydroxide (NaOH) (20 ml) at 150 °C for 90 min under a nitrogen (N_2) atmosphere in a CEM MARS5 microwave accelerated reaction system (Goñi and Montgomery, 2000). After the oxidation, the alkaline supernatant was transferred and acidified to pH 1, and the reaction products were extracted into ethyl acetate. Traces of water remaining in ethyl acetate were removed by Na_2SO_4. The ethyl acetate was evaporated under N_2 close to dryness.

The extracts were first pre-cleaned with a Supelclean ENVI-18 solid phase extraction (SPE) cartridge (Supelco, 1 g), through which part of the undesired compounds were absorbed on the stationary phase while phenolic compounds were eluted with acetonitrile. The phenolic compounds were further separated on Supelclean LC-NH_2 SPE cartridges (Supelco, 0.5 g). The lignin phenols with aldehyde and ketone groups, i.e. vanillin (Vl), syringaldehyde (Sl), acetovanillone (Vn) and acetosyringone (Sn) were eluted with MeOH and the lignin phenols with acid groups, i.e. vanillic acid (Vd), syringic acid (Sd), *p*-coumaric acid (*p*-Cd) and ferulic acid (Fd) were subsequently rinsed out with MeOH: 12 N HCl 95:5 (v:v). The lignin phenols were extracted from these two fractions with ethyl acetate and re-dissolved in MeOH. These pre-separated lignin phenols of interest were isolated by preparative high-performance liquid chromatography (prep-HPLC), using an Agilent 1200 HPLC with a diode array detector (DAD) and a fraction collector unit. The lignin phenols in the aldehyde and ketone fraction were purified with a Phenomenex Synergi Polar-RP column (4.6×250 mm, 4 μm particle size) coupled with a Polar–RP guard column (4.0×3.0 mm, 4 μm particle size) followed by further purification with a ZORBAX Eclipse XDB-C18 column (4.6×160 mm, 4 μm particle size) coupled with a ZORBAX Eclipse C18 guard column (4.6×12.5 mm, 5 μm particle size). The lignin phenols in the acid fraction were purified with identical columns but in a reversed order. The specific settings for the prep-HPLC system were given in detail by Feng et al. (2013a). Aliquots of collected lignin phenols were derivatized with bis-trimethylsilyl-trifluoroacetamide (BSTFA) +1 % trimethylchlorosilane (TMCS) and injected to GC-FID for quantification and to check the purity.

4.3.3. Radiocarbon analysis

4.3.3.1. Radiocarbon analysis of TOC

Dried and homogenized sediments were fumigated with 12N HCl at 60 °C for 72 hours to remove carbonates (Komada et al., 2008). Samples were subsequently heated with solid NaOH at 60 °C for 72 hours to remove excess acid and dry the samples. The ^{14}C compositions of TOC were determined from gaseous CO_2 introduced to a MICADAS accelerator mass spectrometer (AMS) coupled with an elemental analyser at the Laboratory of Ion Beam Physics, ETH Zürich (McIntyre et al., 2016; Ruff et al., 2010; Wacker et al., 2010). Oxalic acid II (NIST-SRM-4990C) and ancient carbon dioxide were used for the calibration and blank correction for the ^{14}C measurements.

4.3.3.2. Radiocarbon analysis of biomarkers

Individual purified *n*-alkanoic acid methyl esters and lignin phenols were flame-sealed with pre-combusted CuO in pre-combusted quartz tubes (850 °C, 5 h) under vacuum conditions. The sealed quartz tubes were heated at 850 °C for 5 hours to oxidize organic compounds to CO_2. The CO_2 was cryogenically dried and quantified on the vacuum line and subsequently transferred to glass ampoules (63 mm× 4 mm o.d.) that fit the ampoule cracker unit connected to the MICADAS. Samples that contained less than 15 μg C (estimated by GC-FID quantification) were directly flame-sealed in 4 mm o.d. quartz ampoules and combusted with CuO (850 °C, 5 h), i.e. the step of cryogenic drying and quantification of CO_2 on the vacuum line was omitted for small samples. The gaseous ^{14}C measurements were performed by the MICADAS AMS system equipped with a gas inlet system at the Laboratory of Ion Beam Physics, ETH Zürich (Ruff et al., 2007). The calibration and blank correction for the AMS data were conducted with the same standards used for radiocarbon analysis of TOC.

4.3.3.3. Data report and blank correction

^{14}C composition is reported as fraction modern carbon ($F^{14}C$), conventional radiocarbon age (^{14}C age) and $\Delta^{14}C$ value according to the conventions of Reimer et al. (2004) and Stuiver and Polach (1977).

The procedural blank for compound-specific ^{14}C analysis was estimated by analysing a series of modern and radiocarbon dead (fossil) standards (Sun et al., submitted). *n*-C_{16} alkanoic acid (extracted from apple peel) and *n*-C_{30} alkanoic acid (Sigma, Prod. No.T3527-100MG, Lot 018K3760, Rethemeyer et al., 2013) were methylated to corresponding *n*-alkanoic acid methyl esters and purified with the procedure described in section 4.3.2.1 and used as the modern and fossil standards for *n*-alkanoic acid methyl esters, respectively. Vanillin (extracted from wood chips) and ferulic acid (Aldrich, Prod. No.12,870-8, Lot STBB6360) were isolated with the procedure described in section 4.3.2.2 and represent the modern and fossil standards for lignin phenols. The amount and ^{14}C composition of the procedural blank contributions were indirectly assessed based on the method developed by Sun et al. (submitted). Briefly, the mass and $F^{14}C$ of the procedural blank were determined by the intersection point of the linear regression lines of different sizes of modern and fossil standards. The linear regression lines

were yielded with a Bayesian model to take the analytical error of each standard into account. A detailed description of the blank assessment and correction is given in the supplementary material. The ^{14}C compositions of n-alkanoic acid methyl esters and lignin phenols are calculated after the correction for the blank carbon using an isotopic mass balance. ^{14}C compositions of n-alkanoic acid methyl esters are further corrected for the methyl group carbon added during methylation to obtain the ^{14}C compositions of n-alkanoic acids. The ^{14}C composition of lignin is calculated as weighted average based on the abundance of individual lignin phenols.

4.4. Results

4.4.1. Radiocarbon data of TOC

The ^{14}C compositions of TOC are shown in Table 4.1. Riverbed sediments and marine surface sediments exhibit a relatively wide range of ^{14}C compositions between $\Delta^{14}C$ -457.8±6.5 ‰ and -64.1±10.2 ‰, which correspond to conventional ^{14}C ages from 4860±100 to 470±90 years before present (yr BP). Riverbed sediments show slightly lower $\Delta^{14}C$ values of TOC ($\Delta^{14}C_{TOC}$) (-133.6±13.9 ‰ to -91.4±13.9 ‰) compared to marine surface sediments in the south-east sector (SE) (-112.5±9.8 ‰ to -64.1±10.2 ‰). The distribution of $\Delta^{14}C_{TOC}$ values of marine surface sediments is shown in Fig. 4.2. The lowest $\Delta^{14}C_{TOC}$ value was obtained at station GeoB16210-2, located in the north-west sector (NW) near the Amazon River mouth and has the lowest TOC value (Table 4.1, Fig. 4.1). The highest $\Delta^{14}C_{TOC}$ value was detected at station GeoB16203-2 in the far SE sector, where a relatively high $\delta^{13}C_{TOC}$ value was found. The marine surface sediments from the NW sector exhibit lower and more variable $\Delta^{14}C_{TOC}$ values (-457.8±6.5 ‰ to -138.1±9.6 ‰) than the SE sector. For marine surface sediments, $\Delta^{14}C_{TOC}$ and $\delta^{13}C_{TOC}$ values are positively correlated (r^2=0.69, p<0.05, n=11) (Fig. 4.3).

4.4.2. Radiocarbon data of n-alkanoic acids

The ^{14}C compositions of short- and long-chain n-alkanoic acids are displayed in Table 4.2. Riverbed sediments in station MAO19 located in the mainstream of the Amazon River (Fig. 4.1) displays the highest $\Delta^{14}C$ values of both n-C_{16+18} alkanoic acids (-18.5±11.9 ‰) and n-$C_{24+26+28+30}$ alkanoic acids (-147.5±8.9 ‰) compared to other samples. Riverbed sediments from station MAO13c from the Solimões River and MC12-1 from the Amazon River mainstream near the mouth show lower $\Delta^{14}C$ values for n-$C_{24+26+28+30}$ alkanoic acids than riverbed sediments from station MAO19. The $\Delta^{14}C$ values of n-C_{16+18} alkanoic acids in marine surface sediments are lower than in MAO19. The lowest $\Delta^{14}C$ values of n-C_{16+18} alkanoic acids (-84.0±22.8 ‰) and n-$C_{24+26+28+30}$ alkanoic acids (-366.9±47.6 ‰) are both observed in marine surface sediments from station GeoB16218-3, which is located far away from the Amazon River mouth. Compared to n-C_{16+18} alkanoic acids, n-$C_{24+26+28+30}$ alkanoic acids in all samples are consistently lower in $\Delta^{14}C$ values. The $\Delta^{14}C$ values of n-C_{16+18} alkanoic acids and n-$C_{24+26+28+30}$ alkanoic acids in marine surface sediments are generally lower than those in riverbed sediments.

4.4.3. Radiocarbon data of lignin

The ^{14}C compositions of lignin are reported as weighted averages of individual lignin phenols in Table 4.2. The ^{14}C compositions of individual lignin phenols are shown in Table S4.4 in the supplementary information. Similar to the n-C$_{24+26+28+30}$ alkanoic acids, the highest and lowest Δ^{14}C values of lignin are observed in stations MAO19 (-103.3$\pm$13.8 ‰) and GeoB16218-3(-406.7$\pm$8.2 ‰), respectively. The Δ^{14}C values of lignin in marine surface sediments (-406.7 ‰ to -238.9 ‰) tend to be slightly lower than those detected in riverbed sediments (-265.8 ‰ to -103.3 ‰). The Δ^{14}C values of lignin are highly correlated to the corresponding Δ^{14}C values of n-C$_{24+26+28+30}$ alkanoic acids (r^2=0.93, p<0.05, n=5).

Table 4.2. New total organic carbon radiocarbon data and published geochemical data of the riverbed and marine surface sediments by Häggi et al. (2016) and Sun et al. (2017).

Sample	Long	Lat	Water[H] depth (m)	TOC[H, S] (%)	$\delta^{13}C_{TOC}$[S] (‰)	$\Lambda 8$[S] (mg/100mg OC)	$(Ad/Al)_V$[S]	Al/Si[H, S]	TOC F[14]C	TOC Δ^{14}C (‰)	TOC ^{14}C age (yr BP)
Riverbed
MAO13c	-59.88	-3.20	9	0.77	-28.4	6.44	0.28	0.37	0.873±0.014	-133.6±13.9	1090±130
MAO19	-59.13	-3.18	12	1.00	-29.4	4.22	0.48	0.37	0.916±0.014	-91.4±13.9	710±125
MC12-1*	-51.05	-0.08	20	1.01	-28.1	7.20	0.42	0.36	n.a.	n.a.	n.a.
South-east Sector
GeoB16202-1	-41.59	-1.91	2247	0.47	-18.6	0.06	0.50	0.37	0.917±0.009	-90.3±8.9	700±80
GeoB16203-2	-41.72	-2.04	1590	0.75	-19.1	0.08	0.51	0.41	0.943±0.010	-64.1±10.2	470±90
GeoB16206-2	-43.02	-1.58	1367	0.55	-18.9	0.07	0.59	0.39	0.894±0.010	-112.5±9.8	900±90
North-west Sector
GeoB16209-2	-49.37	2.83	24	0.11	-23.2	0.19	0.64	0.15	0.688±0.007	-316.9±7.0	3000±90
GeoB16210-2	-49.36	2.87	40	0.11	-24.1	0.39	0.50	0.17	0.546±0.006	-457.8±6.5	4860±100
GeoB16211-2	-49.35	2.88	64	0.18	-24.1	1.08	0.46	0.22	0.596±0.007	-409.0±6.7	4160±100
GeoB16212-2	-49.39	3.10	77	0.73	-25.7	1.55	0.51	0.46	0.763±0.009	-243.8±9.3	2180±100
GeoB16216-2	-51.26	6.24	2851	0.79	-20.4	0.18	0.66	0.41	0.868±0.010	-138.1±9.6	1130±90
GeoB16217-1	-51.29	6.07	2433	0.50	-20.3	0.18	1.16	0.30	0.846±0.010	-160.3±9.5	1340±100
GeoB16218-3	-51.52	4.77	40	0.76	-23.7	1.18	0.47	0.47	n.a.	n.a.	n.a.
GeoB16223-1	-52.12	6.63	2251	0.79	-20.5	0.19	0.65	0.38	0.797±0.009	-209.2±8.8	1830±90
GeoB16225-2	-52.86	5.67	34	0.27	-21.7	1.05	0.37	0.14	0.763±0.008	-242.5±8.4	2170±90

n.a.: not available. The sample denoted by an asterisk is the identical sample labelled as '*7/5 P95 MACAPA NORTE MEIO' in Häggi et al. (2016). The parameters denoted by an H and S have been published in Häggi et al. (2016) and Sun et al. (2017), respectively.

Table 4.3. Compound-specific radiocarbon data of riverbed and marine surface sediments.

Sample	n-C_{16+18} alkanoic acids F[14]C	Δ^{14}C (‰)	[14]C age (yr BP)	n-C_{24+26+28+30} alkanoic acids F[14]C	Δ^{14}C (‰)	[14]C age (yr BP)	Lignin (weighted average) F[14]C	Δ^{14}C (‰)	[14]C age (yr BP)	$\Sigma 8$ (mg/10g dry sediments)	Content of n-C_{24+26+28+30} alkanoic acids (µg/g dry sediment)
Riverbed
MAO13c	n.a.	n.a.	n.a.	0.778±0.010	-227.9±9.9	2020±100	0.782±0.015	-224.2±15.3	1980±160	4.94	5.47
MAO19	0.989±0.012	-18.5±11.9	90±100	0.859±0.009	-147.5±8.9	1220±80	0.904±0.014	-103.3±13.8	820±120	4.22	n.a.
MC12-1	n.a.	n.a.	n.a.	0.702±0.011	-303.4±10.9	2840±130	0.740±0.009	-265.8±8.8	2420±100	7.29	1.05
North-west Sector
GeoB16212-2	0.938±0.016	-69.1±15.9	510±140	0.727±0.011	-278.5±10.9	2560±120	0.767±0.011	-238.9±11.3	2130±120	1.05	4.20

GeoB16218-3	0.923±0.023	-84.0±22.8	640±200	0.638±0.048	-366.9±47.6	3610±600	0.598±0.008	-406.7±8.2	4130±110	0.95	0.89
GeoB16225-2	n.a.	n.a.	n.a.	n.a.	n.a.	n.a.	0.728±0.024	-277.5±24.0	2550±270	0.33	n.a.

n.a.: not available.

4.5. Discussion

4.5.1. Δ^{14}C and δ^{13}C values of TOC in marine surface sediments

It has been shown that both the lignin contents and $\delta^{13}C_{TOC}$ values of sedimentary OC are dependent on the relative contributions of terrigenous and marine OC on the Amazon shelf (Showers and Angel, 1986; Sun et al., 2017). Therefore, the $\Delta^{14}C_{TOC}$ values of sedimentary OC on the Amazon shelf are also expected to reflect the mixing of differentially aged OC from terrigenous and marine sources. Indeed, higher $\Delta^{14}C_{TOC}$ (average -89.0 ‰) values were found in the SE sector (Fig. 4.2), where the sedimentary OC is dominated by marine input (Sun et al., 2017) as indicated by low lignin contents (average 0.07 mg/100mg OC) and high $\delta^{13}C_{TOC}$ values (average -18.9 ‰) (Table 4.1). The $\Delta^{14}C_{TOC}$ value at station GeoB16225-2 (-242.5±8.4 ‰) is comparable to the results of samples from the nearby mud belt (-253.4 ‰ to -198.63 ‰) obtained in the study of Williams et al. (2015). In the NW sector, the $\Delta^{14}C_{TOC}$ values tend to become higher towards locations that receive more marine organic matter (Table 4.1, Fig. 4.1). The correlation between $\Delta^{14}C_{TOC}$ and $\delta^{13}C_{TOC}$ values (Fig. 4.3) implies that the Amazon-derived pre-aged terrestrial OC is progressively diluted by younger marine-derived organic matter as the sediment is transported north-westward of the Amazon River mouth.
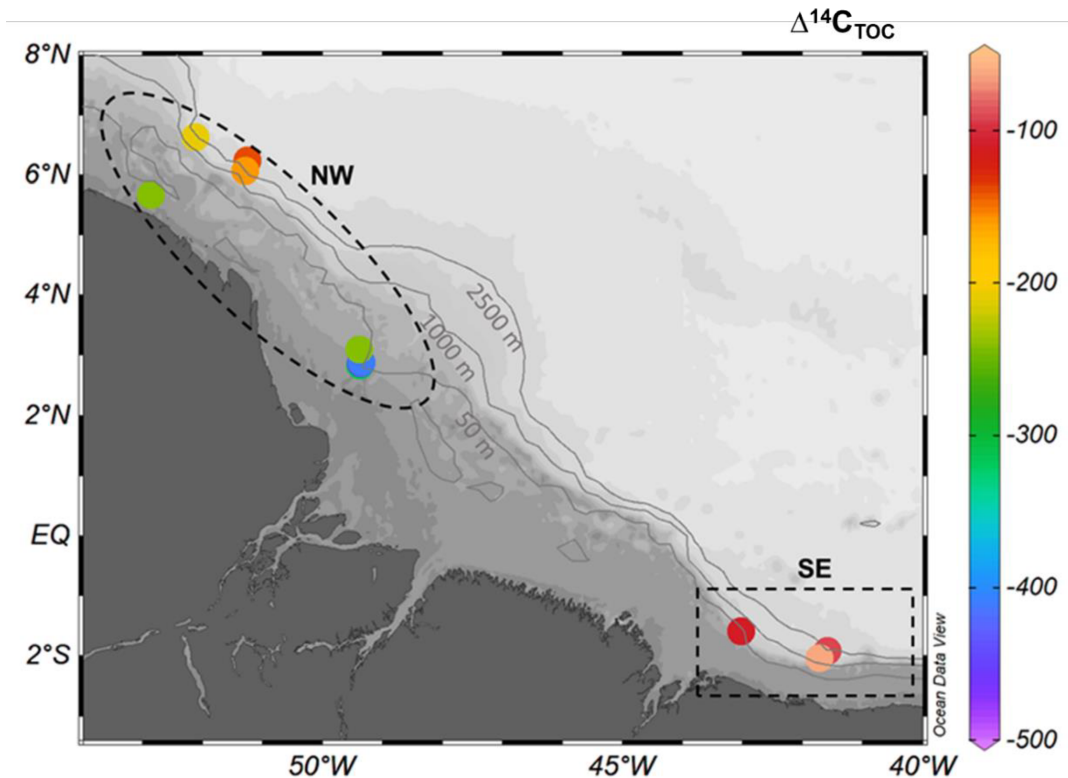
Figure 4.2. Spatial distribution of ^{14}C compositions of total organic carbon ($\Delta^{14}C_{TOC}$) in marine surface sediments from the Amazon continental margin. The dashed ellipse and rectangle represent the north-west sector (NW) and the south-east sector (SE), respectively.

Using $\delta^{13}C_{TOC}$ and $\Delta^{14}C_{TOC}$ values, it is possible to estimate the average age of terrigenous organic matter deposited in the marine surface sediments. Assuming that the average $\delta^{13}C_{TOC}$ value of surface sediment samples in the SE sector (-18.9±0.3 ‰) represents the end-member value of marine organic matter (Sun et al., 2017), an extrapolation of the correlation between $\delta^{13}C_{TOC}$ and $\Delta^{14}C_{TOC}$ (Fig. 4.3) yields the corresponding average $\Delta^{14}C_{TOC}$ value of marine organic carbon (-107.4±78.4 ‰). The average $\delta^{13}C_{TOC}$ value of riverbed sediments from the Amazon River mainstream (-28.2±0.2 ‰) published in the study of Sun et al. (2017) is used as the end-member value of terrestrial OC. A binary mixing model is employed to assess the relative contribution of marine and terrestrial OC to the marine surface sediments. The model is expressed by the following equations:

$$f_M \times (\delta^{13}C_{TOC\text{-}M}) + f_T \times (\delta^{13}C_{TOC\text{-}T}) = \delta^{13}C_{TOC} \qquad (1)$$

$$f_M + f_T = 1 \qquad (2)$$

where f_M and f_T represent the fraction of marine and terrestrial OC, respectively. $\delta^{13}C_{TOC\text{-}M}$, $\delta^{13}C_{TOC\text{-}T}$ and $\delta^{13}C_{TOC}$ represent the end-member values of marine OC, terrestrial OC, and the $\delta^{13}C_{TOC}$ of the specific sample, respectively. The estimated contribution of marine and terrestrial OC is shown in Table 4.3. The $\Delta^{14}C_{TOC}$ value of terrestrial OC can be further assessed based on isotopic mass balance as described by equation 3:

$$f_M \times (\Delta^{14}C_{TOC\text{-}M}) + f_T \times (\Delta^{14}C_{TOC\text{-}T}) = \Delta^{14}C_{TOC} \qquad (3)$$

where $\Delta^{14}C_{TOC\text{-}M}$, $\Delta^{14}C_{TOC\text{-}T}$ and $\Delta^{14}C_{TOC}$ represent the end-member $\Delta^{14}C$ value of marine OC (-107.4±78.4 ‰), the estimated average $\Delta^{14}C$ values of terrestrial OC, and the measured $\Delta^{14}C_{TOC}$ values of specific samples, respectively. The calculated $\Delta^{14}C$ values and ^{14}C ages of terrestrial OC are shown in Table 4.3. The three samples in the SE sector are not discussed here because they receive very limited terrestrial input. For the sediments in the NW sector, the estimated $\Delta^{14}C$ values of terrestrial OC ($\Delta^{14}C_{TOC\text{-}T}$) vary widely (-734.1±95.1 ‰ to -293.9±81.8 ‰) and are approximately linearly related to Al/Si ratios (Sun et al., 2017) reflecting the grain size of terrestrial mineral particles ($r^2=0.40$, $p<0.05$, $n=8$) (Fig. 4.4). This correlation suggests that the terrestrial OC associated with the finer-grained particles is more effectively protected against degradation during the transport offshore the Amazon River mouth.
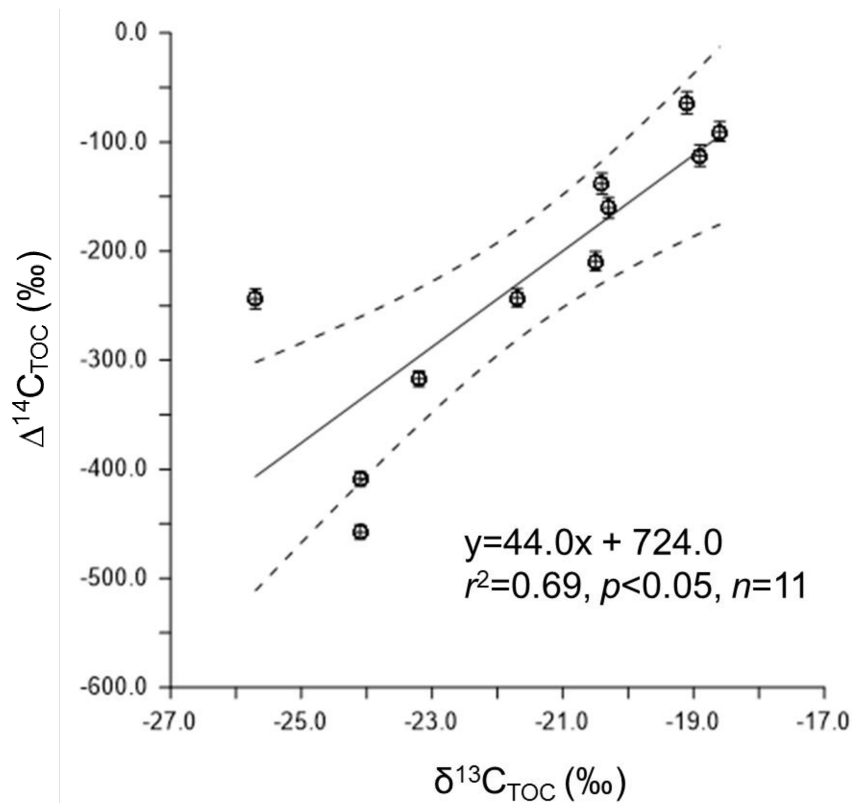
Figure 4.3. Correlation between total organic carbon Δ^{14}C ($\Delta^{14}C_{TOC}$) and δ^{13}C ($\delta^{13}C_{TOC}$) values of marine surface sediments. The continuous line represents a linear regression (given also in numerical form) and the dashed lines refer to the 95 % confidence interval.

Bulk terrestrial OC and its Δ^{14}C age have to be interpreted as a mixture of materials with different ages and reactivities, where labile components tend to be younger than refractory ones. As a result, a higher relative contribution of older refractory components (e.g., after degradative loss of the young labile fraction) will result in lower Δ^{14}C values of bulk terrestrial OC. Considering this, our data suggest that the terrigenous organic matter in coarser-grained sediments consists to a large part of pre-aged refractory fractions (e.g., petrogenic particles) and the relatively young and easily-degradable counterparts are not preserved well on coarser-grained particles. These findings mirror previous suggestions by Bouchez et al. (2014), who found a similar relationship in suspended sediment samples from the Amazon River. The influence of grain size on $\Delta^{14}C_{TOC}$ values of terrestrial OC also corroborates the conclusion based on the correlation between lignin contents and Al/Si ratios from Sun et al. (2017) that lignin is better preserved and protected from degradation on finer-grained particles in the riverbed sediments of the lowland Amazon basin. It also confirms the trend observed by Keil et al. (1997) that POC contents are positively correlated to the specific surface area of suspended particles, which indicates high loading of POC on finer suspended particles.

Table 4 Radiocarbon data of terrestrial organic carbon in marine surface sediments estimated based on a binary mixing model (see section 4.5.1). $f_T = (\delta^{13}C_{TOC} - \delta^{13}C_{TOC-M})/(\delta^{13}C_{TOC-T} - \delta^{13}C_{TOC-M})$ and $f_M = 1 - f_T$. Δ^{14}C value of terrestrial organic carbon is calculated as $(\Delta^{14}C_{TOC} - \Delta^{14}C_{TOC-M} \times f_M)/f_T$. The weight percentage of terrestrial organic carbon is calculated as $TOC \times f_T$. The errors of the estimation are propagated according

to the uncertainties of the considered associated parameters. ^{14}C ages and their errors are rounded to the nearest 10 and 5 years, respectively.

Sample	f_M (%)	f_T (%)	Weight percentage of terrestrial OC (wt %)	Δ^{14}C value of terrestrial OC (‰)	^{14}C Age of terrestrial OC (yr BP)
GeoB16209-2	54±4	46±4	0.05	-560.5±92.1	6550±1090
GeoB16210-2	44±4	56±4	0.06	-734.1±95.1	10580±1410
GeoB16211-2	44±4	56±4	0.10	-646.8±91.9	8300±1250
GeoB16212-2	27±5	73±4	0.53	-293.9±81.8	2740±870
GeoB16216-2	84±4	16±4	0.13	-297.7±120.9	2800±1130
GeoB16217-1	85±4	15±4	0.08	-458.8±150.0	4890±1440
GeoB16223-1	83±4	17±4	0.14	-699.1±173.5	9620±1760
GeoB16225-2	70±4	30±4	0.08	-556.1±106.3	6470±1130

n.a.: not available.
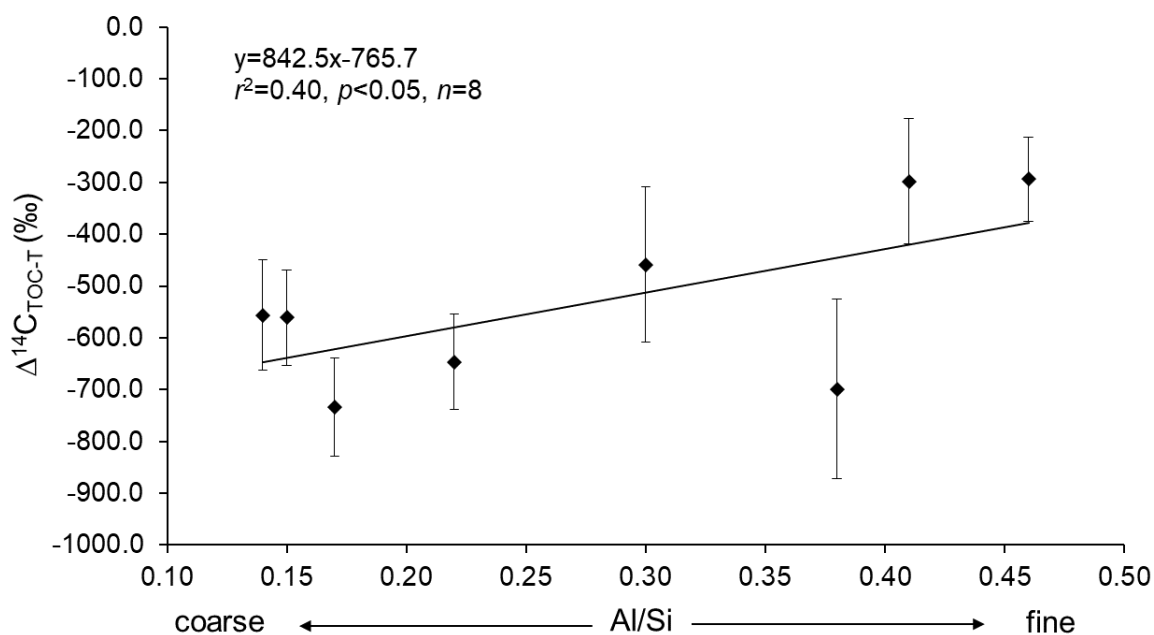
Figure 4.4. Correlation between total organic carbon Δ^{14}C of terrestrial organic carbon (Δ^{14}C$_{TOC-T}$) and Al/Si ratios representing variations in grain size from marine surface sediments. The continuous line represents a linear regression (given also in numerical form).

4.5.2. Δ^{14}C values of compounds from different sources and with various reactivities

Although there is considerable uncertainty in the specific source of short-chain n-alkanoic acids, they are commonly assumed to be mainly produced by microorganisms indicating autochthonous input from algal and/or bacterial sources (Volkman et al., 1998). Indeed, a study conducted in the Amazon Plume found that δD of short-chain n-alkanoic acids reflect local salinity conditions and hence represent a modern autochthonous OC fraction in aquatic environments (Häggi et al., 2015). This is reflected by the highest Δ^{14}C values of n-C$_{16+18}$ alkanoic acids in the riverbed and marine sediments compared to the Δ^{14}C values of TOC and other components (Table 4.2, Fig. 4.5). Compared to the Δ^{14}C values of dissolved inorganic carbon (DIC) in the lowland Amazon basin (89±44 ‰) (Mayorga et al., 2005), n-C$_{16+18}$ alkanoic acids in the riverbed sediment from station MAO19 exhibit a slightly lower Δ^{14}C value (-18.5±11.9 ‰) and a near modern ^{14}C age (90±100 yr BP), which suggests predominant input from

recently produced material and rapid turnover. The Δ^{14}C values of n-C$_{16+18}$ alkanoic acids in the marine surface sediment samples (-84.0±22.8 ‰ to -69.1±15.9 ‰) agree with that of their riverine counterparts within uncertainties (Table 4.2, Fig. 4.5).
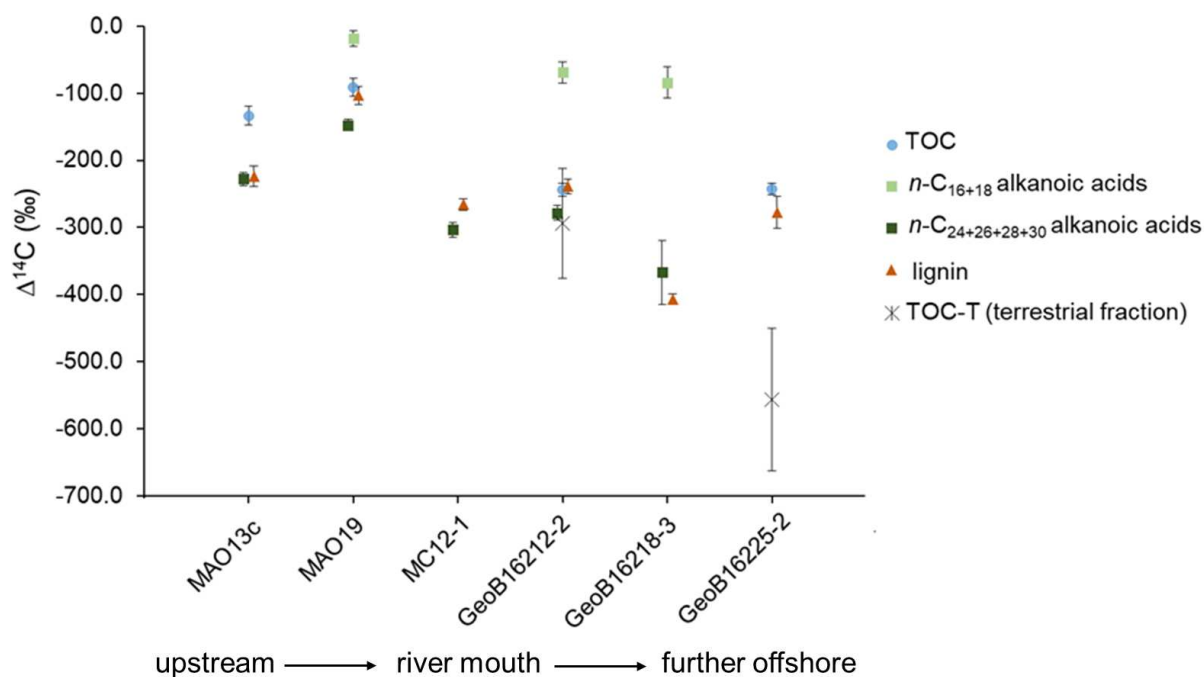

Figure 4.5. Radiocarbon data (reported as Δ^{14}C values) of total organic carbon (TOC) and compounds with different reactivities for riverine and marine sediments, as well as the terrestrial fraction of organic carbon (TOC-T) in marine sediments. The samples are plotted in an upstream-offshore order.

As a major class of leaf wax-derived biomarkers produced by vascular plants, long-chain n-alkanoic acids are used to trace the distribution of terrestrial OC (Feng et al., 2013a; Hedges et al., 2000; Mollenhauer and Eglinton, 2007). In contrast to the short-chain homologues, the n-C$_{24+26+28+30}$ alkanoic acids consistently display the lowest Δ^{14}C values except for the marine surface sediments from station GeoB16218-3, in which the Δ^{14}C value is higher than that of lignin and has a larger uncertainty due to the small sample size (Table S4.2, Fig. 4.5). This pattern of Δ^{14}C values of short- and long-chain n-alkanoic acids suggests heterogeneous sources and different turnover times. Moreover, the difference in the Δ^{14}C values between short- and long-chain n-alkanoic acids increases from the riverbed sediment in the middle of the Amazon River mainstream (i.e. station MAO19) to marine surface sediments far away from the river mouth (Table 4.2). The increasing age offset (1130-2970 years) suggests that during the long-distance transport from the lowland Amazon basin to the ocean, the long-chain n-alkanoic acids are continuously aged and become increasingly older compared to the *in-situ* produced OC. The lignin in our samples exhibits the same spatial distribution pattern of the Δ^{14}C values as the long-chain n-alkanoic acids, in which they show a trend towards lower values with transport distance from upstream of the Amazon mainstream to the offshore area (Table 4.2).

The correlation between the $\Delta^{14}C$ values of long-chain *n*-alkanoic acids and lignin and their coincident variations with distance from upstream source suggests that they derive from a similar source and undergo similar processes during transport. The $\Delta^{14}C$ values of long-chain *n*-alkanoic acids are marginally lower than, or about the same as lignin within errors. The general pattern of long-chain *n*-alkanoic acids being lower in $\Delta^{14}C$ values than lignin has also been found in other regions with different environmental conditions, for example, in suspended sediments of the Yellow River basin, estuarine sediments from Eurasian Arctic river basins, and sediments from fjord systems in Fiordland, New Zealand (Cui et al. 2017; Feng et al., 2013b; Tao et al., 2015). This suggests that long-chain *n*-alkanoic acids intrinsically have a higher potential to survive in the longer term under various climatic and hydrodynamic conditions irrespective of the dominant local plant composition.

Not all studies mentioned above observed a correlation between long-chain *n*-alkanoic acids and lignin $\Delta^{14}C$. In particular in the Arctic, based on their relatively high $\Delta^{14}C$ values, lignin phenols were inferred to be mainly derived from rapidly exported OC from topsoil layers which are rich in relatively fresh OC in various stages of decomposition and transported via surface runoff. Instead, long-chain *n*-alkanoic acids exhibiting lower $\Delta^{14}C$ values were inferred to originate more likely from aged OC associated to mineral soil released from deeper permeable permafrost layers (Feng et al., 2013b). The lowland Amazon basin, in contrast, is different in various biogeochemical aspects from the Arctic (e.g., soil properties and hydrodynamic processes). First, the age differences between organic matter in upper and deeper soil layers are observed to be less significant in the lowland Amazon basin than in the Arctic, with drainage basins of the latter covered by discontinuous and/or continuous permafrost (Trumbore, 1993). Second, the grain size influence on the content and composition of lignin in the Amazon system suggests that the transport of lignin as well as long-chain *n*-alkanoic acids is intimately associated with soil minerals (Sun et al., 2017). In addition, compared to the Arctic, deep soils in the lowland Amazon basin might be better drained so that the lignin in deeper soils has equal potential to be released along with long-chain *n*-alkanoic acids (Quesada et al., 2011; Wynn, 2007). For these reasons, in contrast to Arctic environments, the mechanisms that control the fate of lignin and long-chain *n*-alkanoic acids in soils and their transfer to rivers in the lowland Amazon basin are inferred to be similar. Because we do not observe a significant discrepancy in ages between lignin and long-chain *n*-alkanoic acids, it appears that in the lowland Amazon basin lignin as well as long-chain *n*-alkanoic acids can be used as tracer for terrigenous pre-aged OC.

In our riverbed sediments, bulk terrestrial OC shows higher $\Delta^{14}C$ values compared to the refractory components (e.g. long-chain *n*-alkanoic acids and lignin) (Tables 4.1, 4.2, Fig. 4.5). However, in corresponding marine surface sediments, the terrestrial fraction of the sedimentary OC exhibits lower $\Delta^{14}C$ values than the long-chain *n*-alkanoic acids and lignin. This is particularly the case for the sample from station GeoB16225-2, which is likely grain-size related (Tables 4.2, 4.3, Fig. 4.5). The low $\Delta^{14}C$ value of terrestrial OC in the marine sediments illustrates that terrestrial OC contains material

predominantly more recalcitrant and aged than long-chain *n*-alkanoic acids and lignin which has survived remineralization.

Lignin in sample GeoB16218-3 from the shelf off French Guiana is approximately 2000±160 yr older in ^{14}C age than lignin in GeoB16212-2 (Table 4.2), the marine sample close to the river mouth. Yet, its (Ad/Al)$_V$ value indicating the degree of lignin degradation is not elevated (Table 4.1). The age difference in long-chain *n*-alkanoic acids between GeoB16218-3 and GeoB16212-2 is about 1050±610 yr. These differences suggest that it takes about 2000±160 years and 1050±610 years, respectively, to transport lignin and long-chain *n*-alkanoic acids about 100 km from the Amazon River mouth to station GeoB16218-3. It has been reported that the aging of long-chain *n*-alkanoic acids during the 600 km long transport from the Lena River to the Laptev Sea shelf edge is around 3600±300 years (Bröder et al., 2018). While these estimated transport times are on the same order of magnitude, the transport of lignin and long-chain *n*-alkanoic acids on the Amazon shelf appears to be slower than on the Laptev Sea shelf. Our estimates for the Amazon shelf, however, are based on only two sites and should thus be interpreted with caution.

The ^{14}C age of lignin in the surface sediment GeoB16225-2 (2550±270 yr BP), located even more distant from the Amazon River mouth than GeoB16218-3, does not follow the aging trend along the transport pathway but displays a younger ^{14}C age of lignin than that of the sample GeoB16218-3 (4130±110 yr BP) (Table 4.2). The coarser sediments (reflected by lower Al/Si ratio in GeoB16225-2) suggest additional input of fine sand particles (Table 4.1), with which plant debris might be deposited. Thus, the unexpectedly young lignin in GeoB16225-2 could result from contributions of fresher lignin from local rivers mixed with Amazon-derived pre-aged lignin. The fresh lignin introduced from local rivers in GeoB16225-2 is both reflected by its lower (Ad/Al)$_V$ value (0.37; Sun et al., 2017) and a large age difference between lignin and the terrestrial fraction of bulk OC (Fig. 4.5; see discussion above). The ^{14}C age of lignin in marine surface sediments from station GeoB16225-2 (2550±270 yr BP) (Table 4.2) generally agrees with the results (2150±285 yr BP) obtained by Williams et al. (2015) in nearby mud belt sediments.

4.5.3. Constraints on the origin of terrestrial OC in the Amazon system

The river-transported OC consists of components that originate from different sources with various reactivities, such as recently biosynthesized labile OC, pre-aged refractory OC released from soils, and highly resistant fossil rock-derived material (Marwick et al., 2015). When terrestrial OC is exported to the ocean, labile components will be replaced by modern OC produced by marine plankton while pre-aged and fossil components will potentially be preserved and stored along with marine OC. With the help of radiocarbon and $\delta^{13}C_{TOC}$ values, a three end-member mixing model can be established to provide better constraints on the origin of sedimentary OC in continental and marine carbon reservoirs of the Amazon system. The model is expressed using the following equations:

$$f_{bio} \times F^{14}C_{bio} + f_{pre\text{-}aged} \times F^{14}C_{pre\text{-}aged} + f_{fossil} \times F^{14}C_{fossil} = F^{14}C_{TOC} \qquad (4)$$

$$f_{bio} \times (\delta^{13}C_{bio}) + f_{pre\text{-}aged} \times (\delta^{13}C_{pre\text{-}aged}) + f_{fossil} \times (\delta^{13}C_{fossil}) = \delta^{13}C_{TOC} \qquad (5)$$

$$f_{bio} + f_{pre\text{-}aged} + f_{fossil} = 1 \qquad (6)$$

where f_{bio}, $f_{pre\text{-}aged}$ and f_{fossil} represent the fractions of modern biosynthesized OC, pre-aged OC and fossil OC, respectively. $F^{14}C_{bio}$, $F^{14}C_{pre\text{-}aged}$, $F^{14}C_{fossil}$, and $F^{14}C_{TOC}$ refer to the $F^{14}C$ values of modern biosynthesized OC, pre-aged OC, fossil OC and bulk OC of specific samples, respectively. $\delta^{13}C_{bio}$, $\delta^{13}C_{pre\text{-}aged}$, $\delta^{13}C_{fossil}$ and $\delta^{13}C_{TOC}$ refer to the $\delta^{13}C$ values of modern biosynthesized OC, pre-aged OC, fossil OC and bulk OC of specific samples, respectively. As discussed above, the short-chain n-alkanoic acids are mainly derived from local aquatic production, therefore, their $F^{14}C$ values are used as $F^{14}C_{bio}$, 0.989±0.012 for riverbed sediments and 0.931±0.020 (average of two samples of marine surface sediments) for marine sediments. Because the major plant source of terrestrial OC is non-woody tissues of C3 vascular plants (Häggi et al., 2016; Sun et al., 2017), a typical average $\delta^{13}C$ of -30±0.9 ‰ for C3 plants is assigned to $\delta^{13}C_{bio}$ for riverbed sediments (Hedges et al., 1986). The $\delta^{13}C$ of -18.9±0.3 ‰ is taken for $\delta^{13}C_{bio}$ in marine sediments. It has to be noted that, as GeoB16212-2 might receive terrestrial input of modern biospheric OC, the end-member $\delta^{13}C$ of -18.9±0.3 ‰ would result in an underestimation of the terrestrial contribution. Both the long-chain n-alkanoic acids and lignin have $F^{14}C$ values suggesting moderate degradation histories. Considering that lignin accounts for more biomass in plants and might be more abundant in soils than lipids (Ingalls et al., 2010), the specific $F^{14}C$ values of lignin are accordingly used as the $F^{14}C_{pre\text{-}aged}$ for individual samples. An average $\delta^{13}C$ of (-27.0 ‰) of wetland soil (Sobrinho et al., 2016) with an assumed uncertainty of 0.8 ‰ is set to represent $\delta^{13}C_{pre\text{-}aged}$ of OC in soils under C3 forest in the Amazon basin. Bouchez et al. (2014) have reported that the $\delta^{13}C$ value of fossil rock-derived OC in the Amazon basin is around -25.0‰, therefore, the $F^{14}C_{fossil}$ and $\delta^{13}C_{fossil}$ are set as 0 and -25.0±0.7 ‰, respectively.

Two riverbed samples and two marine samples have sufficient data for the calculation of this dual isotope mixing model. A Monte Carlo simulation with 1000 iterations is implemented to evaluate the contributions of these OC pools and uncertainties. The results are shown in Table 4.4 and Fig. 4.6. The relative contributions of different OC reservoirs vary greatly along the transport pathway from station MAO13c in the Solimões River to station GeoB16225-2 in the mobile mud belt off French Guiana. The modern biospheric OC and/or pre-aged soil OC are the predominant components of sedimentary OC in all samples. For the riverbed sediments, modern OC constitutes the predominant fraction in sample MAO13c in the Solimões River (60±13 %) and MAO19 in the Amazon River mainstream (71±14 %). The pre-aged soil OC makes smaller contributions relative to modern OC, 35±15 % in sample MAO13C and 24±15 % in sample MAO19, respectively. Compared to MAO19, the high proportion of soil OC in MAO13c is probably due to a greater contribution of sediments derived from erosion of Late Pleistocene and Holocene sediments (Rossetti et al., 2005), which form soft substrates drained by the Solimões

River and its tributaries. In contrast, the location of MAO19 in the Amazon River mainstream also receives contributions from the Negro River that drains the Guiana shield, where forests cover older substrates more resistant to erosion and probably introduce younger OC from surface soil layers. This may explain the larger proportion of modern OC in MAO19.

Fossil OC is consistently a minor fraction with a large uncertainty, 5±3 % and 5±2 % of TOC in riverbed sediments MAO13c and MAO19, respectively, which accounts for absolute contents (TOC × f_{fossil}) of around 0.04 % of dry weight. These calculated values are similar to the extrapolated results obtained by the binary mixing model applied by Bouchez et al. (2010), which shows that the absolute contents of fossil OC in the Amazon basin are constant in individual rivers, e.g., 0.03±0.02 % in the Solimões River and 0.06±0.05 % in the Amazon mainstream.

Table 4.4. Percentages of organic carbon from different sources estimated according to the ternary mixing model in riverbed and marine surface sediments, as described in section 4.5.3.

Sample	f_{bio} (%)	$f_{pre\text{-}aged}$ (%)	f_{fossil} (%)
MAO13c	60±13	35±15	5±3
MAO19	71±14	24±15	5±2
GeoB16212-2	16±7	80±8	4±2
GeoB16225-2	62±4	25±6	13±2

For the marine surface sediments, pre-aged soil OC accounts for the major proportion of sedimentary OC (80±8 %) in sample GeoB16212-2 near the mouth of the Amazon River (Table 4.4, Figs. 1, 6). Sample GeoB16225-2 further away from the Amazon River mouth contains less soil OC (25±6 %) and is slightly more enriched in the proportion of fossil OC (13±2 %) relative to GeoB16212-2. In terms of terrestrial OC, the preservation of soil OC decreases while fossil OC progressively becomes a more important component away from the Amazon River mouth. In the view of absolute contents, there is a substantial decrease of soil OC during the transport from GeoB16212-2 (0.58±0.06 %) to GeoB16225-2 (0.07±0.02 %). The marked depletion of the absolute content of soil OC is not only the consequence of increasing dilution by marine OC and inorganic particles but likely also reflects loss of the relatively labile components in the soil OC by decomposition. The substantial loss of the labile soil OC in GeoB16225-2 is very likely related to the coarser grain size (reflected by a low Al/Si ratio of 0.14) of terrestrial particles in GeoB16225-2 (Table 4.1). As discussed in section 4.5.1, the preservation of terrestrial OC in the Amazon system is highly dependent on grain size of the mineral particles, i.e., soil OC is likely to adsorb to finer-grained particles and is better preserved through association with mineral surfaces. Unlike soil OC, the absolute contents of fossil OC in marine sediments appear to be almost invariant, 0.03±0.01 % in GeoB16212-2 and 0.02±0.01 % in GeoB16225-2 (Fig. 4.6), respectively. The absolute contents of fossil OC in riverbed and marine sediments do not change with Al/Si ratios. This observation suggests that the burial of fossil OC in the Amazon is spatially almost constant on the

Amazon shelf and the distribution of absolute contents of fossil OC in sediments is not influenced by the variation of sediment grain size. This also suggests that fossil OC is not remobilized to a large degree during transport in the Amazon system. The proportion of the refractory terrestrial OC in GeoB16225-2 (37±8 %) is in accordance with the results obtained with the Ramped PyrOX method in the study of Williams et al. (2015). These authors found that the refractory terrestrial OC preserved in a nearby location to be at least 36 %. The contributions of terrestrial OC in GeoB16212-2 and GeoB16225-2 estimated with the three end-member mixing model (around 84 % and 38 %, respectively) are higher than the results obtained by the binary mixing model used in section 4.5.1 (about 73 % and 30 %, respectively) (Tables 4.3, 4.4). This difference arises from the fact the three end-member model utilizing both radiocarbon and stable carbon isotopic data takes into account that terrestrial OC contains components with different origins and reactivities. Hence, the more detailed quantitative view can avoid underestimation of terrestrial OC and provides better constraints on the origin of sedimentary OC.
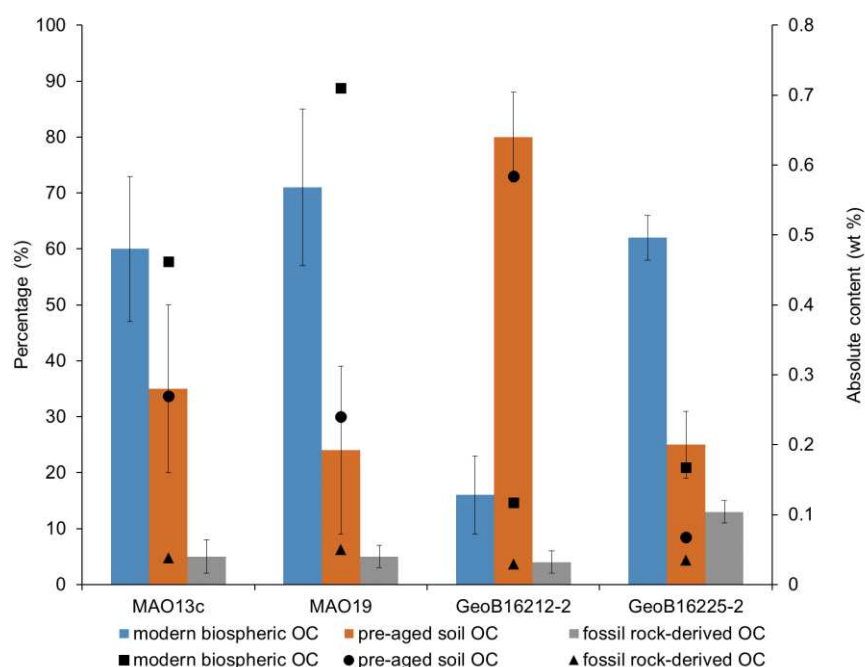
Figure 4.6. Quantitative estimation of proportion of organic carbon derived from different origins with different reactivities. The histograms with error bars represent the percentages of organic carbon from different pools. The black squares, circles and triangles refer to the absolute contents of modern biospheric organic carbon (OC), pre-aged soil OC and fossil rock-derived OC in the sediments, respectively.

4.5.4. Degradation and cycling of terrestrial OC in the Amazon system

Terrestrial OC is exposed to various physical and biogeochemical processes resulting in transformation or decomposition of terrestrial OC during residence within and transfer between different carbon pools (e.g., soils, fluvial deposits and coastal sediments). Consequently, the abundances, degrees of degradation, and ages of residual terrestrial organic matter varies widely along the transport trajectory. The radiocarbon ages of terrestrial OC represent the residence time in the reservoirs where various processes induce degradation of terrestrial OC. By plotting the absolute contents of terrestrial OC

normalized to mass in our riverbed and marine surface sediments with their ^{14}C ages, we observe an exponential relation (Fig. 4.7a), which fits the single exponential decay model of organic matter (Catalán et al., 2016). The model can be described as $OC(t) = OC(0) \times e^{-kt}$, in which $OC(t)$ and $OC(0)$ are defined as the remaining and initial mass of OC during decomposition, respectively. The constant k represents the decay rate and t is the residence time of the terrestrial OC.
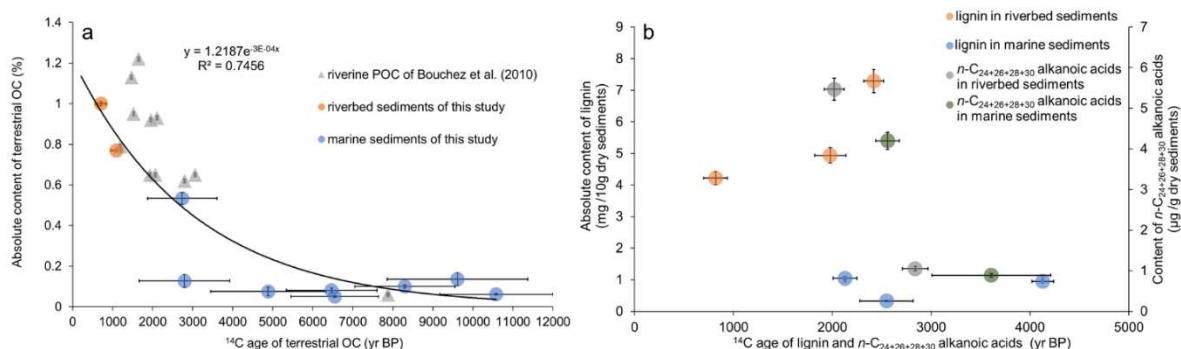

Figure 4.7. Absolute content of terrestrial organic carbon (OC) (a), lignin and long-chain alkanoic acids (b) versus the corresponding ^{14}C age from riverine and marine samples. For marine sediments, the absolute content of terrestrial OC was corrected by the corresponding fraction of terrestrial OC, as estimated in section 4.5.1 (i.e., TOC * f_M). The calculated age of terrestrial OC (as estimated in section 4.5.1) is applied here.

In Fig. 4.7a, the data of our two riverbed sediments and marine sediments in the NW sectors are compiled with the results of riverine suspended sediments from lowland Amazon basin reported by Bouchez et al. (2010). As shown in Fig. 4.7a, our riverbed sediments and most of the suspended sediments exhibit relatively younger ^{14}C ages and more abundant terrestrial OC. The data of riverbed sediments (Table 4.1) and riverine suspended sediments reflect the initial ^{14}C age, composition or degradation status of the terrestrial OC entering the Amazon River system, i.e. $OC(0)$. The data of marine sediments are regarded as reflecting the composition and degradation status of terrestrial OC at ^{14}C age t after residence in the Amazon system and transport to offshore areas (Table 4.3), i.e. $OC(t)$. Terrestrial OC becomes older while losing the less stable components until deposition in the marine sediments. This variation from the riverine to the marine sediments reflects loss of terrestrial OC since it is exported to the river until its (final) deposition in marine surface sediments, i.e., the degradation during transport. Our finding is consistent to the global pattern of older riverine POC age with decreasing POC content, which suggests preferential decomposition of younger and more labile OC during the residence time within the river network (Marwick et al., 2015). It should be noted that the loss of terrestrial OC in our study is not necessarily caused by decomposition alone, but also includes other effects, such as the burial within the river and/or dilution by marine inorganic particles. The latter point could be especially relevant for the marine samples off the inner shelf, where limited present-day terrestrial sedimentation takes place.

Based on our data we attempt an approximation of the decay rate of terrestrial OC. Based on the obtained correlation, k is $3 \times 10^{-4} \pm 3 \times 10^{-5}$ yr^{-1} and the half-life of terrestrial OC can be calculated as T(1/2)

= ln (2)/k. The half-life of terrestrial OC is estimated to be about 2310±230 years. Aller and Blair (2006) have estimated a so-called "conditional" (i.e., based on a set of assumptions, see Aller and Blair, 2006) reactivity of terrestrial OC during the transport from the Amazon River to the mobile mud belt surface sediments based on the approximate residence time of particles and the change in terrestrial OC loading. They estimated that the "conditional" rate constant for terrestrial OC is around 0.2 yr^{-1} and the corresponding T(1/2) is about 3.5 years, suggesting that most terrestrial OC is remineralized within a few years (Aller and Blair 2006). The difference in the estimation of the decay rate of terrestrial OC in our and their study most likely derives from the different ways of constraining the residence time of terrestrial OC. In the study of Aller and Blair (2006), the transport time of particles (carrier of terrestrial OC) in the mud belt surface sediments is used for the estimation. However, ages and contents of terrestrial OC are not necessarily related to the depositional locations. Therefore, our findings are based on the residence time of terrestrial OC itself in the intermediate reservoirs and reveals the cycling kinetics of terrestrial OC in the Amazon system before deposition. A similar approach has been applied to investigate the decay rate of terrestrial OC on the Laptev Sea shelf, which gave a degradation rate of $2.4 \times 10^{-3} \pm 6 \times 10^{-4}$ yr^{-1} (Bröder et al., 2018). Compared to the decay rate of terrestrial OC on the Laptev Sea shelf, our estimate of decay rate of terrestrial OC in the Amazon system is approximately 10 times lower. This is consistent with more rapid organic matter degradation in tropical soils compared to high latitude permafrost systems, resulting in the release of less bioavailable terrestrial organic matter to the ocean in the tropics than in the Arctic. It is also in agreement with our observation that terrestrial OC exported by the Amazon is older than lignin and lipids and hence inferred to consist predominantly of highly refractory material (see discussion above).

As an indicator for the degradation degree of lignin, the $(Ad/Al)_V$ ratio can be used to reflect the decomposition status of terrestrial OC. In our riverbed and marine sediments, $(Ad/Al)_V$ ratios are not correlated with either ^{14}C ages of terrestrial OC or ^{14}C ages of lignin (Table 4.1, 4.2 and 4.3). Similarly, no correlation between lignin composition and ^{14}C ages of lignin has been observed in high latitude regions (e.g., the Eurasian Arctic river basins; Feng et al., 2013b), or in tropical settings (e.g., the Mekong River; Martin et al., 2013). This suggests that the microbial degradation of lignin is not necessarily related to its residence time within intermediate reservoirs, and instead it is more likely dependent on the specific environmental conditions. Lignin in settings favouring preservation might show low $(Ad/Al)_V$ ratios but old ^{14}C ages. Conversely, if lignin is preserved under conditions promoting degradation, their $(Ad/Al)_V$ ratios are probably high while their ^{14}C ages are young. The absolute contents of lignin in riverbed and marine sediments do not show any correlation with their ^{14}C ages of lignin (Fig. 4.7b) as the decay curve of terrestrial OC (Fig. 4.7a). As illustrated by the large range of the absolute contents of lignin ($\Sigma 8$) and ^{14}C ages of lignin in riverbed sediments, the riverbed sediments probably do not represent the initial status before the decay, as decay may already start prior to or during riverine transport (e.g., within soils). Because marine sediments from GeoB16225-2 are

potentially influenced by contributions of lignin from local small rivers, it may not properly characterize the final status after the decay either. Therefore, we only consider here the decomposition of lignin during the transport between GeoB16212-2 and GeoB16218-3. Assuming that the decay of lignin follows the same exponential model, the decay rate k of lignin decomposition occurring during transport from GeoB16212-2 to GeoB16218-3 can be estimated from the corresponding $\Sigma 8$ values and ^{14}C ages. This result in a lignin decay rate of 5×10^{-5} yr^{-1} and corresponding half-life of ~ 13860 years. The longer half-life of lignin compared to terrestrial OC is consistent with expectations because lignin is thought to be one of the most refractory components in terrestrial OC pools. Therefore, if our estimate is correct, it highlights the great preservation potential of lignin in the mud belt on the Amazon shelf. The absolute contents and ^{14}C ages of long-chain alkanoic acids riverbed and marine sediments are also plotted in Fig. 4.7b. The decay rate k of long-chain alkanoic acids (1.5×10^{-3} yr^{-1}) obtained by the exponential model based on GeoB16212-2 and GeoB16218-3 is strikingly higher than that of lignin corresponding to a half-life of 470 years. The high decay rate of long-chain alkanoic acids is the consequence of marked decreased of its content from GeoB16212-2 to GeoB16218-3, while the ages of long-chain alkanoic acids and lignin hardly differ. The rapid loss of long-chain alkanoic acids might imply that organic matter degradation in marine sediments favours long-chain alkanoic acids over lignin, as the degradation of lignin occurs mostly in soils by fungi under oxic conditions (Hedges et al., 1988). Compared to the decay rates of lignin and long-chain alkanoic acids on the Laptev Sea shelf ($2.8\times10^{-3}\pm0.2\times10^{-3}$ yr^{-1} and $4.0\times10^{-3}\pm0.9\times10^{-3}$ yr^{-1}, respectively) (Bröder et al., 2018), our estimate of the decay rate of lignin is lower by two orders of magnitude but the decay rate of long-chain alkanoic acids is comparable.

Decay of terrestrial OC during the transport is influenced by many factors, such as burial loss, variable degree of adsorption onto particles of different grain sizes, hydrodynamic processes, oxygen exposure time, etc., and the available data used for our estimation is relatively small with decay rates of lignin and long-chain alkanoic acids based on only two samples. While our preliminary estimates should be regarded as a starting point for future studies in the Amazon system, they provide important new constraints on the dynamics of terrestrial OC during land-ocean transfer.

4.6. Conclusions

In this study, we use radiocarbon and stable carbon isotopic composition of the TOC and source-specific biomarkers to investigate the characteristics of terrestrial OC in the Amazon system. The Δ^{14}C$_{TOC}$ and δ^{13}C$_{TOC}$ values of marine surface sediments on the Amazon continental margin are positively correlated, suggesting that the pre-aged terrestrial OC dispersed from the Amazon River is progressively diluted by younger marine-derived OC as the sediment is transported towards the north-west along the Amazon mobile mud belt. Δ^{14}C values of terrestrial OC on the Amazon continental margin are negatively correlated to sediment grain size indicating that terrestrial OC associated with finer-grained particles

have a greater preservation potential during the passage from inland floodplains to the Amazon continental margin. Thus, grain size might be the dominant controlling factor of terrestrial OC cycling in the Amazon system. The different radiocarbon compositions of individual biomarkers indicate variations in their sources and pre-depositional histories. In the Amazon system, short-chain *n*-alkanoic acids represent the recently biosynthesized organic matter from aquatic primary production, whereas both the long-chain *n*-alkanoic acids and lignin derive from pre-aged soil OC associated to mineral surfaces and show generally similar radiocarbon ages. Application of a ternary mixing model using $\Delta^{14}C$ and $\delta^{13}C$ compositions suggests variable compositions of fresh biospheric and pre-aged soil organic carbon in riverbed and marine sediments during transport, but a relatively constant burial of fossil rock-derived OC. Estimates of the decay rates of terrestrial OC, lignin and long-chain alkanoic acids based on their absolute contents and ^{14}C ages suggest a half-life of about 2310 years for terrestrial OC during transport from the lowland Amazon basin to the Amazon continental margin. For the transport along the Amazon mobile mud belt the half-lives of lignin and long-chain alkanoic acids are estimated to be around 13860 and 470 years, respectively. Based on these findings, we infer that the terrestrial OC buried in the Amazon-Guianas mobile mud belt is highly refractory, and subject only to long-term degradation.

Acknowledgements

4.7. Supplementary information

4.7.1. Blank assessment and correction of *n*-alkanoic acid methyl esters

Our method for the assessment of the extraneous carbon contaminants is based on the study of Shah and Pearson (2007). This method relies on the assumption that the contaminants introduced before the purification on preparative capillary gas chromatography (PCGC) or preparative high-performance liquid chromatography (prep-HPLC) are removed. Hence, the contaminants include contributions from the chromatographic collection of target compounds, pre-treatments for flame-sealing and the processes carried out on the vacuum line. Another key premise is that the size and the isotopic composition of contamination are constant. Based on these assumptions, a graphical presentation of the masses and $F^{14}C$ values of modern (*n*-C_{30} alkanoic acid methyl ester) and fossil (*n*-C_{16} alkanoic acid methyl ester) standard compounds can be applied to assess the mass and the $F^{14}C$ value of the procedural blank. The basic concept of the blank assessment method can be found in Sun et al. (submitted for publication).

Briefly, a range of standard compounds of different masses of carbon were collected by PCGC, which account for 24 μgC, 63 μgC, and 89 μgC for *n*-C_{30} alkanoic acid methyl ester (fossil standard) and 22 μgC, 67 μgC, μgC 119 μgC and 151 μgC for *n*-C_{16} alkanoic acid methyl ester (modern standard), respectively. The data of 24 μgC *n*-C_{30} alkanoic acid methyl ester and 22 μgC and 151 μgC *n*-C_{16} alkanoic acid methyl ester were measured by Winterfeld et al. (submitted for publication). Their masses and $F^{14}C$ values were measured with MICADAS and the results are displayed in Table S4.1. The $F^{14}C$ value of unprocessed *n*-C_{30} alkanoic acid methyl ester was calculated based on known $F^{14}C$ values of *n*-C_{30} alkanoic acid (0.002±0.001) (Rethemeyer et al., 2013) and MeOH (0.001±0.000) using isotopic mass balance. The calculated $F^{14}C$ value of unprocessed *n*-C_{30} alkanoic acid methyl ester is regarded as the true $F^{14}C$ value of *n*-C_{30} alkanoic acid methyl ester without the influence of any extraneous blank (Table S4.1). The bulk organic carbon from a piece of apple peel was graphitized and analysed for the $F^{14}C$ value. The obtained $F^{14}C$ value of the bulk organic carbon from the apple peel is 1.031±0.004, which was used to calculate the $F^{14}C$ value of *n*-C_{16} alkanoic acid methyl ester. The calculated $F^{14}C$ value of *n*-C_{16} alkanoic acid methyl ester is 0.970±0.004 and regarded as the true $F^{14}C$ of pure *n*-C_{16} alkanoic acid methyl ester (Table S4.1).

The $F^{14}C$ values were plotted against the reciprocal of masses of carbon (Fig. S4.1a). It is clear that the $F^{14}C$ values of both the fossil and modern standards deviate from their true $F^{14}C$ values towards each other as their masses decrease. This trend implies that as the masses of compounds decrease, their measured mass and $F^{14}C$ value increasingly approach the values of the blank. The true $F^{14}C$ values of fossil and modern standards were set as the intercepts to obtain the linear relations. The intersection point of these two trend lines can represent the reciprocal of mass and $F^{14}C$ of the blank. In order to take the measurement errors in the mass and the $F^{14}C$ values of these standards into account, a Bayesian regression model was applied to estimate the distribution of the intersection of the regression lines. This

model was established by Sun et al. (submitted for publication) using an R script. The distribution of the regression lines and intersections are plotted in Fig. S4.1a and Fig. S4.1b, respectively. The output from the Bayesian model gives the mass and $F^{14}C$ values of the procedural blank to be 4.85±0.62 µgC with a $F^{14}C$ value of 0.721±0.079. The $F^{14}C$ values of *n*- alkanoic acid methyl esters from our samples were corrected for the procedural blank by isotopic mass balance and the propagated error are shown in Table S4.2.

The $F^{14}C$ values of the corresponding *n*-alkanoic acids were further corrected for the methyl group carbon added during the methylation step. Because our samples are a mixture of *n*-alkanoic acid methyl esters with different carbon numbers, the ratios of methyl group carbon were first calculated based on the abundance of individual *n*-alkanoic acid methyl esters and the results are shown in Table S4.2. Using the isotopic mass balance, the $F^{14}C$ values of *n*-alkanoic acids methyl esters were calculated and shown in Table S4.2.

4.7.2. Blank assessment and correction of lignin phenols

Similar to the blank assessment for *n*-alkanoic acid methyl esters, a range of standard compounds of different masses of carbon were collected by prep-HPLC, which account for 6 µgC, 13 µgC, 33 µgC, 51 µgC, and 83 µgC for ferulic acid (fossil standard), and 6 µgC, 11 µgC, 29 µgC, 50 µgC, and 70 µgC for vanillin (modern standard), respectively. Their masses and $F^{14}C$ values were measured with MICADAS and the results are displayed Table S4.3. The $F^{14}C$ value of unprocessed ferulic acid is regarded as the true $F^{14}C$ value without the influence of any extraneous blank (Table S4.3) and set as the intercept for the linear regression of masses and $F^{14}C$ values of fossil standards.

Fig. S4.2a shows the relation between $F^{14}C$ values and the reciprocal of masses of carbon of the modern and fossil standards. The possible regression lines of modern and fossil standards stimulated by the Bayesian model cross each other at the points that give the distribution of the mass and $F^{14}C$ values of the procedural blank Fig. S4.2b. The output estimation of the procedural blank is 0.90±0.23 µgC with a $F^{14}C$ value of 0.813±0.155. The $F^{14}C$ values of lignin phenols were corrected for the blank carbon using isotopic composition and shown in Table S4.4.

Table S4.5. Mass and $F^{14}C$ values of standard compounds for the blank assessment for *n*-alkanoic acid methyl ester.

Standard compound	Mass of carbon (µgC)	$F^{14}C$	σ_{F14C}
fossil standard			
Unprocessed *n*-C30 alkanoic acid methyl ester	n.a.	0.002 [R]	0.001 [R]
	89	0.040	0.002
Processed *n*-C30 alkanoic acid methyl ester	63	0.057	0.003
	24 [W]	0.145 [W]	0.004 [W]
modern standard			
Bulk OC of the apple peel	n.a.	0.970	0.004
Processed *n*-C16 alkanoic acid methyl ester	151 [W]	0.965 [W]	0.008 [W]

119	0.996	0.015
67	0.944	0.009
22 [W]	0.901 [W]	0.008 [W]

n.a.: not available. The superscript R and W refer to the data adopted from Rethemeyer et al. (2013) and Winterfeld et al. (submitted for publication).

Table S4.6. Masses and $F^{14}C$ values of *n*-alkanoic acid methyl esters from the samples and the correction for blank carbon of 4.85±0.62 µgC with a $F^{14}C$ value of 0.721±0.079 and methyl group carbon from MeOH (0.001±0.000).

Sample	Mass of carbon (µgC)	$F^{14}C$ value of *n*-alkanoic acid methyl esters±1σ		Ratio of carbon from MeOH in *n*-alkanoic acid methyl esters (%)	$F^{14}C$ value of *n*-alkanoic acids±1σ
		Uncorrected for blank carbon	Corrected for blank carbon		
MAO13c *n*-$C_{24+26+28+30}$	69	0.748±0.007	0.750±0.010	3.64	0.778±0.010
MAO19 *n*-C_{16+18}	63	0.915±0.008	0.932±0.011	5.75	0.989±0.012
MAO19 *n*-$C_{24+26+28+30}$	101	0.822±0.008	0.828±0.009	3.71	0.859±0.009
MC12-1 *n*-$C_{24+26+28+30}$	61	0.680±0.007	0.677±0.010	3.55	0.702±0.011
GeoB16212-2 *n*-C_{16+18}	40	0.864±0.008	0.884±0.015	5.68	0.938±0.016
GeoB16212-2 *n*-$C_{24+26+28+30}$	53	0.703±0.006	0.701±0.011	3.54	0.727±0.011
GeoB16218-3 *n*-C_{16+18}	26	0.840±0.008	0.869±0.022	5.88	0.923±0.023
GeoB16218-3 *n*-$C_{24+26+28+30}$	14	0.652±0.008	0.615±0. 046	3.60	0.638±0.048

Table S4.7. Masses and F^{14}C values of standard compounds for the blank assessment of lignin phenols.

Standard compound	Mass of carbon (μgC)	F^{14}C	σ_{F14C}
fossil standard			
Unprocessed ferulic acid	n.a.	0.000	n.a.
	83	0.010	0.001
	51	0.008	0.001
Processed ferulic acid	33	0.011	0.001
	13	0.013	0.002
	6	0.145	0.007
modern standard			
vanillin	70	1.213	0.012
vanillin	50	1.200	0.011
vanillin	29	1.224	0.012
vanillin	11	1.188	0.013
vanillin	6	1.158	0.023

n.a.: not available.

Table S4.8. Masses and $F^{14}C$ values of lignin phenols from the samples and the correction for blank carbon of 0.90±0.23 µgC with a $F^{14}C$ value of 0.813±0.155.

Sample	Mass of carbon (µgC)	$F^{14}C$ value of lignin phenols±1σ	
		Uncorrected for blank carbon	Corrected for blank carbon
MAO13c Vl	19	0.697±0.013	0.691±0.015
MAO13c Vn	6	0.829±0.016	0.833±0.030
MAO13c Vd	72	0.882±0.011	0.883±0.012
MAO13c Sl	12	0.833±0.011	0.835±0.016
MAO13c Sn	25	0.653±0.008	0.647±0.010
MAO13c Sd	56	0.903±0.009	0.905±0.010
MAO19 Vl	26	0.913±0.009	0.917±0.011
MAO19 Vn	4	0.858±0.026	0.872±0.051
MAO19 Vd	101	0.930±0.010	0.931±0.010
MAO19 Sl	28	0.934±0.010	0.939±0.011
MAO19 Sn	36	0.713±0.008	0.710±0.008
MAO19 Sd	95	0.908±0.010	0.909±0.010
MC12-1 Vl	39	0.714±0.008	0.712±0.009
MC12-1 Vn	57	0.741±0.008	0.740±0.009
MC12-1 Vd*	68	0.755±0.009	0.754±0.009
	113	0.750±0.009	0.750±0.009
MC12-1 Sl	102	0.735±0.009	0.734±0.009
MC12-1 Sn*	53	0.757±0.009	0.756±0.010
	35	0.743±0.008	0.741±0.008
MC12-1 Sd*	38	0.757±0.008	0.756±0.009
	55	0.760±0.008	0.759±0.008
GeoB16212 Vl	11	0.656±0.009	0.642±0.016
GeoB16212 Vd	19	0.821±0.009	0.822±0.012
GeoB16212-2 Vn+Sl+Sn+Sd	38	0.810±0.009	0.810±0.009
GeoB16218-3 V and S phenols	83	0.600±0.008	0.598±0.008
GeoB16225-2 V and S phenols	7	0.739±0.013	0.728±0.024

The samples denoted with an asterisk were analysed in duplicate.
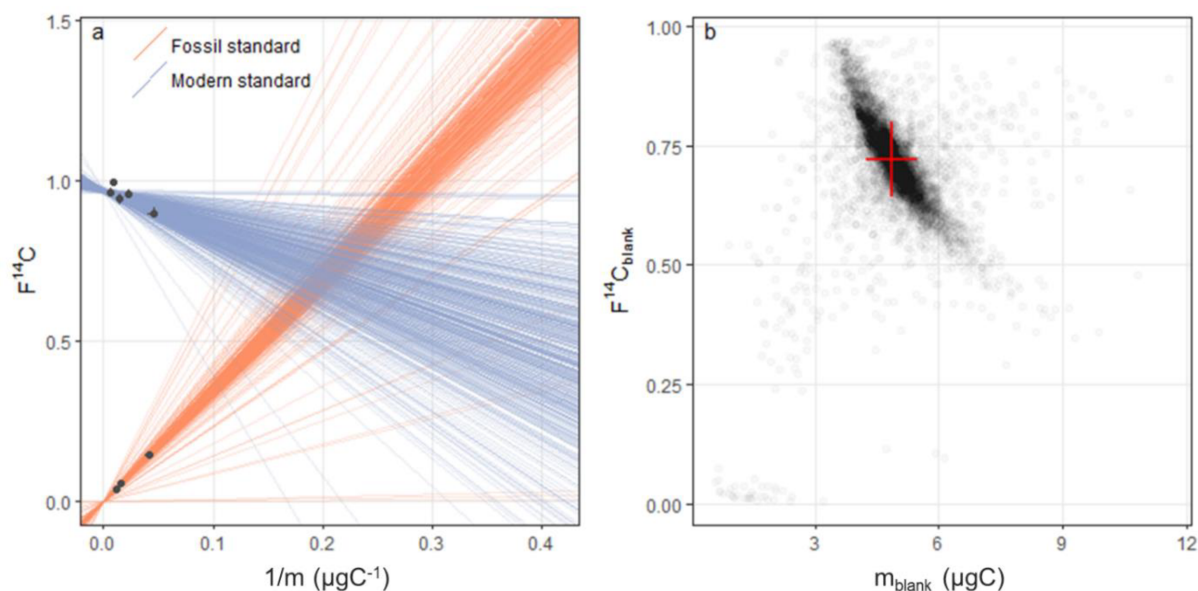
Figure S4.1. (a) The probable regression lines of the fossil and modern standards of *n*-alkanoic acid methyl esters. (b) The posterior distribution of masses and $F^{14}C$ values of the procedural blank. The red cross indicates the probability of 68 %.
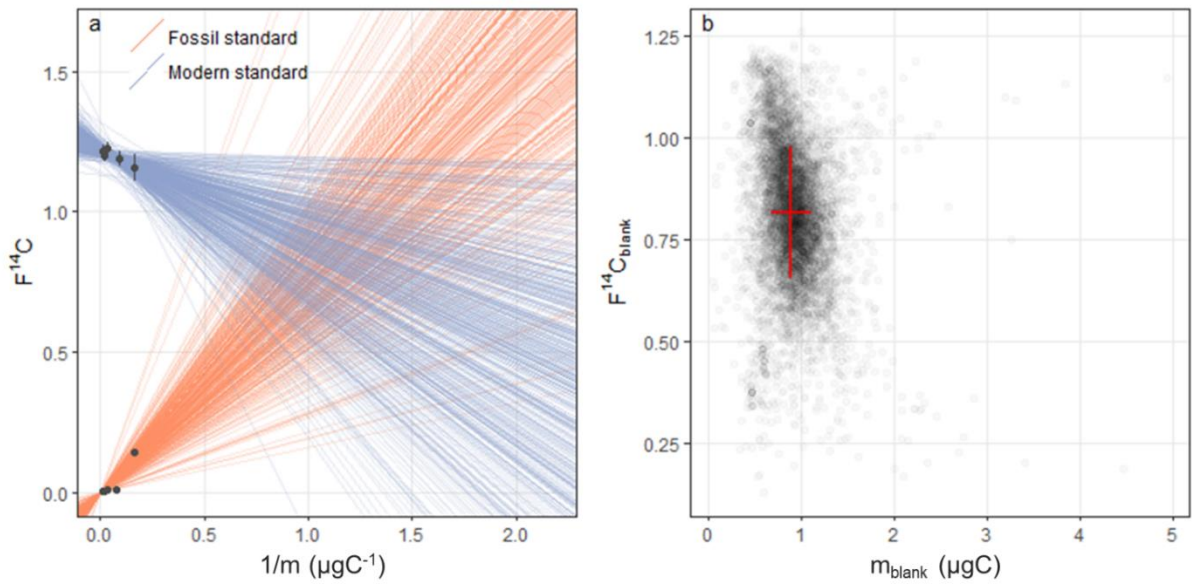
Figure S4.2. (a) The probable regression lines of the fossil and modern standards of lignin phenols. (b) The posterior distribution of masses and $F^{14}C$ values of the procedural blank. The red cross indicates the probability of 68 %.

5. Manuscript IV:

Using compound-specific δ^{13}C analysis of lignin phenols to investigate terrigenous organic matter discharge in the Amazon system

Shuwen Sun[1, 2, 3], Enno Schefuß[2], Stefan Mulitza[2], Christoph Häggi[2], Cristiano M. Chiessi[4], André. O. Sawakuchi[5], Paul A. Baker[6,7], Jens Hefter[3], Gesine Mollenhauer[1, 2, 3]

[1]Department of Geosciences, University of Bremen, 28359 Bremen, Germany

[2]MARUM-Center for Marine Environmental Sciences, University of Bremen, 28359 Bremen, Germany

[3]Alfred Wegener Institute, Helmholtz Centre for Polar and Marine Research, 25570 Bremerhaven, Germany

[4]School of Arts, Sciences and Humanities, University of São Paulo, 03828-000 São Paulo, Brazil

[5]Institute of Geosciences, Department of Sedimentary and Environmental Geology, University of São Paulo, 05508-080 São Paulo, Brazil

[6]Nicolas School of the Environment, Duke University, 301 Old Chemistry, Box 90227, Durham, NC 27708, USA

[7]School of Geological Sciences and Engineering, Yachay Tech, Yachay City of Knowledge, 100650 Urcuqui, Equador

Abstract. As lignin is unique to terrestrial vascular plants, its stable carbon isotope composition (δ^{13}C) could potentially be a powerful tool to identify sources of terrestrial organic carbon (OC) in sediments. However, lignin is subject to various biodegradation processes, which may cause isotope fractionation and influences the δ^{13}C values. This complicates the interpretation of δ^{13}C of lignin used to reconstruct vegetation changes. We present δ^{13}C data of individual lignin phenols from marine surface sediments from the Amazon shelf and sediment core GeoB16224-1 recovered from the continental margin NW of the Amazon mouth. The weighted average δ^{13}C values of lignin indicate that the modern terrestrial OC on the Amazon shelf is dominated by C3 plants and the vegetation source remained constant over the past 50-12.8 kyr, in agreement with previous studies. A general pattern of phenolic δ^{13}C values is observed with the acid monomers of V and S phenols displaying lower δ^{13}C values than their aldehyde counterparts, while C phenols are always more enriched in ^{13}C than V and S phenols. However, the effects of biodegradation on δ^{13}C values of lignin phenols are not very clear based our results. We use lignin content and composition paired with δ^{13}C of lignin to reconstruct the characteristics of terrestrial OC deposited on the continental margin NW of the Amazon mouth over the period 50-12.8 kyr. Based on the in-phase variation between lignin composition, δ^{13}C values of lignin, δ^{13}C and δD values plant-wax lipids, we propose that next to vegetation change, the variation of δ^{13}C values of lignin and plant-wax lipids during HS could reflect either enhanced discharge of more degraded terrestrial OC and/or more contributions of terrestrial from high altitude regions. These two possible scenarios suggest that

the Amazon basin was still a stable ecological system dominated by C3 forest and the increases of δ^{13}C values of lignin and plant-wax lipids were actually the consequence of changes of sources of terrestrial OC. The discharge of terrestrial OC is largely governed by hydrologic conditions in the Amazon system.

5.1. Introduction

Compound-specific stable isotope composition (δ^{13}C) is widely used to trace the source of sedimentary organic carbon (OC) in various environments (Hockun et al., 2016; Pearson et al., 2001; Tao et al., 2016; Vogts et al., 2012). Particularly the δ^{13}C values of biomarkers of terrestrial OC, such as leaf wax lipids and lignin, are important tools to accurately differentiate the terrestrial OC from marine OC; by using source specific terrigenous biomarkers the complication in estimating terrigenous OC input arising from mixed C3 (δ^{13}C around -27 ‰)and C4 (δ^{13}C around -14 ‰) plant sources can be circumvented. (Collister et al., 1994). For example, Goñi et al. (1997) have used δ^{13}C values of lignin and found that the proportion of terrestrial OC in offshore sediments in the Gulf of Mexico has been significantly underestimated due to contributions of C4 plants that had not been recognized (Hedges and Parker, 1976; Jasper and Gagosian, 1989). The relative contributions of C3 and C4 plants reflected by δ^{13}C values of vascular plant biomarkers can be used to infer vegetation change, which is related to climate variation. Vogts et al. (2012) have applied δ^{13}C values of long-chain *n*-alkanes from deep sea sediments off southwest Africa to calculate contributions of C3 and C4 plants reflecting continental vegetation and climate conditions. In applications of compound-specific δ^{13}C analysis, isotope fractionation effects between different molecules have been observed widely. The isotope fractionation may be caused by isotope discrimination occurring during photosynthesis and degradation by heterotrophic microorganisms (Dümig et al., 2013; Fernandez et al., 2003; Kodina, 2010; Wang et al., 2015). Apart from isotope fractionation, δ^{13}C values of plant wax biomarkers have been found to be sensitive to altitude and have the potential to serve as a proxy for paleoaltimetry (Wu et al., 2017). When interpreting compound-specific δ^{13}C values for vegetation variation, it is necessary to also consider these effects.

The Amazon basin is a complex ecosystem due to its enormous diversity of vegetation species and has received considerable attention with regard to the link between biodiversity and climate change (Cheng et al., 2013). The Refugia Hypothesis proposed by Haffer (1969) is a theory suggesting that the Amazon rainforest was contracted to discrete patches of small forests due to expansion of savannahs during the Last Glacial Maximum (LGM). These isolated forest 'islands' served as the refuges for forest species to survive. This theory was supported by some pollen records but also has been challenged by contradictory evidence derived from both isotope composition and vascular plant biomarker records obtained in sedimentary archives (Boot et al., 2006; Kastner and Goñi, 2003; Schlünz et al., 1999). For instance, the record of δ^{13}C values of terrestrial OC in the Amazon fan did not show a change from a C3- to a C4-dominated signal, which did not suggest the expansion of savannah during LGM (Schlünz

et al., 1999). The lignin composition in a sediment core from the Amazon fan indicates constancy of vegetation sources of terrestrial OC from 10 to 70 kyr (Kastner and Goñi, 2003). Recently, Häggi et al. (2017) have used δ^{13}C and δD values of long-chain n-alkanes to reconstruct shifts of vegetation and precipitation regimes of the Amazon basin for the late Pleistocene (50-12.8 kyr before present). They have found that the glacial climate variation controls the hydrological conditions in the Amazon basin and further influences vegetation, while the evidence of shifts in vegetation are not enough to prove the large-scale replacement of forests by savannah. As lignin is the major component of vascular plants, its δ^{13}C value could be capable of providing knowledge about the sources of terrestrial OC and its response to climate change. However, to date, compound-specific δ^{13}C analyses in paleoclimatology have been predominantly conducted on plant wax lipids. Only a few studies have carried out δ^{13}C analyses of lignin phenols (Bianchi et al., 2002; Huang et al., 1999). In the Amazon basin and adjacent offshore area, information about δ^{13}C values of lignin phenols has not been reported yet.

Here we present compound-specific δ^{13}C data of individual lignin phenols in marine surface sediments from the Amazon shelf area and a sediment core retrieved from the continental margin off French Guiana receiving sediments from the Amazon. We interpret the data in context of vegetation types in the source area and test whether the isotope variation associated with biodegradation of lignin have a substantial influence on δ^{13}C values of individual lignin phenols. We further apply δ^{13}C lignin of the sediment core to reconstruct potential changes in vegetation over the late Pleistocene (50-12.8 kyr). In addition, we combine the δ^{13}C values and composition of lignin with Branched and Isoprenoid Tetraether (BIT) index and published inorganic geochemical data, δD and δ^{13}C values of plant-waxes from the same cores to reconstruct the hydrological control on discharge of terrestrial OC in the Amazon system.

5.2. Study area

The research area is located on the Amazon shelf and continental slope offshore the coast of northern Brazil and French Guiana to the north of the Amazon River mouth. Today, the Amazon shelf receives large amounts of sediments originating from the Amazon River. The terrestrial sediments are transported north-westward to our study area under the influence of the North Brazil Current and tides forming the 1600 km-long and 50-150 km-wide sediment deposition and resuspension mudbelt along Amazon-Guianas coast (Geyer et al., 1996; Nittrouer and DeMaster, 1996). When sea level is low, such as during glacial periods, most of the sediments discharged by the Amazon River are transported to the Amazon fan forming an about 3.3×10^5 km^2 depo-center of the terrestrial OC (Damuth and Flood, 1984; Schlünz et al., 1999).

5.3. Material and methods

5.3.1. Sample collection

The GeoB marine surface sediments and a 7.6 m-long sediment core GeoB16224-1 (2510 water depth) were collected from stations on the Amazon shelf during the *R/V Maria S. Merian* cruise MSM 20/3 in February/March 2012 (Fig. 5.1). Another two marine surface sediments (BC61C and MC33A) on the Amazon shelf were taken during cruise KNR197-4 in February/March 2010. The information regarding the locations, the sampling and processing of the sediments have been presented in Häggi et al. (2016, 2017), Häggi et al. (2017) and Sun et al. (2017).

The age model for core GeoB16224-1 was first established by Zhang et al. (2015) and amended by Häggi et al. (2017). Due to a potential hiatus between 50 and 66 cm core depth (dated as 6.3 kyr and 12.6 kyr, respectively), results in intervals of the first 12.8 kyr are not not displayed in this study (Häggi et al. 2017). Selected sediment horizons (62 samples) from core GeoB16224-1 were analysed for lignin content and a subset of intervals (11 samples) were measured for $\delta^{13}C$ of lignin phenols. The intervals for analyses of lignin content and $\delta^{13}C$ were selectively sampled based on published $\delta^{13}C$ values of plant-waxes in Häggi et al. (2017) that higher resolution sampling in depth with larger variation in $\delta^{13}C$ values of plant-waxes.
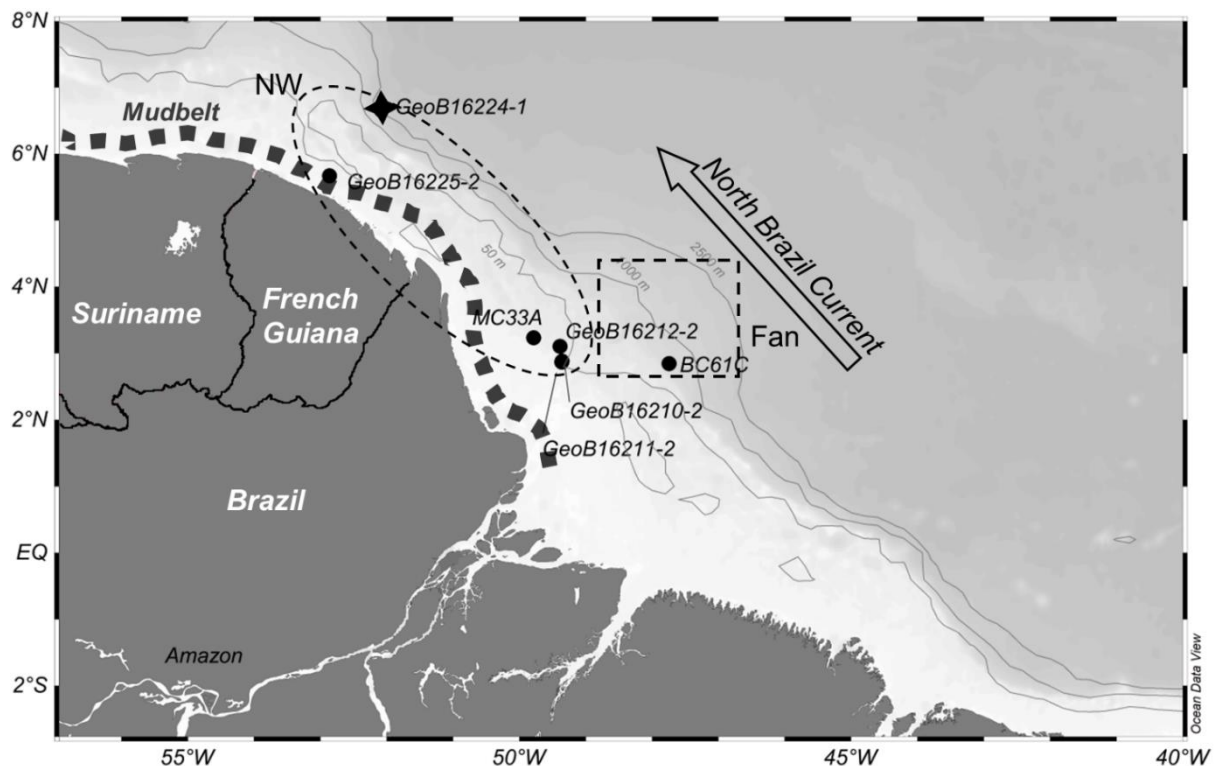
Figure 5.1. Map of the Amazon offshore area with sample locations. The marine surface sediments are indicated with black dots. The core GeoB16224-1 is indicated with a cross star. The dashed ellipse and rectangle indicate the northwest area of the Amazon shelf and the Amazon fan. The mudbelt is marked by the chain of small filled squares. The map was created using Ocean Data View 4.7.10 (Schlitzer, 2017).

5.3.2. Lignin analysis and the $\delta^{13}C$ values of lignin phenols

The extraction of lignin phenols for irm-GC-MS analysis was carried out based on the method of Goñi and Eglinton (1996) and described in detail in Sun et al. (2017). Dried sediment samples were oxidized with copper oxide and ferrous ammonium sulfate in 2 N NaOH under anoxic conditions. The oxidation was conducted with a CEM MARS5 microwave accelerated reaction system at 150 °C for 90 min. After the oxidation, known amounts of ethyl vanillin and *trans*-cinnamic acid were added to each reaction vessel as recovery standards. The solution was acidified to pH 1 with concentrated HCl after being separated from the sediments by centrifugation. The reaction products were subsequently recovered by liquid-liquid extraction by using ethyl acetate. The extracts were dehydrated with Na_2SO_4 and the ethyl acetate was then evaporated under a stream of nitrogen. The dried extracts were re-dissolved in 400 μl ethyl acetate and an aliquot (50 μl) was taken for quantification. This aliquot of extracts was dried and dissolved in 50 μl pyridine. 50 μl of *bis*-trimethylsilyl-trifluoroacetamide (BSTFA)+1% trimethylchlorosilane (TMCS) was added to derivatize lignin phenols (70 °C for 40 min). The concentrations of lignin phenols were quantified using gas chromatography-mass spectrometry (GC-MS). The mass spectrometer was operated in the electron impact (EI) mode at 70 eV ionization energy and scanned from 50 to 600 m/z with a scanning rate of 2.5 cycles per second. The GC-MS system was equipped with a DB-1 MS column (30 m × 0.25 mm i.d., film thickness 0.25 μm). The temperature of the GC-MS column was programmed 100 °C initially and followed by 4 °C/min ramp to 300 °C with a hold of 10 min. According to the quantification results, the ethyl acetate of the remnant solution was dried and the extracts were redissolved in pyridine to prepare the appropriate concentrations (~50 ng/μl) of lignin phenols for the measurement of $\delta^{13}C$ values. An equal volume of BSTFA+1% TMCS was added to the pyridine solution and derivatized at 70 °C for 40 min for the $\delta^{13}C$ analysis.

The measurement of the $\delta^{13}C$ values of lignin phenols was carried out by using an isotope ratio monitoring gas chromatography mass spectrometry (irm-GC-MS), which mainly consists of a Thermo Fisher Scientific Trace GC equipped with a DB-1 MS column (30 m × 0.25 mm i.d., film thickness 0.25 μm) and an on-column injector, a GCC combustion interface, and a Thermo Fisher Scientific MAT 252 isotope ratio mass spectrometer. The lignin phenols eluted from the GC column were combusted to CO_2 by the GCC combustion interface maintained at 1000 °C. The $\delta^{13}C$ values of lignin-phenol CO_2 peaks were measured and calibrated based on the known $\delta^{13}C$ value of CO_2 reference gas, which was injected at the beginning and end of each run. $\delta^{13}C$ values are reported in ‰ relative to Vienna Pee Dee Belemnite (VPDB). The stability of the $\delta^{13}C$ analysis on the irm-GC-MS was assured by routine measurements of the $\delta^{13}C$ values of laboratory *n*-alkane standards ('Arndt B2') against their offline-determined $\delta^{13}C$ values every five samples during the analysis sequence. The integration of derivatized lignin-phenol peaks were approached manually with Isodat software 3.0 according to the method by Goñi and Eglinton (1996). The $\delta^{13}C$ value of the trimethylsilyl carbon, which was added to replace the active hydrogens of lignin phenols, was calculated based on the known $\delta^{13}C$ value of ethyl vanillin (-

28.9±0.2 ‰) and isotope mass balance. The $\delta^{13}C$ values of lignin phenols were further corrected for the $\delta^{13}C$ value of the trimethylsilyl carbon by using isotope mass balance. For marine surface sediments, duplicate injections of the real samples are unfortunate not available. The analytical precision of the $\delta^{13}C$ values of individual lignin phenols were estimated based on the discrepancy between the irm-GC-MS determined and offline-determined $\delta^{13}C$ values of lignin standards, which ranged from 0.2 ‰ to 1.8 ‰. For GeoB16224-1 down-core samples, duplicate measurements were conducted to calculate the average and uncertainty, which varied from 0.2 ‰ to 2.2 ‰.

Eight lignin-derived phenols were analyzed in this study. They can be classified into three groups according to their plant sources and structures. The vanillyl phenols (V) exist in all vascular plant and include vanillin (Vl), acetovanillone (Vn), and vanillic acid (Vd). The syringyl phenols (S) derive only from angiosperms and include syringaldehyde (Sl), acetosyringone (Sn), and syringic acid (Sd). The cinnamyl phenols (C) are unique to non-woody tissues of vascular plants and consist of *p*-coumaric acid (*p*-Cd) and ferulic acid (Fd). The OC- and sediment-normalized content of lignin (Λ8 and Σ8) are the sum of S, V and C phenols in 100 mgTOC and 10 g dry sediment, respectively, which reflect the contribution of lignin to TOC carbon and total sediment. The ratios of S/V and C/V can be used as proxies to indicate the plant sources of lignin, such as non-woody and woody tissues of angiosperms and gymnosperms. The acid to aldehyde ratios of V and S, $(Ad/Al)_V$ and $(Ad/Al)_S$, can serve as indices to reflect degradation of lignin (Ertel and Hedges, 1985). Except for these 8 phenols, lignin-derived para-hydroxybenzenes (P) including *p*-hydroxybenzaldehyde (Pl), *p*-hydroxybenzophenone (Pn), and *p*-hydroxybenzoic acid (Pd) can also be used with V and S, i.e. P/(V+S), to indicate degradation.

5.3.3. BIT index

The BIT index refers to the abundance ratio of branched glycerol dialkyl glycerol tetraether (GDGTs) to isoprenoid GDGTs (Hopmans et al., 2004). As branched GDGTs are unique to peats and soils (Kim et al., 2006; Weijers et al., 2004) and isoprenoid GDGTs originate from marine source, their relative amount can reflect terrestrial soil OC in marine sediments (Sinninghe Damsté et al., 2002) that higher BIT values suggest more contributions from terrestrial soil OC.

The extraction of GDGTs has been described in detail in Meyer et al. (2016). Briefly, 5 g dry sediments with 10 µg C_{46}-GDGT (internal standard) were extracted with dichloromethane (DCM): methanol (MeOH) 9:1 (v/v) using accelerated solvent extractor (Dionex ASE 200) at 100 °C and 1000psi for 15 minutes (with three cycles). After drying with a rotary evaporator, the total lipid extracts were hydrolysed with 0.1 N potassium hydroxide (KOH) in MeOH:H20 9:1 (v/v). The neutral fraction with GDGTs was extracted into *n*-hexane and further separated with by chromatography with a column filled with deactivated SiO_2. The polar compounds including GDGTs were eluted with MeOH: DCM 1:1 (v/v). Afterwards, the polar compounds were dissolved in *n*-hexane: isopropanol 99:1 (v/v) and filtered with a PTFE filter (0.45 µm pore size) for quantification (Hopmans et al., 2004). GDGTs were analysed

by a high-performance liquid chromatography -atmospheric pressure chemical ionization-mass spectrometry (HPLC-APCI-MS). Selective ion monitoring (SIM) was applied to identify and quantify the target GDGTs and the detailed instrumental parameters have been given in (Crivellari et al., 2018). The BIT index was calculated as ([I]+[II]+[III])/([I]+[II]+[III]+[IV]). [I], [II], and [III] refer to the concentrations of branched GDGTs and [IV] refers to the concentration of isoprenoid GDGT. Their concentrations were determined by their respective peak areas and the response factor of the internal standard.

5.4. Results

5.4.1. δ^{13}C values of lignin phenols

The δ^{13}C values of individual lignin phenols in marine surface sediments and core GeoB16224-1 are shown in Table 5.1 and Fig. 5.2. For the marine surface sediments, the δ^{13}C values of individual lignin phenols display obvious differences within a sample. The largest intra-sample variation in δ^{13}C values of lignin phenols is observed in GeoB16211-2 from Sd of -39.4±0.9 ‰ to p-Cd of -28.3±1.8 ‰. Despite that we were not able to obtain for δ^{13}C values for all lignin phenols, the δ^{13}C values of individual lignin phenols in GeoB16225-2 show the smallest variation, from Vd of -34.8±1.3 ‰ to Sl of -29.1±0.7 ‰. The Sd in GeoB16212-2 has the lowest δ^{13}C values (-39.6±0.9 ‰). The highest δ^{13}C values (-25.7±0.9 ‰) is observed in Sd in GeoB16210-2. The Sd is inclined to exhibit large inter-sample variation in the δ^{13}C values, with a discrepancy of 13.9 ‰ between the highest and lowest observed δ^{13}C values. In contrast, the δ^{13}C values of Vl and Sn are relatively consistent in our samples, the discrepancies between highest and lowest δ^{13}C values are 3 ‰ and 2.3 ‰ for Vl and Sn, respectively. The abundance weighted average δ^{13}C values of lignin (δ^{13}C$_{lignin}$) range from -33.3±0.5 ‰ in GeoB16212-2 to -28.9±0.4 ‰ in GeoB16210-2. The weighted average δ^{13}C values of C phenols are consistently higher than V and S phenols in each sample.
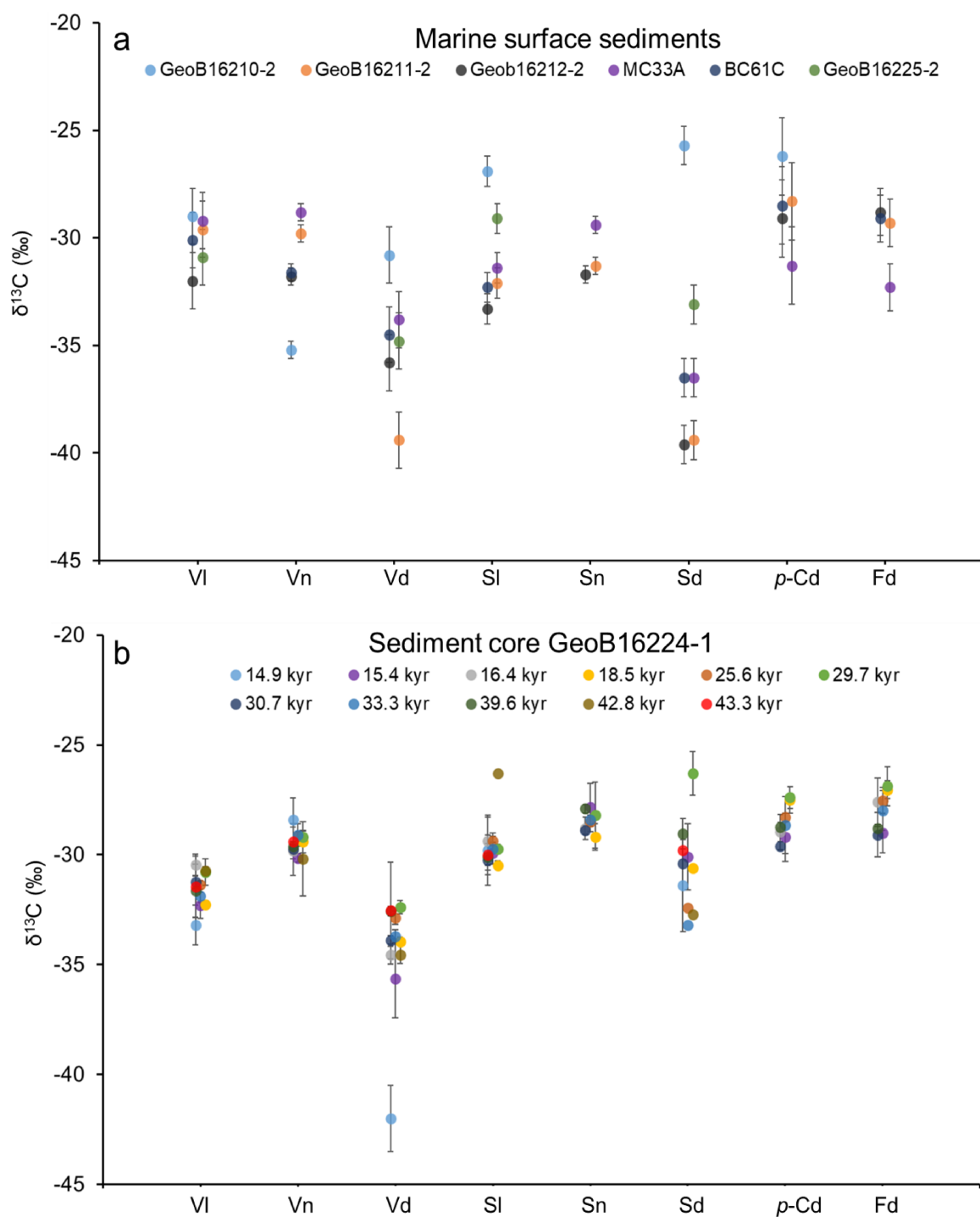
Figure 5.2. (a) δ^{13}C values (‰) of individual lignin phenols in marine surface sediments. (b) δ^{13}C values (‰) of individual lignin phenols in the sediment core GeoB16224-1.

For the sediment core GeoB16224-1, there is also variation in δ^{13}C values of individual lignin phenols within each sediment horizon (Fig. 5.2b). The largest variation is observed in the interval 14.9 kyr BP, from Vd of -42.0±1.5 ‰ to Sl of -29.8±1.6 ‰. The smallest variation is observed in the interval 43.3 kyr BP, from -32.5±2.2 ‰ of Vd to -29.4±0.8 ‰ of Vn. The lowest and highest δ^{13}C values in core GeoB16224-1 are observed in Vd in 14.9 kyr BP (-42.0±1.5 ‰) and Sd in 29.7 kyr BP (-26.3±1.0 ‰), respectively. The Sn displays the smallest inter-sample offsets in δ^{13}C values (1.4 ‰), while the δ^{13}C

values of Vd present the largest variation (9.6 ‰). The weighted average $\delta^{13}C$ values of V, S, and C phenols exhibit a pattern with $\delta^{13}C(V) < \delta^{13}C(S) < \delta^{13}C(C)$.

Table 5.1. δ¹³C values (‰) of individual lignin phenols of marine surface sediments and core samples. The δ¹³C values of V, S and C phenol groups and lignin are reported as weighted averages.

Sample	Vl	Vn	Vd	Sl	Sn	Sd	*p*-Cd	Fd	Lignin	V	S	C
GeoB16210-2	-29.0(1.3)	-35.2(0.4)	-30.8(1.3)	-26.9(0.7)	n.a.	-25.7(0.9)	-26.2(1.8)	n.a.	-28.9(0.4)	-32.0(0.6)	-26.4(0.6)	-26.2(1.8)
GeoB16211-2	-30.6(1.3)	-29.8(0.4)	-39.4(1.3)	-32.1(0.7)	-31.3(0.4)	-39.4(0.9)	-28.3(1.8)	-29.3(1.1)	-32.6(0.5)	-32.5(0.8)	-33.6(0.6)	-28.9(1.0)
GeoB16212-2	-32.0(1.3)	-31.8(0.4)	-35.8(1.3)	-33.3(0.7)	-31.7(0.4)	-39.6(0.9)	-29.1(1.8)	-28.8(1.1)	-33.3(0.5)	-32.9(0.8)	-34.6(0.6)	-28.9(1.0)
MC33A	-29.2(1.3)	-28.8(0.4)	-33.8(1.3)	-31.4(0.7)	-29.4(0.4)	-36.5(0.9)	-31.3(1.8)	-32.3(1.1)	-31.6(0.4)	-30.8(0.8)	-32.3(0.5)	-31.9(1.0)
BC61C	-30.1(1.3)	-31.6(0.4)	-34.5(1.3)	-32.3(0.7)	n.a.	-36.5(0.9)	-28.5(1.8)	-29.9(1.1)	-32.5(0.4)	-32.0(0.7)	-34.0(0.6)	-29.4(0.9)
GeoB16225-2	-30.9(1.3)	n.a.	-34.8(1.3)	-29.1(0.7)	n.a.	-33.1(0.9)	n.a.	n.a.	-31.3(0.5)	-33.8(1.0)	-30.0(0.6)	n.a.
Core GeoB165224-1												
111-122 cm	-33.2(0.9)	-28.4(1.0)	-42.0(1.5)	-29.8(1.6)	n.a.	-31.4(2.1)	n.a.	n.a.	-32.6(0.7)	-34.6(0.7)	-30.3(1.3)	n.a.
122-123 cm	-32.3(0.6)	-30.1(0.2)	-35.6(1.8)	-29.9(0.5)	-27.8(1.1)	-30.1(1.5)	-29.2(1.1)	-29.0(0.9)	-30.8(0.4)	-33.3(0.8)	-29.5(0.5)	-29.1(0.7)
146-147 cm	-30.5(0.5)	-29.8(1.1)	-34.6(0.4)	-29.4(1.1)	-28.8(0.5)	n.a.	-29.0(0.8)	-27.6(1.1)	-30.0(0.4)	-31.7(0.4)	-29.2(0.8)	-28.2(0.7)
195-196 cm	-32.3(0.2)	-29.4(0.5)	-33.9(0.2)	-30.5(0.2)	-29.2(0.6)	-30.6(n.a.)	-27.5(0.6)	-27.0(0.4)	-30.6(0.1)	-32.2(0.2)	-30.3(0.2)	-27.2(0.3)
349-350 cm	-31.4(0.2)	-29.2(0.2)	-32.9(0.3)	-29.4(0.2)	-28.5(0.2)	-32.4(n.a.)	-28.3(0.2)	-27.5(0.6)	-30.1(0.1)	-31.3(0.1)	-30.1(0.2)	-27.9(0.4)
431-432 cm	-30.8(0.6)	-29.2(0.3)	-32.4(0.3)	-29.7(0.2)	-28.2(1.5)	-26.3(1.0)	-27.4(0.5)	-26.9(0.9)	-29.3(0.3)	-31.1(0.3)	-28.5(0.4)	-27.1(0.5)
447-448 cm	-31.2(0.3)	-29.7(0.2)	-33.9(0.2)	-30.3(0.2)	-28.9(0.2)	-30.4(n.a.)	-29.6(0.2)	-29.1(1.0)	-30.5(0.1)	-31.8(0.1)	-29.9(0.1)	-29.3(0.5)
491-492 cm	-31.9(0.3)	-29.1(0.5)	-33.7(0.3)	-29.7(0.7)	-28.4(0.2)	-33.2(n.a.)	-28.7(1.3)	-28.0(0.9)	-30.7(0.2)	-31.8(0.2)	-30.6(0.5)	-28.3(0.8)
591-592 cm	-31.6(1.2)	-29.6(0.2)	-32.6(0.2)	-30.1(0.6)	-27.9(0.2)	-29.0(0.7)	-28.7(0.2)	-28.8(0.2)	-30.0(0.2)	-31.6(0.4)	-29.3(0.4)	-28.8(0.1)
645-646 cm	-30.7(0.2)	-30.2(1.7)	-34.5(0.4)	-26.3(n.a.)	n.a.	-32.7(n.a.)	n.a.	n.a.	-30.7(0.3)	-32.2(0.4)	-29.0(n.a.)	n.a.
653-654 cm	-31.5(1.4)	-29.4(0.8)	-32.5(2.2)	-30.0(0.9)	n.a.	-29.8(n.a.)	n.a.	n.a.	-30.7(0.8)	-31.7(1.3)	-29.9(2.1)	n.a.

n.a.: not available. The standard deviation of the δ¹³C value is shown in parentheses.

5.4.2. Lignin composition in core GeoB16224-1

The record of the content, composition, and $\delta^{13}C$ values of lignin are shown in Fig. 5.4. The lignin content $\Sigma 8$ varies between 0.24 and 0.67 mg/10g dry sediment (Fig. 5.4a). Over the last 50 kyr, the lignin content of core GeoB16224-1 displays low values and small variation between Heinrich Stadial (HS) 3 and HS4. Obvious increases of lignin content were observed during HS1, HS4, HS5 and during the interglacial period between HS 4 and HS5. The maximum lignin content was found during HS1. Lignin contents during HS2 and HS3 are lower than during the other periods and present only slight changes.

C/V ratios fluctuate drastically between 0.17 and 0.46 throughout the record, except for 35-40 kyr, during which C/V remains stable (Fig. 5.4d). S/V ratios vary from 1.04 to 2.41. The highest S/V ratios are found between HS4 and HS5. During Marine Isotope Stage (MIS) 3 S/V present larger extent of variation especially from HS4 to HS5. In contrast, S/V in MIS2 show little change except for an increase in the HS1(Fig. 5.4d).

The $\delta^{13}C$ values of lignin present relatively small variations, ranging from -32.6±0.7 ‰ to -29.3±0.3 ‰ (Fig. 5.4e). The lowest value was obtained from the youngest interval dated to the end of HS1 and the highest value was observed during HS3. $\delta^{13}C$ values increase during HS1, HS3 and HS4.

The records of $(Ad/Al)_V$ and $(Ad/Al)_S$ ratios display different variations over the last 50 kyr (Fig. 5.4f). The $(Ad/Al)_V$ change between 0.37 and 0.79, and the $(Ad/Al)_S$ vary between 0.16 and 0.58. During MIS2, $(Ad/Al)_V$ and $(Ad/Al)_S$ have similar average values, 0.45 for $(Ad/Al)_V$ and 0.42 for $(Ad/Al)_S$, respectively. From MIS3 to MIS2, $(Ad/Al)_V$ gradually decreases with peaks during HS3, HS4 and between HS4 and HS5. However, an opposite trend was observed for $(Ad/Al)_S$, increasing towards MIS2. During MIS3, the $(Ad/Al)_S$ (mean=0.32±0.11) are considerably lower than $(Ad/Al)_V$ (mean=0.60±0.07).

5.4.3. BIT index in core GeoB16224-1

The BIT index varies between 0.32 and 0.76 (Fig. 5.4a). Over the last 50 kyr, the BIT index of core GeoB16224-1 displays low values between HS3 and HS5 and late HS1. Higher BIT index values were observed during HS1, HS2, HS3, and HS5. The highest and the lowest BIT index values were found during HS1 and during late HS1 and late HS5, respectively. Obvious increases of BIT index values occurred during early HS1 and HS3. The BIT index values decreased markedly during HS5 and late HS1.

5.5. Discussion

5.5.1. Carbon isotope signatures of lignin phenols

The $\delta^{13}C_{lignin}$ in marine surface sediments (-33.3 ‰ ~ -28.9‰, mean=-31.7±1.6 ‰) and core GeoB16224-1 (-32.6 ‰ ~ -29.3‰, mean=-30.5±0.8 ‰) are lower than $\delta^{13}C$ values of TOC in the Amazon riverbed sediments (-29.9 ‰ ~ -26.1 ‰, mean=-28.5±0.9 ‰) (Table 5.1) (Sun et al., 2017). In our marine surface sediments and sediment core, lignin is more ^{13}C-enriched compared to the corresponding C_{29} and C_{31} n-alkanes (mean $\delta^{13}C$ n-C_{29-31}=-33.4±0.1 ‰ and -33.0±0.5 ‰ for surface sediments and core GeoB16224-1, respectively) (Häggi et al., 2016, 2017). It has been reported that the typical $\delta^{13}C_{lignin}$ of C3 and C4 plants are around 4 ‰ and 1 ‰ lower relative to the corresponding $\delta^{13}C$ values of bulk OC (Dümig et al., 2013), which suggests $\delta^{13}C_{lignin}$ of C3 and C4 plants are generally -31 ‰ and -15 ‰, respectively. Bulk OC is enriched in ^{13}C compared to lignin because it consist of main polymers that are isotopically heavier such as starch and hemicellulose ($\delta^{13}C \sim$ -26 ‰) (Kodina, 2010). Both the $\delta^{13}C$ values of lignin and long chain n-alkanes in marine surface sediments and in the sediment core suggest that the dominant vegetation source of terrestrial OC deposited on the Amazon shelf is C3 plants. The discrepancy between $\delta^{13}C$ values of lignin and n-C_{29-31} alkanes is expected as the result of isotope fractionation of ^{13}C during the biosynthesis and/or biodegradation of main polymers of higher plants (Kodina, 2010). The differences in isotope composition are detected not only between lignin and n-C_{29-31} alkanes, but also observed within different lignin phenols.

In the marine surface sediments, the $\delta^{13}C$ values of individual lignin phenols within a sample show significant offsets with magnitudes of 5.7-11.1 ‰. In the sediment core GeoB16224-1, the intra-sample variation in $\delta^{13}C$ values of lignin phenols display magnitudes of 3.2-13.6 ‰. Large intra-sample differences between individual lignin phenols have also been found in other regions, such as the surface sediments in the Mississippi plume region (offsets of 3.8-15.8 ‰; Bianchi et al., 2011) and a sediment core in the Sacred Lake, Mount Kenya (offsets of up to 9.5 ‰; Huang et al., 1999). In these previous studies, the differences were interpreted as the consequence of different contributions from C3 and C4 plants to different lignin phenol groups (Bianchi et al., 2011; Huang et al., 1999). Given that C phenols are more abundant in C4 plants, C phenols would be expected to be more ^{13}C-enriched if the contributions from C3 vs. C4 plants controls the isotopic signature. However, in our marine surface sediments only the S and C phenols of GeoB16210-2 exhibit slightly higher $\delta^{13}C$ values (-26.9±0.7 ‰ to -25.7±0.9 ‰) that can potentially be caused by C4 plant influence (Table 5.1). The C phenols in the other samples (-32.3±1.1 ‰ to -28.3±1.8 ‰) are depleted in ^{13}C and compared to the typical C4 plant signal.

In sediment core GeoB16224-1, the $\delta^{13}C$ values of C phenols also imply predominant C3 plant contribution (mean=-28.2±0.8 ‰) (Table 5.1), corroborating previous findings based on $\delta^{13}C$ values of n-C_{29-31} alkanes (Häggi et al., 2017). Thus, the intra-sample variation in $\delta^{13}C$ of different lignin phenols

cannot be explained solely by the mixing of C3 and C4 plants for our marine surface sediments. Instead, it stems more likely from the isotope fractionation effects occurring during both biosynthetic processes and long-term degradation. Except for GeoB16210-2, the $\delta^{13}C$ values of lignin phenols in our marine sediments exhibit a general pattern with the phenolic acids Vd and Sd being always poorest in ^{13}C within V and S phenol groups, respectively (Table 5.1 and Fig. 5.2a). The phenolic ketones Vn and Sn are inclined to be more enriched in ^{13}C within V and S phenols, respectively. The $\delta^{13}C$ values of C phenols are relatively higher than those of the other lignin phenols. The $\delta^{13}C$ values of lignin in GeoB16224-1 basically display the same pattern (Table 5.1 and Fig. 5.2b). Similar patterns were also found in fresh plant tissues and soils (Dignac et al., 2005; Goñi and Eglinton, 1996). This pattern suggests that the isotopic discrepancy among lignin monomers intrinsically exist when they are still in growing plants. The variation in initial fresh plants implies that these phenols are probably incorporated into the lignin polymer precursor through different photorespiratory steps (Goñi and Eglinton, 1996). Apart from the isotope fractionation associated with biosynthesis, the degradation of lignin might make further changes of $\delta^{13}C$ values after lignin enters the intermediate reservoirs such as soils, riverbed and marine sediments.

Previous research has shown that microbial degradation of lignin can cause structural alteration of lignin polymers resulting in the increase of the (Ad/Al) ratios of V and S phenols and decrease of C/V and S/V ratios (Hedges et al., 1988; Thevenot et al., 2010). Together with the changes of the contents and composition, $\delta^{13}C$ values of lignin might also change due to the preferential consumption of ^{13}C or ^{12}C by microorganisms. Dümig et al. (2013) have found ^{13}C enrichment of lignin phenols in C3 forest soils during decomposition compared to fresh plants. It was therefore hypothesized that the $\delta^{13}C$ values of lignin phenols may be related to the degradation degree, which is indicated by (Ad/Al) ratios of V and S phenols. However, the $\delta^{13}C$ values of phenolic aldehydes and acids of V and S groups do not show any clear correlation with the corresponding (Ad/Al) ratios in our marine surface sediments and sediment core GeoB1224-1 (Fig. 5.5a, b). Although the phenolic aldehydes are decomposed faster than the phenolic acids of the V and S groups, the $\delta^{13}C$ offset between phenolic aldehydes and acids are not correlated to the degradation degree (Fig. 5.5a, b). The ambiguous evidence for the influence of degradation on $\delta^{13}C$ values can be attributed to the complicated degradation pathways employed (Loftis, 2013). For example, aromatic ring cleavage, side-chain oxidation and demethylation are all probably involved in the microbial degradation of the lignin polymer. These different pathways might result in different effects on isotope composition of lignin monomers (Loftis, 2013). Although the $\delta^{13}C$ values of individual lignin phenols do not show clear trend with the degradation degree, the weighted average $\delta^{13}C$ values display slight enrichment with decreasing sediment-normalized lignin contents ($\Sigma8$) in both marine surface sediments ($r^2=0.17$) and the sediment core GoeB16224-1 ($r^2=0.45$) (Fig. 5.5c). This suggests the loss of lignin might indeed lead to the increase of the $\delta^{13}C$ values of lignin in the sediment. In the sediment core GeoB16224-1, the pattern with $\delta^{13}C(V) < \delta^{13}C(S) < \delta^{13}C(C)$, is likely associated to

the effect of degradation, as the rates of degradation are known to increase from V to S to C phenols (Hedges et al., 1988).

Because there is only a very limited number of studies investigating $\delta^{13}C$ values of lignin phenols, it is difficult to compare our results to available published data. According to our data, it seems the degradation of lignin might increase the $\delta^{13}C$ values of lignin. Therefore, our findings can provide evidence about the influence of degradation of lignin in 'real word' on the isotope composition. This hypothesis can be tested in lab and/or in-situ incubation studies in future.

5.5.2. Sources and processing of terrestrial OC discharge from the Amazon River

The sediment-normalized lignin contents ($\Sigma 8$) in sediment core GeoB16224-1 show large variations during HS1 and over the period from HS4 to HS5 but smaller variations between HS4 and the LGM. This reflects changes of inputs of terrestrial organic matter (OM) from the Amazon River (Fig. 5.4a). $\Sigma 8$ values throughout the sediment core GeoB16224-1 (0.24-0.67 mg/10 g dry sediments) are larger than those of the modern surface sediments retrieved from the nearby stations (0.10-0.17 mg/10 g dry sediments), which indicates more deposition of terrestrial OM at this position compared to recent periods (Sun et al., 2017). This is probably because the sea level during MIS2 and MIS3 was at least 30 m lower today (Kastner and Goñi, 2003). Thus, the core was closer to the coast and received more terrestrial input. The downcore variations of $\Sigma 8$ are generally in accordance with Fe/Ca ratios, which indicates sediment discharge from the Amazon River. (Fig. 5.4c) (Zhang et al., 2017). This suggests that deposition of terrestrial OM is associated with the preservation of sediment over the last 50kyr and the characteristics of terrestrial OM might be influenced by the sedimentological conditions. A notable mismatch is the period between HS4 and HS5, when there was a peak of $\Sigma 8$ but the Fe/Ca was low and displayed minor change. This exception probably implies that the lignin deposited during this period is not dominantly carried by terrigenous sediment but receives contribution from coastal small rivers. The Andean sediment influence on the characteristics of terrestrial OM is also reflected by the negative correlation between $\Sigma 8$ values and Al/Si ratios (Fig. 5.5a, b). Al/Si rations have been used as an indicator of sediment grain size in the Amazon system (Bouchez et al., 2011; Sun et al., 2017). The co-variation of $\Sigma 8$ values and Al/Si during HS1, HS3, HS4 and HS5 implies that more lignin is preserved in finer-grained sediments. This is in accordance to earlier observations in the Amazon riverbed sediments and marine surface sediments Sun et al. (2017). BIT index and $\Sigma 8$ show approximately the same variation trend during MIS2. However, they are not correlated during MIS3, particularly before HS4, when they are even anti-phased with each other (Fig. 5.4a). This discrepancy might derive from the slight difference in the sources of lignin and branched GDGTs. As BIT index reflects contribution from soil OM and lignin might exist as plant debris in addition to soil OM. Therefore, the opposite variation trend before HS4 probably suggests there were substantially higher contribution of lignin existing as plant debris apart from as soil OM.
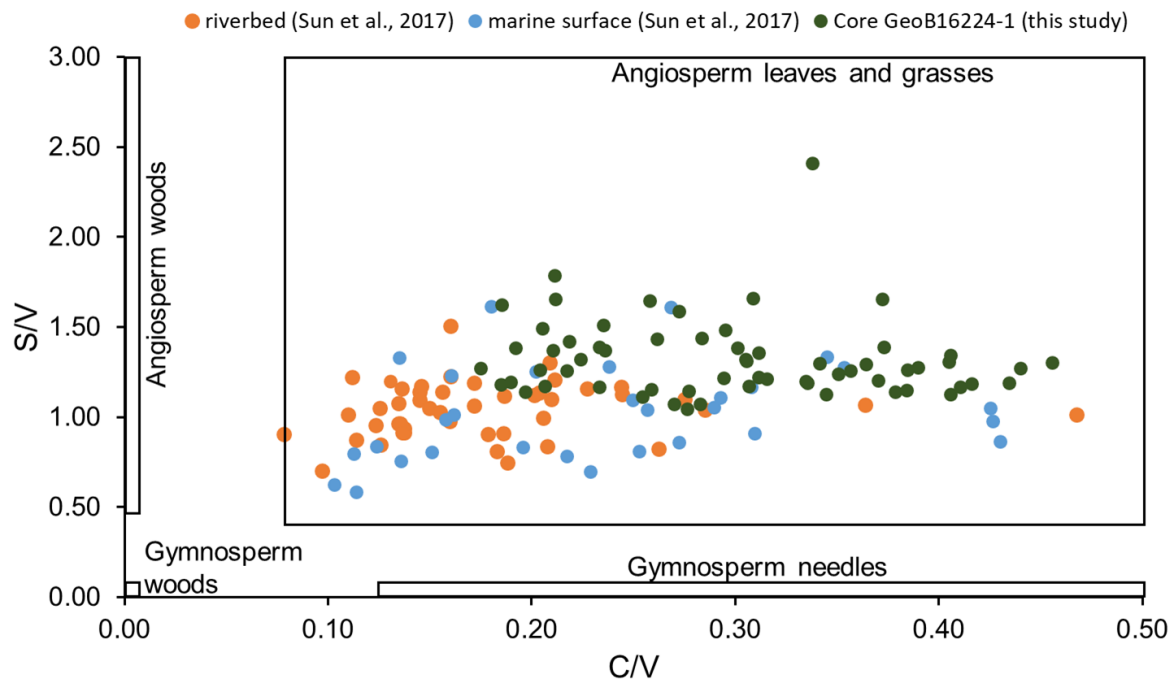
Figure 5.3. Syringyl/vanillyl (S/V) vs. cinnamyl/vanillyl (C/V) ratios of lignin in the Amazon basin riverbed sediments, marine surface sediments, and the core GeoB16224-1. The black rectangles indicate the typical ranges for different vascular plant tissues according to the study of Hedges et al. (1986) and Goñi et al. (1998).

The plant sources of lignin are indicated by S/V and C/V ratios. The data suggest that non-woody angiosperm plants are the predominant source (Fig. 5.3). Compared to the large variation of C/V ratios, the S/V ratios changed in a small range over most of the record and exhibit only a large variation between HS4 and HS5, which suggests large contribution of the vegetation characterized with high S/V signals (Fig. 5.4d). The rather uniform composition of lignin suggests that the vegetation within the Amazon basin was relatively invariable from 50 kyr to 12.8 kyr BP. Moreover, the plant sources of lignin deposited between 50 to 12.8 kyr BP were comparable to those of lignin deposited in the modern riverbed sediments of the lowland Amazon basin and marine surface sediments on the Amazon shelf (Sun et al., 2017).
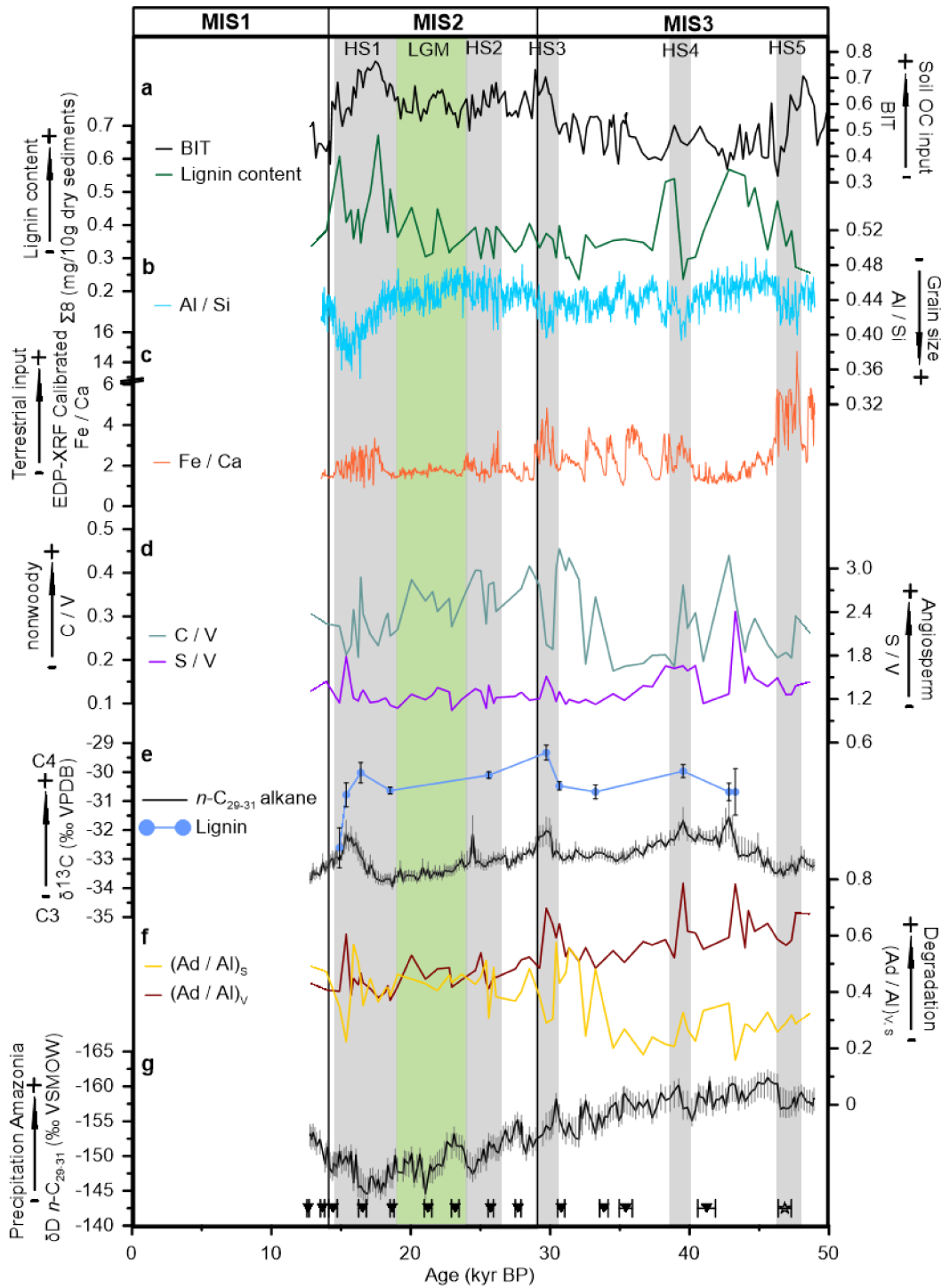
Figure 5.4. Downcore records of the content, composition and δ¹³C values of lignin and other isotope records in the core GeoB16224-1. Age model is based on the ¹⁴C ages of planktonic foraminifera (triangles) and U/Th dated El Condor speleothem record (the tie-point is marked as a star), and the error bars represent 2σ on the calibrated ages. (Cheng et al., 2013; Häggi et al., 2017; Zhang et al., 2015). (a) Lignin content (dark green line) and the Branched and Isoprenoid Tetraether (BIT) index (black line) in the sediments. (b) The ratio of Al/Si (Zhang et al., 2017). (c) The EDP-XRF calibrated Fe/Ca (Zhang et al., 2017). (d) C/V (green line) and S/V (purple line) ratios of lignin. (e) δ¹³C values of long-chain C₂₉ and C₃₁ n-alkanes (black line, grey error bars represent 1σ) (Häggi et al., 2017) and lignin (blue line and data points, grey error bars represent 1σ). (f) Acid to aldehyde ratios for vanillyl phenols (Ad/Al)ᵥ (red line) and syringyl phenols (Ad/Al)ₛ (yellow line). (g) Ice volume corrected δD values of long chain C₂₉ and C₃₁ n-alkanes (grey error bars represent 1σ) (Häggi et al., 2017). The grey-shaded boxes mark the approximate timing of

102

Slight increases of $\delta^{13}C_{lignin}$ occurred during HS1, HS3 and HS4, which is in agreement with the pattern of $\delta^{13}C$ n-C$_{29-31}$ (Fig. 5.4e). Enrichment of $\delta^{13}C$ n-C$_{29-31}$ observed during HS was interpreted to reflect the expansion of savannah or more open vegetation types (Häggi et al. 2017). Both enhanced contributions of C4 plants and decreased canopy effects of more open vegetation can shift the $\delta^{13}C$ n-C$_{29-31}$ towards higher $\delta^{13}C$ values. However, this explanation is incompatible with the record of precipitation as deduced from the stable hydrogen isotopes of n-C$_{29-31}$ alkanes (δD n-C$_{29-31}$) (Fig. 5.4g) where decreases of δD n-C$_{29-31}$ during HS1, HS2, and HS5 suggest more precipitation. The observed increases of $\delta^{13}C_{lignin}$ and $\delta^{13}C$ n-C$_{29-31}$ implying higher C4 plant input thus occur during phases of increased rainfall, which is indicated by the decreases of δD n-C$_{29-31}$. However, development of C4 plants and more open vegetation types are assumed to occur under relatively hot and arid climate conditions.
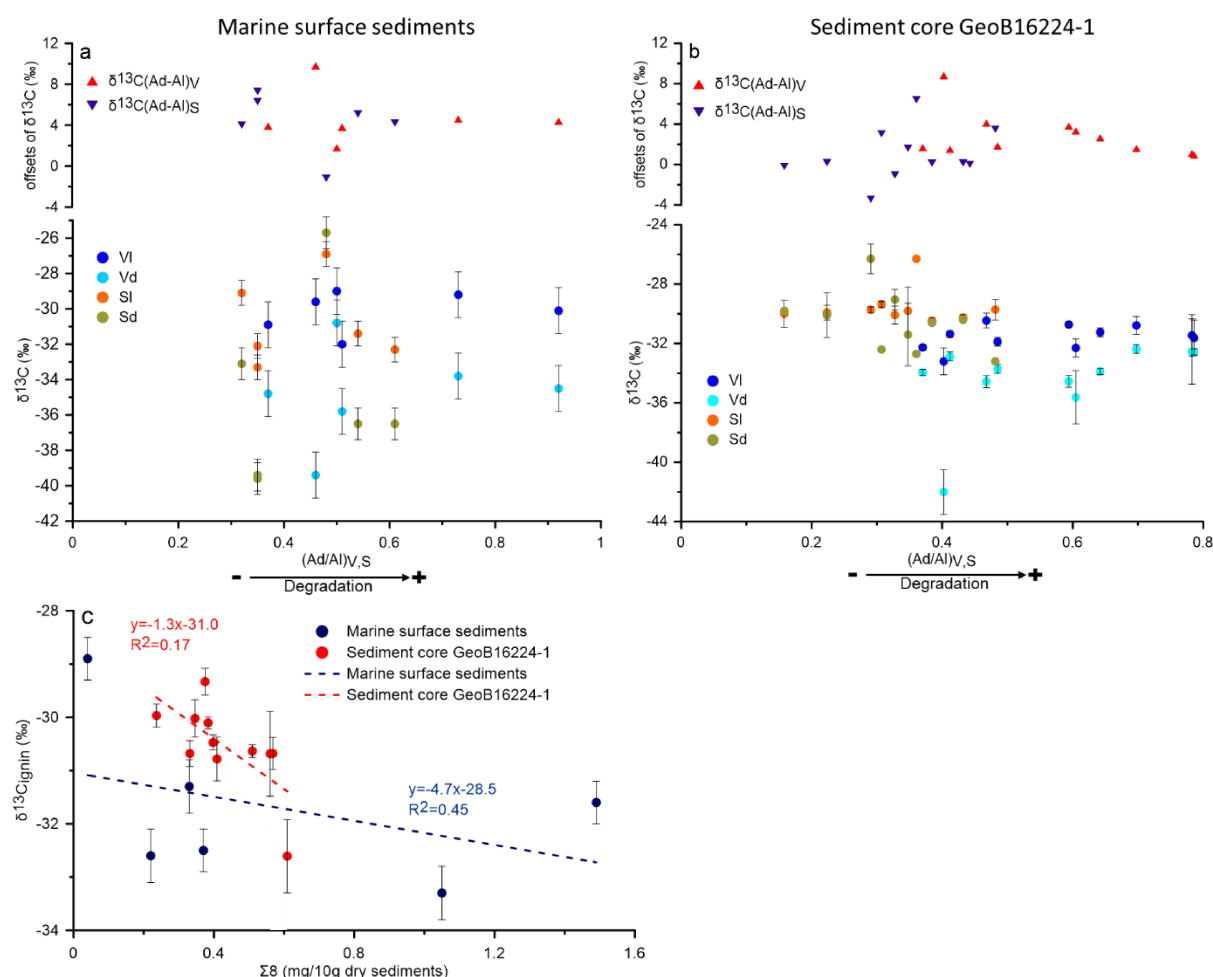
Figure 5.5. (a) $\delta^{13}C$ **values of aldehyde and acid phenols of V and S phenols vs. Ad/Al ratios of V and S phenols (circles) and the offsets of $\delta^{13}C$ values of aldehyde and acid phenols of V and S phenols, vs. corresponding Ad/Al ratios of V and S phenols (triangles) of marine surface sediments. (b) $\delta^{13}C$ values of aldehyde and acid phenols of V ($\delta^{13}C(Ad-Al)_V$) and S phenols ($\delta^{13}C(Ad-Al)_S$), $\delta^{13}C(Ad-Al)_V$ vs. corresponding Ad/Al ratios of V and S phenols (circles) and the offsets of $\delta^{13}C$ values of aldehyde and acid**

phenols of V (δ^{13}C(Ad-Al)$_V$) and S phenols (δ^{13}C(Ad-Al)$_S$) vs. Ad/Al ratios of V and S phenols (triangles) of sediment core GeoB16224-1. (c) Weighted average δ^{13}C values lignin vs. sediment-normalized lignin contents ($\Sigma 8$) in marine surface sediments (blue circles) and in the sediment core GeoB16224-1 (red circles).

In the following, we discuss alternative scenarios to explain the increases of δ^{13}C$_{lignin}$ and δ^{13}C n-C$_{29-31}$ during HS. As discussed in section 5.5.1, the influence of biodegradation on δ^{13}C$_{lignin}$ is not very clear and the effects of n-alkanes degradation on isotope changing has not been studied intensively either. It is, however, plausible that the changes of δ^{13}C$_{lignin}$ and δ^{13}C n-C$_{29-31}$ might be attributed to isotope fractionation effects associated to biodegradation of lignin and n-alkanes, as the increases of δ^{13}C$_{lignin}$ and δ^{13}C n-C$_{29-31}$ during HS are in phase with increases of (Ad/Al)$_V$ ratios (Fig. 5.4f) indicating a higher degree of degradation of lignin. This suggests that when there was more precipitation during HS, more degraded terrestrial OM with slightly higher δ^{13}C$_{lignin}$ and δ^{13}C n-C$_{29-31}$ were eroded from the Amazon basin and transported to the Amazon offshore area.

Another possible explanation for the changes of δ^{13}C$_{lignin}$ and δ^{13}C n-C$_{29-31}$ is the altitude effect on isotope composition. The altitude dependency of δ^{13}C values of bulk OC and leaf wax biomarkers has been observed in the Andes Mountains by Wu et al. (2017). δ^{13}C n-C$_{29-31}$ increases by 1.45±0.33 ‰ km^{-1} with increasing elevation, and this trend is observed for various tree species. Despite that the elevation effects on δ^{13}C$_{lignin}$ has not been tested yet, δ^{13}C$_{lignin}$ could potentially display the same pattern as lignin and leaf wax biomarkers are both major components of vascular plants and should respond to environment conditions in a similar way. Due to this inference, the increases of δ^{13}C$_{lignin}$ and δ^{13}C n-C$_{29-31}$ during HS can be interpreted as evidence that a larger proportion of terrestrial OM from the highland regions was transported by the Amazon River during high precipitation events. Terrestrial OM sourced from highland regions experienced longer-term degradation processes, in agreement with the observation of elevated (Ad/Al)$_V$ ratios during HS. In sum, both the isotope variation associated to biodegradation of terrestrial OM and higher contributions of highland-derived terrestrial OM can lead to the changes of δ^{13}C$_{lignin}$ and δ^{13}C n-C$_{29-31}$ during HS. It is notable that these two effects are actually driven by high precipitation. Therefore, the Amazonian hydrology plays an important role in the discharge of terrestrial OM in the Amazon system.

The degree of lignin degradation as indicated by the (Ad/Al)$_V$ ratio co-varies with the changing pattern of precipitation not only during HS but also over long time scales from MIS3 to MIS2 (Fig. 5.4f). This suggests that more degraded lignin was discharged from the Amazon basin during phases of enhanced precipitation. The increases of the (Ad/Al)$_V$ ratio during HS are in parallel with slight decreases of the Al/Si ratio, which indicates slight increases of grain size of sediments. This suggests that more degraded lignin associated with coarser sediment particles was discharged during HS, when precipitation was enhanced. This observation in the downcore record is in accordance with the results found in the riverbed sediments in the Amazon basin, where lignin associated to coarser-grained particles has higher (Al/Al)$_V$ ratios (Sun et al. 2017). Unlike the riverbed sediments and marine surface sediments on the

Amazon shelf (Sun et al. 2017), the $(Ad/Al)_V$ and $(Ad/Al)_S$ ratio in sediment core GeoB16224-1 are not correlated with each other and even exhibit opposite trends during MIS3 (Fig. 5.4f). This is unexpected because both ratios serve as proxies for the degree of lignin degradation. Instead of being correlated with $(Ad/Al)_V$, the record of $(Ad/Al)_S$ presents a positive relationship with P/(V+S) (Fig. 5.6), which is also an indicator of lignin biodegradation by the pathway of demethylation (Dittmar and Lara, 2001). When $(Ad/Al)_V$ and $(Ad/Al)_S$ showed opposite patterns, especially during MIS3, the S/V ratio also displayed large increases (Fig. 5.4d). Thus, the much lower $(Ad/Al)_S$ ratios compared to corresponding $(Ad/Al)_V$ values can probably be interpreted as suddenly increasing supply of fresh tissues with high S/V signals. This inference is in agreement with the above reasoning for the opposite changes of BIT index and $\Sigma 8$ during MIS3.
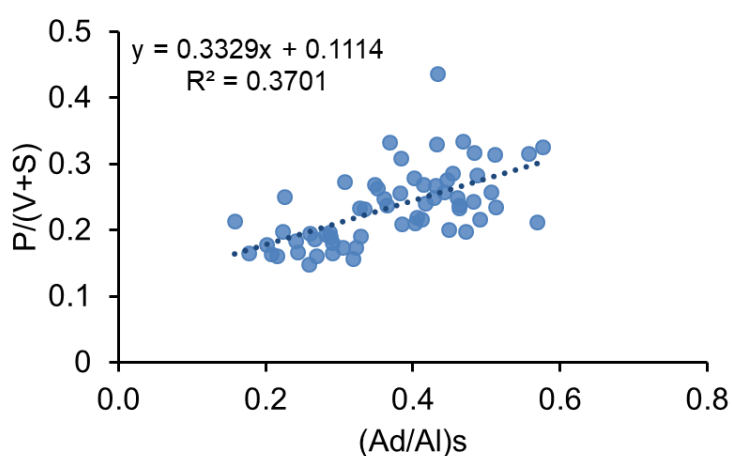
Figure 5.6. P/(V+S) vs. (Ad/Al)$_S$ of the sediment core GeoB16224-1.

5.6. Conclusions

We use compound-specific $\delta^{13}C$ of lignin phenols in marine surface sediments and sediment core GeoB16224-1 to explore the potential of $\delta^{13}C$ of lignin phenols as proxies for vegetation changes and degradation of terrigenous OM in marine sediments and inspect the influence of degradation on $\delta^{13}C$ of individual lignin phenols. Our results show that the weighted average $\delta^{13}C$ values of lignin are consistently slightly higher than those of long-chain *n*-alkanes but lower than those of bulk OC, which implies isotope fractionation between different biomarkers of terrestrial OC. The dominant plant source of lignin is C3 plants and the contribution of C4 plants is limited. Some distinct patterns of the isotope compositions of lignin phenols have been observed, with the acid monomers of V and S phenols tending to have lower $\delta^{13}C$ than their aldehyde counterparts, and C phenols being always enriched in ^{13}C relative to V and S phenols. Although the degradation effect on isotope variation of lignin phenols is not clear according to our results, it should not be neglected when we interpreting variations of $\delta^{13}C$ values of various biomarkers.

Combined with lignin content and composition, $\delta^{13}C$ of lignin has been applied to reconstruct the characteristics of terrestrial OM over the past 50 kyr. The correlation between lignin contents, Fe/Ca and Al/Si corroborates our expectation that discharge of lignin should be tied to total discharge of terrigenous materials and lignin is more abundant in fine-grained sediments. In addition to vegetation change, we propose two likely scenarios to explain the increases of $\delta^{13}C_{lignin}$ and $\delta^{13}C$ n-C_{29-31} during HS based on the covariation $\delta^{13}C_{lignin}$ with $(Ad/Al)_V$ and δD n-C_{29-31}. First, enhanced precipitation will increase the erosion of more degraded terrestrial OC, which has higher $(Ad/Al)_V$. The increases of $\delta^{13}C_{lignin}$ and $\delta^{13}C$ n-C_{29-31} during HS could result from isotope variation associated to the degradation. Alternatively, enhanced precipitation leads to more discharge of terrestrial OC from highland regions with higher $(Ad/Al)_V$ because of longer residence time during transport. Terrestrial OM from these highland regions is expected to display higher $\delta^{13}C$ values due to the altitude effect Both of these two mechanisms reflect significant hydrologic control on carbon discharge in the Amazon system.

Acknowledgements

6. Synthesis and perspectives

In this thesis, lignin and its ^{13}C and ^{14}C isotope compositions were used as the major tools, combined with other biomarkers (e.g., n-alkanoic acids and BIT index), isotope compositions (^{13}C and ^{14}C) of bulk OC and inorganic geochemical data (Al/Si), to reflect the characteristics of terrestrial particulate OC in the Amazon basin and achieve the main objectives: (1) to investigate the origins and processing of terrestrial OC based on the $\delta^{13}C$ of bulk OC and content and composition of lignin in riverbed sediments of the Amazon basin and marine surface sediments on the Amazon shelf area; (2) to develop insights into the influence of grain size on the preservation and fate of terrestrial OC in the Amazon system; (3) to quantify OC from different pools and reveal the pre-depositional history and fate of terrestrial OC; (4) to reconstruct the past vegetation change of the Amazon basin during the late Pleistocene.

In the following sections, the key findings from the main chapters are summarized and the major concepts of this thesis are presented to provide a clear understanding of the origin and fate of terrestrial OC in the Amazon system.

6.1. Sources and compositions of terrestrial OC in the Amazon system today

The relatively low $\delta^{13}C$ values of bulk OC in the riverbed sediments from the Amazon basin suggest that terrestrial OC in the Amazon system originate mainly from C3 plants with only limited contribution of C4 plants. The dominant source of terrestrial OC of C3 plants is also corroborated by the low $\delta^{13}C$ values of lignin phenols obtained in marine surface sediments from the Amazon continental shelf (see chapter 5). The composition of lignin in both the Amazon basin and the adjacent continental margin further indicates that the most important plant sources of terrestrial OC in the Amazon system are non-woody angiosperm C3 plants (see chapter 2). Although the Amazon River and its tributaries drain large area with different vegetation types, the compositions of lignin obtained in different main streams show similar signatures.

Despite that the predominant and essential source of terrestrial OC is C3 plants, more specific information of the sources of terrestrial OC in the Amazon system are further constrained and divided into three main fractions, i.e., recently biosynthesized OC, soil OC, and rock-derived OC. The OC from these three fractions have different reactivities and pre-depositional histories, which are revealed by the ^{14}C compositions of biomarkers. The recently biosynthesized OC is represented by short-chain n-alkanoic acids, which are labile and show young ^{14}C ages. Soil OC is relatively pre-aged and resistant to degradation, which is indicated by older ^{14}C ages of long-chain n-alkanoic acids and lignin. The rock-derived OC is fossil and the most refractory component of terrestrial OC (see chapter 4). The proportions of individual fractions were estimated based on dual-carbon-isotope (^{13}C and ^{14}C) mixing model. We found that the relative abundance of fresh biospheric and pre-aged soil organic carbon in

riverbed and marine sediments vary during transport in the Amazon system. Fossil OC accounts for only a minor fraction of terrestrial OC in the riverbed sediments and its abundance remains relatively constant. The proportion of fossil OC rises as terrestrial OC is discharged into the ocean and transported further away from the Amazon river mouth on the continental margin (see chapter 4).

6.2. Spatial distribution of terrestrial OC on the Amazon continental margin

Both the distribution of lignin and $\delta^{13}C$ values of bulk OC in the marine surface sediments indicate that the terrestrial OC is transported to the north-western region of the Amazon continental shelf under the influence of the North Brazil Current. The south-eastern region of the Amazon continental shelf receives little terrestrial OC supplied by local rivers but not Amazon River-derived terrestrial OC and dominated by marine OC (see chapter 2). The correlation between lignin content and $\delta^{13}C$ values of bulk OC suggests that lignin is a reliable tracer of tracer of terrestrial OC in the Amazon continental margin. The sedimentary OC in the modern Amazon Fan is composed predominantly of marine OC. Moreover, the terrestrial OC in the Amazon Fan is extensively degraded and composed of with a significant proportion of petrogenic organic matter (see chapter 2).

The spatial distribution pattern of $\Delta^{14}C$ values of bulk OC are similar to those of lignin and $\delta^{13}C$ values of bulk OC in the Amazon continental margin (see chapter 4). It verifies the conclusion that the south-eastern region of the Amazon continental margin is dominated by young marine OC while the north-western part is the depositional regime of pre-aged terrestrial OC (see chapter 4).

6.3. Influence of grain size on terrestrial OC preservation

In the Amazon basin, neither the composition of lignin nor $\delta^{13}C$ values of terrestrial OC are obviously related to the deposition position and environments. Instead, the variability of content of TOC and lignin are more clearly influenced by the grain size of the mineral particles, to which the terrestrial OC is associated. In all the riverbed sediments, the TOC contents increase with decreasing grain sizes (indicated by Al/Si), which suggests fine particles can carry more TOC. Except for the Xingu River, the contents of lignin in riverbed sediments of the main tributaries increase with decreasing grain sizes. This means lignin is preferentially preserved on finer particles compared to other components. This is corroborated by less degradation degree of lignin on finer particles observed in the riverbed sediments in the Madeira River and the Solimões River. The correlation between contents of TOC and lignin and grain sizes were also observed in the marine surface sediments on the Amazon continental margin. Thus, grain size of particles remains relevant in the preservation of sedimentary OC in the Amazon continental margin (see chapter 2).

The influence of grain size of mineral particles on preservation of OC is further proved by the correlation between $\Delta^{14}C$ values of terrestrial OC and Al/Si ratios, which suggests the terrestrial OC associated with finer particles have younger ^{14}C ages, while the terrestrial OC adsorbed to coarse

particles are substantially older (see chapter 4). This trend is interpreted as a result of more effective protection of young and labile fraction of the terrestrial OC on the finer-grained particles. Whereas the coarse particles cannot protect young and easily-degradable OC, only the pre-aged refractory fractions can survive the long-distance transport associated with the coarse particles (see chapter 4).

Therefore, grain size of mineral particles is a dominant power to control the preservation and composition of terrestrial OC in the Amazon system. And lignin is selectively preserved and can be efficiently protected from degradation on the finer particles.

6.4. Fate of terrestrial OC in the Amazon system

Based on the ^{14}C ages of long-chain n-alkanoic acids and lignin, the time spent during the about 100 km transport in the Amazon-Guianas mud belt is estimated to be 1050±610 years and 2000±160 years for long-chain n-alkanoic acids and lignin, respectively. The time it takes to transport terrestrial OC through the Amazon system can substantially control the fate of terrestrial OC. Based on the contents and ^{14}C ages of terrestrial OC, the decay rate of terrestrial OC is estimated with an exponential decay model to be $3\times10^{-4}\pm3\times10^{-5}$ yr^{-1} corresponding to a half-life of terrestrial to be 2310±230 years in the Amazon system. The similar method was applied to assess the half-life of long-chain n-alkanoic acids and lignin during the 100 km transport in the Amazon-Guianas mud belt. The results show that the half-lives of lignin and long-chain n-alkanoic acids are approximately 13860 and 470 years, respectively. The estimate of decay rate of terrestrial OC in the Amazon system is considerably lower compared to the finding of Aller and Blair (2006), which imply the half-life of terrestrial OC is only 3.5 years during the transport in the Amazon-Guianas mud belt (see chapter 4).

Altogether, the terrestrial OC buried in the Amazon-Guianas mud belt is highly refractory and subject only to long-term degradation and the preservation of terrestrial OC is more efficient than previously assumed.

6.5. Discharge of terrestrial OC during the late Pleistocene

In this thesis, the compound-specific δ^{13}C of lignin phenols is for the first time applied in marine surface sediments and a sediment core GeoB16224-1 in the Amazon system. We tested the potential of δ^{13}C of lignin phenols as proxies for reconstructing vegetation changes and investigate the influence of degradation of terrigenous OM on δ^{13}C of individual lignin phenols. The results demonstrate that the weighted average δ^{13}C values of lignin are consistently slightly higher than those of long-chain n-alkanes but lower than those of bulk OC due to the isotope fractionation between different biomarkers of terrestrial OC (see chapter 5). The degradation of lignin might increase the δ^{13}C values of lignin, which should be considered when using δ^{13}C values of lignin to reconstruct vegetation changes.

In the sediment core GeoB16224-1, lignin content and composition, $\delta^{13}C$ of lignin were employed to reconstruct the characteristics of terrestrial OM over the past 50 kyr. The contents of lignin are correlated to the amount of sediments input from the Amazon River and the precipitation in the Amazon system. The discharge of lignin is closely associated with mineral particles and might be controlled by hydrologic conditions. The correlation between lignin content and Al/Si ratios in the sediment core is the same to results found in the riverbed sediments and this corroborate the inference that lignin is preferentially preserved in finer particles (see chapter 5). The very small-scale increases of $\delta^{13}C_{lignin}$ during HS periods might not be caused of expansion of savannah. Instead, we two alternative explanations were proposed according to the correlation between $\delta^{13}C_{lignin}$ and lignin degradation. First, increases of $\delta^{13}C_{lignin}$ derive from more discharge of terrestrial OC from degraded layers of the soils because of greater erosion caused by enlarged precipitation. Second, enhanced precipitation brings more terrestrial OC from the highland regions with higher $\delta^{13}C_{lignin}$, which is also revealed by the larger degrees of lignin degradation (see chapter 5).

Thus, the variation of $\delta^{13}C_{lignin}$ more likely reflect the change of sources of the terrestrial OC discharged by the Amazon River instead of the vegetation changes.

6.6. Blank assessment for compound-specific ^{14}C analysis

In order to analyse the ^{14}C compositions of the biomarkers used in this thesis, a good method of assessing the procedural blank is necessary. In chapter 3, a Bayesian model was used to produce the linear fitting between the measured $F^{14}C$ values and masses of a set of processed modern and fossil standards. According to the distributions of the intersection points of the possible regression lines of modern and fossil standards, the procedural blanks were estimated to be 4.88±0.69 μgC with $F^{14}C$ of 0.714±0.077 for *n*-alkanoic acids, and 0.90±0.23 μgC with $F^{14}C$ of 0.813±0.155 for lignin phenols, respectively. The estimate of the procedural blank assures the accuracy of the measurement of the ^{14}C composition of the biomarkers. Compared to previous methods, this method is easy to conduct and not time consuming or labour intensive. Therefore, it can serve as a standardized procedure for blank assessment in small-scale radiocarbon analysis.

6.7. Perspective- origins, processing and fate of terrestrial OC in the Amazon system

This thesis measured the parameters and lignin compositions of riverbed sediments from the main tributaries to reflect the properties of OC in different regions of the Amazon basin. However, the results from the riverbed sediment samples reflect more likely the integrated signal and might be different from OC carried in suspended particles, which are transported to the ocean. In particular, Bouchez et al. (2011) has observed chemical and isotopic compositions of sediments with sampling depth of the suspended sediments. Therefore, the same analysis should also be applied in suspended sediments in the Amazon basin to complement the results.

It has been proved that the deposition centre of terrestrial OC in the Amazon continental margin today is the north-west sector, i.e., the Amazon-Guianas mud belt. Nevertheless, either some of the samples from this region were collected from continental slope, where receives little modern sediment, or were some samples located too closed to each other. The locations of the marine surface sediments do not extend long-distance in high spatial resolution. Because of this, the decay rate of lignin and long-chain *n*-alkanoic acids were estimated based on only two marine surface sediments, which induced large uncertainty in the analysis. Thus, more surface sediments from the Amazon-Guianas mud belt would be helpful to better constrain the fate of terrestrial OC during the transport and preservation in the Amazon system.

6.8. Perspective- matrix association effects on preservation of terrestrial OC

One key finding of this thesis is that grain size strongly influences the composition of terrestrial OC and affect the preservation of terrestrial OC in the Amazon system. The grain sizes of riverbed and marine surface sediments are indicated by Al/Si ratios and actually reflect the average grain sizes of the sediments. However, the bulk sediments are composed of fractions with different sizes and densities. As shown by Tesi et al. (2016), the compositions of OC associated in different density/size/settling velocity fractions are distinct and preferentially accumulated in different regions in coastal sediments. To fully understand the mechanism behind the link between OC and mineral surfaces, density and size fractionations of sediments would be necessary to investigate how the mineral particles influence the adsorbed OC in the Amazon system.

6.9. Perspective- the influence of degradation of lignin on its $\delta^{13}C$ value

The $\delta^{13}C$ values of lignin analysed in the sediment core GeoB16224-1 are low in temporal resolution compared to other geological indicators. First, more $\delta^{13}C$ data of lignin would be more helpful to support the conclusion. Furthermore, the major assumption that degradation of lignin can potentially increase the $\delta^{13}C$ values of lignin was not reflected by the relation between $\delta^{13}C$ values of lignin and $(Ad/Al)_{V,S}$ ratios. This is partly because the degradation degree of lignin in the sediments are not high enough to cause obvious variation in $\delta^{13}C$ values. To test this hypothesis, laboratory incubation experiments are needed to investigate whether and to what extent the $\delta^{13}C$ values of lignin would change with the enhanced degradation. This information would be very important for interpreting $\delta^{13}C$ values of lignin to reflect response of vegetation to climate change.

7. Acknowledgements

Finishing this dissertation would not have been possible without the support, encouragement, and influential presence of many people, whom I am very grateful to and have had the pleasure to work with during this PhD project. It has been a period of intense learning for me, not only in the scientific arena, but also on a personal level.

Foremost, I would like to express my sincere gratitude to my supervisors, Gesine Mollenhauer and Enno Schefuß. Thank you for your faith in my abilities and offering me such a great opportunity to work on this interesting project. It was your kind, patience, encouraging guidance, and immense knowledge that I most appreciate and will incorporate into my own life. When I failed to make progress on the manuscripts and postponed the deadlines time after time, you always tolerated it and were willing to help out. Your generosity and kindness spurred me to keep working. I could not have imagined having better supervisors for my PhD study. Besides my supervisors, I would like to thank my thesis committee members Matthias Zabel and Marcus Elvert for thoughtful feedback and inspiring advices during the meetings.

My sincere thanks also goes to Timothy Eglinton for hosting me to have a three-month research stay in his group at ETH Zürich. It was an exciting experience to work in the world-class lab and turned out to be a very fruitful research stay. During that period, I knew many talented colleagues, from whom I learned so much. I am particular indebted to Daniel Montluçon, Negar Haghipour, Meng Yu, Thomas Blattmann and Tessa van der Voort for their warm-hearted help and technical support.

I am grateful to Stefan Mulitza, Cristiano M. Chiessi, André O. Sawakuchi and Paul A. Baker for providing important samples and constructive ideas in revising my manuscripts. I would also like to thank the fellow doctoral students working in the same project, Christoph Häggi and Yancheng Zhang, for their active cooperation and helpful advices.

I am very fortunate to work in Gesine's group. All the members created a diverse, relaxing environment, which made it very enjoyable to work in this awesome group. We had a lot of fun together. I would like to thank all former and current group members, Maria Winterfeld, Katja Hockun, Wenwen Chen, Vera Meyer, Célia Santos, Eunmi Park, Hendrik Grotheer, Sarah Trojahn, Thorsten Riedel, Julian L. Schukies, Laura Kattein, Bingbing Wei, Jens Hefter, Torben Gentz, Elizabeth Bonk, Milena Ceccopieri, and Ana Dauner.

Special thanks to Vera Meyer for many things. When we shared the office, your highly efficient working attitude and the sound from fast striking keyboard reminded me that 'the most horrific thing in the world is the people who are more talented than you work harder than you too'. Thank you for providing lots of helpful advices and calming me down when I got nervous before meeting with supervisors. Thanks

8. References

Adler, E. (1977) Lignin chemistry-past, present and future. *Wood Sci. Technol.* 11, 169-218.

Aller, R. C. and Blair, N. E. (2006) Carbon remineralization in the Amazon–Guianas tropical mobile mudbelt: a sedimentary incinerator. *Cont. Shelf Res.* 26, 2241–2259.

Aufdenkampe, A. K., Mayorga, E., Hedges, J. I., Llerena, C., Quay, P. D., Gudeman, J., Krusche, A. V. and Richey, J. E. (2007) Organic matter in the Peruvian headwaters of the Amazon: compositional evolution from the Andes to the lowland Amazon mainstem. *Org. Geochem.* 38, 337–364.

Aufdenkampe, A. K., Mayorga, E., Raymond, P. A., Melack, J. M., Doney, S. C., Alin, S. R., Aalto, R. E. and Yoo, K. (2011) Riverine coupling of biogeochemical cycles between land, oceans, and atmosphere. *Front. Ecol. Environ.* 9, 53–60.

Bardy, M., Derenne, S., Allard, T., Benedetti, M. F. and Fritsch, E. (2011) Podzolisation and exportation of organic matter in black waters of the Rio Negro (upper Amazon basin, Brazil). *Biogeochemistry* 106, 71–88.

Battin, T. J., Luyssaert, S., Kaplan, L. a., Aufdenkampe, A. K., Richter, A. and Tranvik, L. J. (2009) The boundless carbon cycle. *Nat. Geosci.* 2, 598–600.

Bendle, J. a., Weijers, J. W. H., Maslin, M. a., Sinninghe Damsté, J. S., Schouten, S., Hopmans, E. C., Boot, C. S. and Pancost, R. D. (2010) Major changes in glacial and Holocene terrestrial temperatures and sources of organic carbon recorded in the Amazon fan by tetraether lipids. *Geochem. Geophys. Geosyst.* 11, Q12007.

Benner, R., Hatcher, P. G. and Hedges, J. I. (1990) Early diagenesis of mangrove leaves in a tropical estuary: bulk chemical characterization using solid-state 13C NMR and elemental analyses. Geochim. Cosmochim. Acta 54, 2003–2013.

Bianchi, T. S. (2011) The role of terrestrially derived organic carbon in the coastal ocean: a chaning paradigm and the priming effect. *Proc. Natl. Acad. Sci. USA* 108, 19473–19481.

Bianchi, T. S., Mitra, S. and McKee, B. A. (2002) Sources of terrestrially-derived organic carbon in lower Mississippi River and Louisiana shelf sediments: implications for differential sedimentation and transport at the coastal margin. *Mar. Chem.* 77, 211–223.

Bianchi, T. S., Wysocki, L. A., Schreiner, K. M., Filley, T. R., Corbett, D. R. and Kolker, A. S. (2011) Sources of terrestrial organic carbon in the Mississippi plume region: evidence for the importance of coastal marsh inputs. *Aquat. Geochem.* 17, 431–456.

Blair, N. E. and Aller, R. C. (2012) The Fate of Terrestrial Organic Carbon in the Marine Environment. *Ann. Rev. Mar. Sci*. 4, 401–423.

Bloom, A. A., Exbrayat, J. F., van der Velde, I. R., Feng, L. and Williams, M. (2015) The decadal state of the terrestrial carbon cycle: global retrievals of terrestrial carbon allocation, pools, and residence times. *Proc. Natl. Acad. Sci. USA* 113, 1285–1290.

Boot, C. S., Ettwein, V. J., Maslin, M. A., Weyhenmeyer, C. E. and Pancost, R. D. (2006) A 35,000 year record of terrigenous and marine lipids in Amazon Fan sediments. *Org. Geochem.*, 37, 208–219.

Bouchez, J., Beyssac, O., Galy, V., Gaillardet, J., France-lanord, C., Maurice, L. and Moreira-Turcq, P. (2010) Oxidation of petrogenic organic carbon in the Amazon floodplain as a source of atmospheric CO_2. *Geology* 38, 255–258.

Bouchez, J., Gaillardet, J., France-Lanord, C., Maurice, L. and Dutra-Maia, P. (2011) Grain size control of river suspended sediment geochemistry: clues from Amazon River depth profiles. *Geochem. Geophys. Geosyst.* 12, Q03008.

Bouchez, J., Galy, V., Hilton, R. G., Gaillardet, J., Moreira-Turcq, P., Pérez, M. A., France-Lanord, C. and Maurice, L. (2014) Source, transport and fluxes of Amazon River particulate organic carbon: Insights from river sediment depth-profiles. *Geochim. Cosmochim. Acta* 133, 280–298.

Bröder L., Tesi T., Andersson A., Semiletov I. and Gustafsson Ö. (2018) Bounding the role of cross-shelf transport and degradation in land-ocean carbon transfer. *Nat. Commun.* 9, 806.

Burd, A. B., Frey, S., Cabre, A., Ito, T., Levine, N. M., Lønborg, C., Long, M., Mauritz, M., Thomas, R. Q., Stephen, B. M., Vanwalleghem, T. and Zeng, N. (2016) Terrestrial and marine perspectives on modelling organic matter degradation pathways. *Glob. Change Biol.* 22, 121-136.

Burdige, D. J. (2005) Burial of terrestrial organic matter in marine sediments : a re-assessment. *Global Biogeochem. Cycles*, 19, GB4011.

Cai, D. L., Tan, F. C. and Edmond, J. M. (1988) Sources and transport of particulate organic carbon in the Amazon River and estuary. *Estuar. Coast. Shelf Sci.*, 26, 1–14.

Callede, J., Kosuth, P., Loup, J. L. and Guimarães, V. S. (2000) Discharge determination by Acoustic Doppler Current Profilers (ADCP): a moving bottom error correction method and its application on the River Amazon at Óbidos. *Hydrol. Sci. J.*, 45, 911–924.

Carpenter B., Gelman A., Hoffman M. D., Lee D., Goodrich B., Betancourt M., Brubaker M., Guo J., Li P. and Riddell A. (2017) Stan: a probabilistic programming language. *J. Stat. Softw.* 76,1.

Catalán, A. N., Marcé, R., Kothawala, D. N. and Tranvik, L. J. (2016) Organic carbon decomposition rates controlled by water retention time across inland waters. *Nat. Geosci.* 9, 501-504.

Cathalot, C., Rabouille, C., Tisnérat-Laborde, N., Toussaint, F., Kerhervé, P., Buscail, R., Loftis, K., Sun, M.-Y., Tronczynski, J., Azoury, S., Lansard, B., Treignier, C., Pastor, L. and Tesi, T. (2013) The fate of river organic carbon in coastal areas: A study in the Rhône River delta using multiple isotopic (δ^{13}C, Δ^{14}C) and organic tracers. *Geochim. Cosmochim. Acta* 118, 33–55.

Cheng, H., Sinha, A., Cruz, F. W., Wang, X., Edwards, R. L., d'Horta, F. M., Ribas, C. C., Vuille, M., Stott, L. D. and Auler, A. S. (2013) Climate change patterns in Amazonia and biodiversity. *Nat. Commun.* 4, 1411.

Christl, M., Vockenhuber, C., Kubik, P. W., Wacker, L., Lachner, J., Alfimov, V. and Synal, H. A. (2013) The ETH Zurich AMS facilities: performance parameters and reference materials. *Nucl. Instrum. Methods Phys. Res. Sect. B* 294, 29–38.

Collins, J. A., Schefuß, E., Govin, A., Mulitza, S. and Tiedemann, R. (2014) Insolation and glacial–interglacial control on southwestern African hydroclimate over the past 140 000 years. *Earth Planet. Sci. Lett.*, 398, 1–10.

Collister, J. W., Rieley, G., Stern, B., Eglinton, G. and Fry, B. (1994) Compound-specific δ^{13}C analyses of leaf lipids from plants with differing carbon dioxide metabolisms. *Org. Geochem.* 21, 619–627.

Cordani, U. G., Sato, K. (1999) Crustal evolution of the South Amarican Platform, based on Nd isotopic systematic on granitoid rocks. *Episodes* 22, 167-173.

Crivellari, S., Chiessi, C. M., Kuhnert, H., Häggi, C., da Costa Portilho-Ramos, R., Zeng, J. Y., Zhang, Y., Schefuß, E., Mollenhauer, G., Hefter, J., Alexandre, F., Sampaio, G. and Mulitza, S. (2018) Increased Amazon freshwater discharge during late Heinrich Stadial 1. *Quat. Sci. Rev.* 181, 144–155.

Cui, X., Bianchi, T. S. and Savage, C. (2017) Erosion of modern terrestrial organic matter as a major component of sediments in fjords. *Geophys. Res. Lett.* 44, 1457–1465.

Damuth, J. E. and Flood, R. D.: Morphology, sedimentation processes, and growth pattern of the Amazon Deep-Sea Fan, Geo-Marine Lett., 3(2–4), 109–117, doi:10.1007/BF02462455, 1984.

Damuth, J. E. and Kumar, N. (1975) Amazon cone: morphology, sediments, age, and growth pattern. *Geol Soc Am Bull.* 86, 863-878.

Dignac, M. F., Bahri, H., Rumpel, C., Rasse, D. P., Bardoux, G., Balesdent, J., Girardin, C., Chenu, C. and Mariotti, A. (2005) Carbon-13 natural abundance as a tool to study the dynamics of lignin monomers in soil: An appraisal at the Closeaux experimental field (France). *Geoderma* 128, 3–17.

Dittmar, T. and Lara, R. J. (2001) Molecular evidence for lignin degradation in sulfate-reducing mangrove sediments (Amazônia, Brazil). *Geochim. Cosmochim. Acta*, 65, 1417–1428.

Drenzek, N. J., Hughen, K. A., Montluçon, D. B., Southon, J. R., dos Santos, G. M., Druffel, E. R. M., Giosan, L. and Eglinton, T. I. (2009) A new look at old carbon in active margin sediments. *Geology* 37, 239-242.

Druffel, E. R. M., Bauer, J. E. and Griffin, S. (2005) Input of particulate organic and dissolved inorganic carbon from the Amazon to the Atlantic Ocean. *Geochem., Geophys. Geosyst.* 6, Q03009.

Dümig, A., Rumpel, C., Dignac, M. F. and Kögel-Knabner, I. (2013) The role of lignin for the $\delta^{13}C$ signature in C4 grassland and C3 forest soils. *Soil Biol. Biochem.* 57, 1–13.

Dunne, T., Mertes, L. A. K., Meade, R. H., Richey, J. E. and Forsberg, B. R. (1998) Exchanges of sediment between the flood plain and channel of the Amazon River in Brazil. *Bull. Geol. Soc. Am.* 110, 450–467.

Eglinton, T. I., Aluwihare, L. I., Bauer, J. E., Druffel, E. R. M. and McNichol, A. P. (1996) Gas chromatographic isolation of individual compounds from complex matrices for radiocarbon dating. Anal. Chem., 68, 904–912.

Ertel, J. R. and Hedges, J. I. (1985) Sources of sedimentary humic substances: vascular plant debris. *Geochim. Cosmochim. Acta* 49, 2097–2107.

Ertel, J. R., Hedges, J. I., Devol, A. H., Richey, J. E. and Ribeiro, M. de N. G. (1986) Dissolved humic substances of the Amazon river system. *Limnol. Oceanogr.* 31, 739–754.

Faravelli, T., Frassoldati, A.,Migliavacca, G., and Ranzi, E. (2010) Detailed kinetic modeling of the thermal degradation of lignins. *Biomass Bioenergy* 34, 290–301.

Farquhar, G. D., Ehleringer, J. R. and Hubick, K. T. (1989) Carbon isotope discrimination and photosynthesis. *Annu. Rev. Plant Physiol. Plant Mol. Biol.* 40, 503-537.

Feng, X., Benitez-Nelson, B. C., Montluçon, D. B., Prahl, F. G., McNichol, A. P., Xu, L., Repeta, D. J. and Eglinton, T. I. (2013a) ^{14}C and ^{13}C characteristics of higher plant biomarkers in Washington margin surface sediments. *Geochim. Cosmochim. Acta* 105, 14–30.

Feng, X., Vonk, J. E., van Dongen, B. E., Gustafsson, Ö., Semiletov, I. P., Dudarev, O. V, Wang, Z., Montluçon, D. B., Wacker, L. and Eglinton, T. I. (2013b) Differential mobilization of terrestrial carbon pools in Eurasian Arctic river basins. *Proc. Natl. Acad. Sci. USA* 110, 14168–14173.

Feng, X., Gustafsson, O., Holmes, R. M., Vonk, J. E., Dongen, B. E., Semiletov, I. P., Dudarev, O. V, Yunker, M. B., Macdonald, R. W., Wacker, L., Montlucon, D. B. and Eglinton, T. I. (2015) Multimolecular tracers of terrestrial carbon transfer across the pan-Arctic: [14]C characteristics of sedimentary carbon components and their environmental controls. *Global Biogeochem. Cycles* 29, 1855–1873.

Fernandez, I., Mahieu, N. and Cadisch, G. (2003) Carbon isotopic fractionation during decomposition of plant materials of different quality. *Global Biogeochem. Cycles* 17, 1075.

Galbe, M. and Zacchi, G. (2007) Pretreatment of lignocellulosic materials for efficient bioethanol production. *Adv. Biochem. Engin./ Biotechnol.* 108, 41–46.

Galy, V., France-Lanord, C., Beyssac, O., Faure, P., Kudrass, H. and Palhol, F. (2007) Efficient organic carbon burial in the Bengal fan sustained by the Himalayan erosional system. *Nature* 450, 407–410.

Galy, V., France-Lanord, C. and Lartiges, B. (2008) Loading and fate of particulate organic carbon from the Himalaya to the Ganga-Brahmaputra delta. *Geochim. Cosmochim. Acta* 72, 1767–1787.

Galy, V. and Eglinton, T. (2011) Protracted storage of biospheric carbon in the Ganges-Brahmaputra basin. *Nat. Geosci.* 4, 843-847.

Galy, V., Eglinton, T., France-Lanord, C. and Sylva, S. (2011) The provenance of vegetation and environmental signatures encoded in vascular plant biomarkers carried by the Ganges-Brahmaputra rivers. *Earth Planet. Sci. Lett.* 304, 1–12.

Galy, V., Peucker-ehrenbrink, B. and Eglinton, T. (2015) Global carbon export from the terrestrial biosphere controlled by erosion. *Nature* 521, 204-207.

Gelman A. and Rubin D. B. (1992) Inference from Iterative Simulation Using Multiple Sequences. *Statist. Sci.* 7, 457–472.

Geyer, W. R., Beardsley, R. C., Lentz, S. J., Candela, J., Limeburner, R., Johns, W. E., Castro, B. M. and Soares, I. D. (1996) Physical oceanography of the Amazon shelf. *Cont. Shelf Res.* 16, 575–616.

Gibbs, R.J. (1967) Amazon River system: environmental factors that control its dissolved and suspended load. *Science* 156, 1734–1737.

Goñi, M. A. (1997) Record of terrestrial organic matter composition in Amazon Fan sediments. *Proc. Ocean Drill. Program. Sci. Results* 155, 519–530.

Goñi, M. A. and Montgomery, S. (2000) Alkaline CuO oxidation with a microwave digestion system: lignin analyses of geochemical samples. *Anal. Chem.* 72, 3116–3121.

Goñi, M. A. and Eglinton, T. I. (1996) Stable carbon isotopic analyses of lignin-derived CuO oxidation products by isotope ratio monitoring gas chromatography mass spectrometry (irm-GC-MS). *Org. Geochem.* 24, 601–615.

Goñi, M. A. and Ruttenberg, K. C. (1997) Sources and contribution of terrigenous organic carbon to surface sediments in the Gulf of Mexico. *Nature* 389, 275–278.

Goulding, M., Barthem, R., Ferreira, E. (2003) The Smithsonian Atlas of the Amazon, Smithsonian Books, Washington, D.C., USA.

Guyot, J. L., Jouanneau, J. M., Soares, L., Boaventura, G. R., Maillet, N. and Lagane, C. (2007) Clay mineral composition of river sediments in the Amazon Basin. *Catena* 71, 340–356.

Haffer, J. (1969) Speciation in Amazonian forest birds. *Science* 165, 131–137.

Hanke U. M., Wacker L., Hagipour N., Schmidt M. W. I., Eglinton T. I. (2017) Comprehensive radiocarbon analysis of benzene polycarboxylic acids (BPCAs) derived from pyrogenic carbon in environmental samples. *Radiocarbon* 59,1103-1116.

Häggi, C., Chiessi, C. M. and Schefuß, E. (2015) Testing the D/H ratio of alkenones and palmitic acid as salinity proxies in the Amazon Plume. *Biogeosciences* 12, 7239–7249.

Häggi, C., Sawakuchi, A. O., Chiessi, C. M., Mulitza, S., Mollenhauer, G., Sawakuchi, H. O., Baker, P. A., Zabel, M. and Schefuß, E. (2016) Origin, transport and deposition of leaf-wax biomarkers in the Amazon Basin and the adjacent Atlantic. *Geochim. Cosmochim. Acta* 192, 149–165.

Häggi, C., Chiessi, C. M., Merkel, U., Mulitza, S., Prange, M., Schulz, M. and Schefuß, E. (2017) Response of the Amazon rainforest to late Pleistocene climate variability. *Earth Planet. Sci. Lett.* 479, 50–59.

Hedges, J. I., Blanchette, R. A., Weliky, K. and Devol, A. H. (1988) Effects of fungal degradation on the CuO oxidation products of lignin: a controlled laboratory study. *Geochim. Cosmochim. Acta* 52, 2717–2726.

Hedges, J. I., Clark, W. A., Quay, P. D., Richey, J. E., Devol, A. H. and Santos, U. de M. (1986) Compositions and fluxes of particlate organic material in the Amazon River. *Limnol. Oceanogr.* 31, 717–738.

Hedges, J. I., Cowie, G. L., Richey, J. E., Quay, P. D., Benner, R., Mike, S. and Forsberg, B. R. (1994) Origins and processing of organic matter in the Amazon River as indicated by carbohydrates and amino acids. *Limnol. Oceanogr.* 39, 743–761.

Hedges, J. I. and Keil, R. G. (1995) Sedimentary organic matter preservation: an assessment and speculative synthesis. *Mar. Chem.* 49, 81–115.

Hedges, J. I., Keil, R. G. and Benner, R. (1997) What happens to terrestrial organic matter in the ocean? *Org. Geochem.* 27, 195-212.

Hedges, J. I. and Mann, D. C. (1979a) The characterization of plant tissues by their lignin oxidation products. *Geochim. Cosmochim. Acta* 43, 1803–1807.

Hedges, J. I. and Mann, D. C. (1979b) The lignin geochemistry of marine sediments from the southern Washington coast. *Geochim. Cosmochim. Acta* 43, 1809–1818.

Hedges, J. I. and Parker, P. L. (1976) Land-derived organic matter in surface sediments from the Gulf of Mexico. *Geochim. Cosmochim. Acta* 40, 1019–1029.

Hedges, J. I., Mayorga, E., Tsamakis, E., McClain, M. E., Aufdenkampe, A., Quay, P. and Richey, J. E. (2000) Organic matter in Bolivian tributaries of the Amazon River: A comparison to the lower mainstream. *Limnol. Oceanogr.* 45, 1449–1466.

Hockun, K., Mollenhauer, G., Ho, S. L., Hefter, J., Ohlendorf, C., Zolitschka, B., Mayr, C., Lücke, A. and Schefuß, E. (2016) Using distributions and stable isotopes of n-alkanes to disentangle organic matter contributions to sediments of Laguna Potrok Aike, Argentina. *Org. Geochem.* 102, 110–119.

Hopmans, E. C., Weijers, J. W. H., Schefuß, E., Herfort, L., Sinninghe Damsté, J. S. and Schouten, S. (2004) A novel proxy for terrestrial organic matter in sediments based on branched and isoprenoid tetraether lipids. *Earth Planet. Sci. Lett.* 224, 107–116.

Houghton, R. A., Lawrence, K. T., Hackler, J. L. and Brown, S. (2001) The spatial distribution of forest biomass in the Brazilian Amazon: a comparison of estimates. *Glob. Chang. Biol.* 7, 731–746.

Huang, Y., Freeman, K. H., Eglinton, T. I. and Street-Perrott, F. A. (1999) $\delta^{13}C$ analyses of individual lignin phenols in Quaternary lake sediments: a novel proxy for deciphering past terrestrial vegetation changes. *Geology* 27, 471–474.

Ingalls, A. E., Ellis, E. E., Santos, G. M., McDuffee, K. E., Truxal, L., Keil, R. G. and Druffel, E. R. M. (2010) HPLC purification of higher plant-derived lignin phenols for compound specific radiocarbon analysis. *Anal. Chem.* 82, 8931-8938.

Jasper, J. and Gagosian, R. (1989) Glacial–interglacial climatically forced $\delta^{13}C$ variations in sedimentary organic matter. *Nature* 342, 60–62.

Jung, B. J., Jeanneau, L., Alewell, C., Kim, B. and Park, J. H. (2015) Downstream alteration of the composition and biodegradability of particulate organic carbon in a mountainous, mixed land-use watershed. *Biogeochemistry* 122, 79–99.

Junk, W. J. (1997) The Central Amazon Floodplain: Ecology of a Pulsing System., Springer, Berlin.

Kastner, T. P. and Goñi, M. A. (2003) Constancy in the vegetation of the Amazon Basin during the late Pleistocene: evidence from the organic matter composition of Amazon fan deep sea sediments. *Geology* 31, 291–294.

Keil, R. G., Mayer, L. M., Quay, P. D., Richey, J. E. and Hedges, J. I. (1997) Loss of organic matter from riverine particles in deltas. *Geochim. Cosmochim. Acta* 61, 1507–1511.

Keil, R. G., Tsamakis, E., Giddings, J. C. and Hedges, J. I. (1998) Biochemical distributions (amino acids, neutral sugars, and lignin phenols) among size-classes of modern marine sediments from the Washington coast. *Geochim. Cosmochim. Acta* 62, 1347–1364.

Killops, S. and Killops, V. (2005) Introduction to Organic Geochemistry Second Edition.

Kim, J. H., Schouten, S., Bonnin, J., Buscail, R., Ludwig, W., Sinninghe Damsté, J. S. and Bourrin, F. (2006) Origin and distribution of terrestrial organic matter in the NW Mediterranean (Gulf of Lions): exploring the newly developed BIT index. *Geochem. Geophys. Geosyst.* 7, Q11017.

Kim, J. H., Zell, C., Moreira-Turcq, P., Pérez, M. A. P., Abril, G., Mortillaro, J. M., Weijers, J. W. H., Meziane, T. and Sinninghe Damsté, J. S. (2012) Tracing soil organic carbon in the lower Amazon River and its tributaries using GDGT distributions and bulk organic matter properties. *Geochim. Cosmochim. Acta* 90, 163–180.

Kodina, L. A. (2010) Carbon isotope fractionation in various forms of biogenic organic matter: I. Partitioning of carbon isotopes between the main polymers of higher plant biomass. *Geochem. Int.* 48, 1157–1165.

Komada, T., Anderson, M. R. and Dorfmeier, C. L. (2008) Carbonate removal from coastal sediments for the determination of carbon carbon and its isotopic signatures, $\delta^{13}C$ and $\Delta^{14}C$: comparison of fumigation and direct acidification by hydrochloric acid. *Limol. Oceanogr.: Methods* 6, 254-262

Komada, T., Druffel, E. R. M. and Hwang, J. (2005) Sedimentary rocks as sources of ancient organic carbon to the ocean: an investigation through $\Delta^{14}C$ and $\delta^{13}C$ signatures of organic compound classes. *Global Biogeochem. Cycles* 19, GB2017.

Kusch, S., Rethemeyer, J., Schefuß, E. and Mollenhauer, G. (2010) Controls on the age of vascular plant biomarkers in Black Sea sediments. *Geochim. Cosmochim. Acta* 74, 7031–7047.

Kuzyk, Z. Z. A., Goñi, M. A., Stern, G. A. and Macdonald, R. W. (2008) Sources, pathways and sinks of particulate organic matter in Hudson Bay: evidence from lignin distributions. *Mar. Chem.* 112, 215–229.

Loftis, K. M. (2013) Geochemistry of lignin biomarkers in marsh environments of the Georgia coast.

Loh, P. S., Chen, C. T. A., Anshari, G. Z., Wang, J. T., Lou, J. Y. and Wang, S. L. (2012) A comprehensive survey of lignin geochemistry in the sedimentary organic matter along the Kapuas River (West Kalimantan, Indonesia). *J. Asian Earth Sci.* 43, 118–129.

Ludwig, W., Probst, J. L. and Kempe, S. (1996) Predicting the oceanic input of organic carbon by continental erosion. *Global Biogeochem. Cycles* 10, 23-41.

Martin, E. E., Ingalls, A. E., Richey, J. E., Keil, R. G., Santos, G. M., Truxal, L. T., Alin, S. R. and Druffel, E. R. M. (2013) Age of riverine carbon suggests rapid export of terrestrial primary production in tropics. *Geophys. Res. Lett.* 40, 5687–5691.

Marwick, T. R., Tamooh, F., Teodoru, C. R., Borges, A. V., Darchambeau, F. and Bouillon, S. (2015) The age of river-transported carbon: a global perspective. *Global Biogeochem. Cycles* 29, 122–137.

Meade, R. H., Dunne, T., Richey, J., Santos, U. de M., and Salati, E. (1985) Storage and remobilization of sediment in the lower Amazon River of Brazil. *Science* 228, 488-490.

Mayer, L. M. (1994) Relationships between mineral surfaces and organic carbon concentrations in soils and sediments. *Chem. Geol.* 114, 347–363.

Mayorga, E., Aufdenkampe, A. K., Masiello, C. A., Krusche, A. V, Hedges, J. I., Quay, P. D., Richey, J. E. and Brown, T. A. (2005) Young organic matter as a source of carbon dioxide outgassing from Amazonian rivers. *Nature* 436, 538-541.

McCallister, S. L. and Giorgio, P. A. (2012) Evidence for the respiration of ancient terrestrial organic C in northern temperate lakes and streams. *Proc. Natl. Acad. Sci. USA* 109, 16963-16968.

McIntyre, C. P., Wacker, L., Haghipour, N., Blattmann, T. M., Fahrni, S., Usman, M., Eglinton, T. I. and Synal, H. (2017) Online 13C and 14C gas measurements by EA-IRMS-AMS at ETH Zürich. *Radiocarbon* 59, 893-903.

Meybeck, M. (1982) Carbon, nitrogen, and phosphorus transport by world rivers. *Am. J. Sci.* 282, 401–450.

Mollenhauer, G. and Eglinton, T. I. (2007) Diagenetic and sedimentological controls on the composition of organic matter preserved in California Borderland Basin sediments. *Limnol. Oceanogr.* 52, 558–576.

Moreira-Turcq, P., Seyler, P., Guyot, J. L. and Etcheber, H. (2003) Exportation of organic carbon from the Amazon River and its main tributaries. *Hydrol. Process.* 17, 1329–1344.

Mounier, S., Braucher, R. and Benaïm, J. Y. (1999) Differentiation of organic matter's properties of the Rio Negro basin by crossflow ultra-filtration and UV-spectrofluorescence. *Wat. Res.* 33, 2363–2373.

Mulitza, S., Chiessi, C. M., Cruz, A. P. S., Frederichs, T., Gomes, J. G., Gurgel, M. H., Haberkern, J., Huang, E., Jovane, L., Kuhnert, H., Pittauerová, D., Reiners, S. -J., Roud, S. C., Schefuß, E., Schewe, F., Schwenk, T. A., Sicoli Seoane, J. C., Sousa, S. H. M., Wagner, D. J., Wiers, S. (2013) Response of Amazon Sedimentation to Deforestation, Land Use and Climate Variability – Cruise No. MSM20/3 – February 19–March 11, 2012 – Recife (Brazil)–Bridgetown (Barbados). Berichte, Fachbereich Geowissenschaften, Universität Bremen, Bremen, Germany, pp. 1–86.

Nittrouer, C. A. and DeMaster, D. J. (1996) The Amazon shelf setting: tropical, energetic, and influenced by a large river. *Cont. Shelf Res.* 16, 553–573.

Nittrouer, C. A., Kuehl, S. A., Sternberg, R. W., Figueiredo, A. G. and Faria, L. E. C. (1995) An introduction to the geological significance of sediment transport and accumulation on the Amazon continental shelf. *Mar. Geol.* 125, 177–192.

Opsahl, S. and Benner, R. (1995) Early diagenesis of vascular plant tissues: lignin and cutin decomposition and biogeochemical implications. *Geochim. Cosmochim. Acta* 59, 4889–4904.

Otto, A. and Simpson, M. J. (2005) Degradation and preservation of vascular plant-derived biomarkers in grassland and forest soils from Western Canada. *Biogeochemistry* 74, 377–409.

Otto, A. and Simpson, M. J. (2006) Sources and composition of hydrolysable aliphatic lipids and phenols in soils from western Canada. *Org. Geochem.* 37, 385–407.

Pearson, A., McNichol, A. P., Benitez-Nelson, B. C., Hayes, J. M. and Eglinton, T. I. (2001) Origins of lipid biomarkers in Santa Monica Basin surface sediment: a case study using compound-specific $\Delta^{14}C$ analysis. *Geochim. Cosmochim. Acta* 65, 3123–3137.

Perez-Pimienta, J. A., Lopez-Ortega, M. G., Varanasi, P., Stavila, V., Cheng, G., Singh, S. and Simmons, B. A. (2013) Comparison of the impact of ionic liquid pretreatment on recalcitrance of agave bagasse and switchgrass. *Bioresour. Technol.* 127, 18–24.

Quesada, C. A., Lloyd, J., Anderson, L. O., Fyllas, N. M., Schwarz, M. and Czimczik, C. I. (2011) Soils of Amazonia with particular reference to the RAINFOR sites. *Biogeosciences* 8, 1415-1440.

R Core Team (2017) R: a language and environment for statistical computing. Vienna, Austria.

Reimer, P. J., Brown, T. A. and Reimer, R. W. (2004) Discussion: reporting and calibration of post-bomb ^{14}C data. *Radiocarbon* 46, 1299–1304.

Rethemeyer, J., Fülöp, R. H., Höfle, S., Wacker, L., Heinze, S., Hajdas, I., Patt, U., König, S., Stapper, B. and Dewald, A. (2013) Status report on sample preparation facilities for ^{14}C analysis at the new CologneAMS center. *Nucl. Instrum. Methods Phys. Res. Sect. B* 294, 168–172.

Rezende, C. E., Pfeiffer, W. C., Martinelli, L. A., Tsamakis, E., Hedges, J. I. and Keil, R. G. (2010) Lignin phenols used to infer organic matter sources to Sepetiba Bay - RJ, Brasil. *Estuar. Coast. Shelf Sci.* 87, 479–486.

Richey, J. E., Hedges, J. I., Devol, A. H., Quay, P. D., Victoria, R., Martinelli, L., Forsberg, B. R. (1990) Biogeochemistry of carbon in the amazon river. *Limnol. Oceanogr.* 35, 352–371.

Richey, J. E., Meade, R. H., Salati, E., Devol, A. H., Nordin, C. F. Jr., and dos Santos U (1986) Water discharge and suspended sediment concentrations in the Amazon River: 1982-1984. *Water Resour. Res.* 22, 756-764.

Rossetti, D. F, Toledo, P. M. and Góes A. M. (2005) New geological framework for Western Amazonia (Brazil) and implications for biogeography and evolution. *Quat. Resear.* 63, 78–89.

Ruff, M., Wacker, L., Gäggeler, H. W. and Szidat, M. S. H. S. S.: A gas ion source for radiocarbon measurements at 200kv, Radiocarbon, 49(2), 2007.

Ruff, M., Szidat, S., Gäggeler, H. W., Suter, M., Synal, H. A. and Wacker, L.: Gaseous radiocarbon measurements of small samples, Nucl. Instruments Methods Phys. Res. Sect. B Beam Interact. with Mater. Atoms, 268(7–8), 790–794, doi:10.1016/j.nimb.2009.10.032, 2010.

Saatchi, S. S., Nelson, B., Podest, E., and Holt, J. (2000) Mapping land cover types in the Amazon Basin using 1 km JERS-1 mosaic. *Int. J. Remote Sens.* 21, 1201-1234.

Salati, E. and Vose, P. B. Amazon basin: a system in equilibrium. *Science* 225, 129-138.

Santos, G. M., Southon, J. R., Drenzek, N. J., Ziolkowski, L. A., Druffel, E., Xu, X., Zhang, D., Trumbore, S., Eglinton, T. I. and Hughen, K. A. (2010) Blank assessment for ultra-small radiocarbon samples: chemical extraction and separation versus AMS. *Radiocarbon* 52, 1322–1335.

Santos, G. M., Alexandre, A., Coe, H. H. G., Reyerson, P. E., Southon, J. R. and De Carvalho, C. N. (2010) The phytolith ^{14}C puzzle : a tale of background determinations and accuracy tests. *Radiocarbon* 52, 113–128.

Santos, G. M., Moore, R. B., Shouthon, J. R., Griffin, S., Hinger, E. and Zhang, D. (2007) AMS ^{14}C sample preparation at the KCCAMS/UCI facility:status report and performance of small samples. *Radiocarbon* 49, 255–269.

Schefuß, E., Eglinton, T. I., Spencer-Jones, C. L., Rullkötter, J., De Pol-Holz, R., Talbot, H. M., Grootes, P. M. and Schneider, R. R. (2016) Hydrologic control of carbon cycling and aged carbon discharge in the Congo River basin. *Nat. Geosci., 9*, 687–690.

Schlitzer, R., Ocean Data View, http://odv.awi.de, 2017

Schlünz, B. and Schneider, R. R. (2000) Transport of terrestrial organic carbon to the oceans by rivers: re-estimating flux and burial rates. *Int. J. Earth Sci.* 88, 599–606.

Schlünz, B., Showers, W. J. and Wefer, G. (1999) Terrestrial organic carbon accumulation on the Amazon deep sea fan during the last glacial sea level low stand. *Chem. Geol.* 159, 263-281.

Schmidt, F., Hinrichs, K. and Elvert, M. (2010) Sources , transport , and partitioning of organic matter at a highly dynamic continental margin. *Mar. Chem.*, 118, 37–55.

Shah, S. R. and Pearson, A. (2007) Ultra-microscale (5-25 μg C) analysis of individual lipids by ^{14}C AMS: assessment and correction for sample processing blanks. *Radiocarbon* 49, 69–82.

Showers, W. J. and Angle, D. G. (1986) Stable isotopic characterization of organic carbon accumulation on the Amazon continental shelf. *Cont. Shelf Res.* 6, 227-244.

Schuur, E. A. G., McGuire, A. D., Schädel, C., Grosse, G., Harden, J. W., Hayes, D. J., Hugelius, G., Koven, C. D., Kuhry, P., Lawrence, D. M., Natali, S. M., Olefeldt, D., Romanovsky, V. E., Schaefer, K., Turetsky, M. R., Treat, C. C. and Vonk, J. E. (2015) Climate change and the permafrost carbon feedback. *Nature* 520, 171-179.

Sinninghe Damsté, J. S., Schouten, S., Hopmans, E. C., van Duin, A. C. T. and Geenevasen, J. A. J. (2002) Crenarchaeol: the characteristic core glycerol dibiphytanyl glycerol tetraether membrane lipid of cosmopolitan pelagic crenarchaeota. *J. Lipid Res.* 43, 1641–1651.

Sobrinho, R. L., Bernardes, M. C., Abril, G., Kim, J. H., Zell, C. I., Mortillaro, J. M., Meziane, T., Moreira-Turcq, P. and Sinninghe Damste, J. S. (2016) Spatial and seasonal contrasts of sedimentary organic matter in floodplain lakes of the central Amazon basin. *Biogeosciences* 13, 467–482.

Sombroek, W. (2001) Spatial and temporal patterns of Amazon rainfall consequences for the planning of agricultural occupation and the protection of primary forests. *AMBIO: A Journal of the Human Environment* 30, 388-396.

Spitzy A. and Ittekkot, V. (1991) Dissolved and particulate organic matter in rivers. In Ocean Margin in Global Change (eds. R. F. C. Mantoura, J. M. Martin and R. Wollast). John Wiley and Sons, New York, pp. 5–17.

Stan Development Team (2018) RStan: the R interface to Stan.

Stuiver, M. and Polach, H. A. (1977) Discussion: reporting of ^{14}C data. *Radiocarbon* 19, 355–363.

Sun, S., Meyer, V., Winterfeld, M., Hefter, J., Dummann, W., McIntyre, C., Montluçon, D. B., Haghipour, N., Wacker, L., Gentz, T. van der Voort, T., Eglinton, T. I. and Mollenhauer, G. (submitted for publication) ^{14}C blank assesment in small-scale compound-specific radiocarbon analysis of lipid biomarkers and lignin phenols. *Radiocarbon*

Sun, S., Schefuß, E., Mulitza, S., Chiessi, C. M., Sawakuchi, A. O., Zabel, M., Baker, P., Hefter, J. and Mollenhauer, G. (2017) Origin and processing of terrestrial organic carbon in the Amazon system: lignin phenols in river, shelf and fan sediments. *Biogeosciences* 14, 2495-2512.

Tao, S., Eglinton, T. I., Montluçon, D. B., McIntyre, C. and Zhao, M. (2015) Pre-aged soil organic carbon as a major component of the Yellow River suspended load: regional significance and global relevance. *Earth Planet. Sci. Lett.* 414, 77–86.

Tao, S., Eglinton, T. I., Montluçon, D. B., McIntyre, C. and Zhao, M. (2016) Diverse origins and pre-depositional histories of organic matter in contemporary Chinese marginal sea sediments. *Geochim. Cosmochim. Acta* 191, 70–88.

Tesi, T., Semiletov, I., Hugelius, G., Dudarev, O., Kuhry, P. and Gustafsson, Ö. (2014) Composition and fate of terrigenous organic matter along the Arctic land–ocean continuum in East Siberia: insights from biomarkers and carbon isotopes. *Geochim. Cosmochim. Acta* 133, 235–256.

Tesi, T., Semiletov, I., Dudarev, O., Andersson, A. and Gustafsson, Ö. (2016) Matrix association effects on hydrodynamic sorting and degradation of terrestrial organic matter during cross-shelf transport in the Laptev and East Siberian shelf seas. *J. Geophys. Res. Biogeosci.* 121, 731–752.

Thevenot, M., Dignac, M. F. and Rumpel, C. (2010) Fate of lignins in soils: a review. *Soil Biol. Biochem.* 42, 1200–1211.

Trumbore, S. E. (1993) Comparison of carbon dynamics in tropical and temperate soils using radiocarbon measurements. *Global Biogeochem. Cycles* 7, 275-290.

van der Voort, T. S., Zell, C. I., Hagedorn, F., Feng, X., McIntyre, C. P., Haghipour, N., Graf Pannatier, E. and Eglinton, T. I. (2017) Diverse soil carbon dynamics expressed at the molecular level. *Geophys. Res. Lett.* 44, 11840-11850.

Vogts, A., Schefuß, E., Badewien, T. and Rullkötter, J. (2012) n-Alkane parameters from a deep sea sediment transect off southwest Africa reflect continental vegetation and climate conditions. *Org. Geochem.* 47, 109–119.

Volkman, J. K., Barrett, S. M., Blackburn, S. I., Mansour, M. P., Sikes, E. L. and Gelin, F. (1998) Microalgal biomarkers: A review of recent research developments. *Org. Geochem.* 29, 1163–1179.

Vonk, J. E., Giosan, L., Blusztajn, J., Montlucon, D. B., Pannatier, E. G., McIntyre, C., Wacker, L., Macdonald, R. W., Yunker, M. B. and Eglinton, T. I. (2015) Spatial variations in geochemical characteristics of the modern Mackenzie Delta sedimentary system. *Geochim. Cosmochim. Acta* 171, 100–120.

Wang, G., Jia, Y. and Li, W. (2015) Effects of environmental and biotic factors on carbon isotopic fractionation during decomposition of soil organic matter. *Sci. Rep.* 5, 1–11.

Ward, N. D., Keil, R. G., Medeiros, P. M., Brito, D. C., Cunha, A. C., Dittmar, T., Yager, P. L., Krusche, A. V. and Richey, J. E. (2013) Degradation of terrestrially derived macromolecules in the Amazon River. *Nat. Geosci.* 6, 530–533.

Ward, N. D., Krusche, A. V., Sawakuchi, H. O., Brito, D. C., Cunha, A. C., Moura, J. M. S., da Silva, R., Yager, P. L., Keil, R. G., and Richey, J. E. (2015) The compositional evolution of dissolved and particulate organic matter along the lower Amazon River-Óbidos to the ocean. *Mar. Chem.* 177, 244-256.

Weijers, J. W. H., Schouten, S., van der Linden, M., van Geel, B. and Sinninghe Damsté, J. S. (2004) Water table related variations in the abundance of intact archaeal membrane lipids in a Swedish peat bog. *FEMS Microbiol. Lett.* 239, 51–56.

Weiss HM, Wilhelms A, Mills N, Scotchmer J, Hall PB, Lind K, Brekke T. 2000. In: Hydro, Norsk (Ed.) *NIGOGA-the Norwegian Industry Guide to Organic Geochemical Analyses* [online]. 4.0 Statoil, Geolab Nor, SINTEF Petroleum Research and the Norwegian Petroleum Directorate.

Williams, E. K., Rosenheim, B. E., Allison, M., McNichol, A. P. and Xu, L. (2015) Quantification of refractory organic material in Amazon mudbanks of the French Guiana Coast. *Mar. Geol.* 363, 93–101.

Winterfeld, M., Goñi, M. A., Just, J., Hefter, J. and Mollenhauer, G. (2015) Characterization of particulate organic matter in the Lena River delta and adjacent nearshore zone, NE Siberia - Part 2: Lignin-derived phenol compositions. *Biogeosciences* 12, 2261–2283.

Winterfeld M, Mollenhauer G, Dummann W, Köhler P, Lembke-Jene L, Meyer VD, Hefter J, McIntyre C, Wacker L, Kokfelt U, Tiedemann R. (submitted for publication) Deglacial mobilization of pre-aged terrestrial carbon from thawing permafrost. *Nat. Commun.*

Wu, M. S., Feakins, S. J., Martin, R. E., Shenkin, A., Bentley, L. P., Blonder, B., Salinas, N., Asner, G. P. and Malhi, Y. (2017) Altitude effect on leaf wax carbon isotopic composition in humid tropical forests. *Geochim. Cosmochim. Acta* 206, 1–17.

Wu, Y., Dittmar, T., Ludwichowski, K. U., Kattner, G., Zhang, J., Zhu, Z. Y. and Koch, B. P. (2007) Tracing suspended organic nitrogen from the Yangtze River catchment into the East China Sea. *Mar. Chem.* 107, 367–377.

Wu, Y., Eglinton, T., Yang, L., Deng, B. and Montluçon, D. (2013) Spatial variability in the abundance, composition, and age of organic matter in sur fi cial sediments of the East China Sea. *J. Geophys. Res. Biogeosci.* 118, 1495–1507.

Wynn, J. G. (2007) Carbon isotope fractionation during decomposition of organic matter in soils and paleosol: implications for paleoecological interpretations of paleosols. *Palaeogeogr. Palaeoclimatol. Palaeoecol.* 251, 437-448.

Zell, C., Kim, J. H., Hollander, D., Lorenzoni, L., Baker, P., Silva, C. G., Nittrouer, C. and Sinninghe Damsté, J. S. (2014) Sources and distributions of branched and isoprenoid tetraether lipids on the Amazon shelf and fan: implications for the use of GDGT-based proxies in marine sediments. *Geochim. Cosmochim. Acta* 139, 293–312.

Zhang, Y., Chiessi, C. M., Mulitza, S., Zabel, M., Trindade, R. I. F., Hollanda, M. H. B. M., Dantas, E. L., Govin, A., Tiedemann, R. and Wefer, G. (2015) Origin of increased terrigenous supply to the NE South American continental margin during Heinrich Stadial 1 and the Younger Dryas. *Earth Planet. Sci. Lett.* 432, 493–500.

Zhang, Y., Chiessi, C. M., Mulitza, S., Sawakuchi, A. O., Häggi, C., Zabel, M., Portilho-Ramos, R. C., Schefuß, E., Crivellari, S. and Wefer, G. (2017) Different precipitation patterns across tropical South America during Heinrich and Dansgaard-Oeschger stadials. *Quat. Sci. Rev.* 177, 1–9.

Zhu, J. Y. and Pan, X. J. (2010) Woody biomass pretreatment for cellulosic ethanol production: technology and energy consumption evaluation. *Bioresour. Technol.* 101, 4992–5002.

Ziolkowski, L. A. and Druffel, E. R. M. (2009) Quantification of extraneous carbon during compound specific radiocarbon analysis of black carbon. *Anal. Chem.* 81, 10156–10161.

Zonneveld, K. A. F., Versteegh, G. J. M., Kasten, S., Eglinton, T. I., Emeis, K. C., Huguet, C., Koch, B. P., de Lange, G. J., de Leeuw, J. W., Middelburg, J. J., Mollenhauer, G., Prahl, F. G., Rethemeyer, J. and Wakeham, S. G. (2010) Selective preservation of organic matter in marine environments; processes and impact on the sedimentary record. *Biogeosciences* 7, 483-511.